

**TWO PROBLEMS IN SPIN-DEPENDENT TRANSPORT IN METALLIC
MAGNETIC MULTILAYERS**

by

Asya Shapiro

A dissertation submitted in partial fulfillment

of the requirements for the degree of

Doctor of Philosophy

Department of Physics

New York University

January, 2004

Thesis Adviser

Peter M. Levy

© Asya Shpiro

All Rights Reserved, 2004

To my parents

Acknowledgements

I would like to express my deepest gratitude to my thesis adviser, Professor Peter M. Levy, for his constant support and guidance, patience and encouragement. I appreciate an opportunity to learn from his expertise, dedication to physics and to the people under his supervision.

Almost all my research was done in a close collaboration with Professor Shufeng Zhang. I am grateful to him for his explanations, suggestions, and constant interest in my work.

I would also like to acknowledge the hospitality of the Laboratoire de Physique des Solides at the Universite Paris-Sud in Orsay, France, where part of my research was done, in particular, Professor Albert Fert and Charles Sommers.

I am thankful to many graduate students, current and former, at Physics Department. Their attitude toward knowledge sharing and supporting each other was a great help. Many of them became good friends of mine.

I am in a great debt to my parents, Polina and Vladimir Shpiro, who first introduced me to the world of science and the world of scientists, who influenced my choice of career, and made me realize that physicists are the best people on Earth. My PhD is their big achievement.

Finally, I would like to thank the people who were next to me during the last stages of my work on the dissertation, my husband Lazar Fleysher and our daughter Sonya, for their love and understanding.

Abstract

Transport properties of magnetic multilayers in current perpendicular to the plane of the layers geometry are defined by diffusive scattering in the bulk of the layers, and diffusive and ballistic scattering across the interfaces. Due to the short screening length in metals, layer by layer treatment of the multilayers is possible, when the macroscopic transport equation (Boltzmann equation or diffusion equation) is solved in each layer, while the details of the interface scattering are taken into account via the boundary conditions. Embedding the ballistic and diffusive interface scattering in the framework of the diffusive scattering in the bulk of the layers is the unifying idea behind the problems addressed in this work: the problem of finding the interface resistance in the multilayered structures and the problem of current-induced magnetization switching.

In order to find the interface resistance, the method of solving the semiclassical linearized Boltzmann equation in CPP geometry is developed, allowing one to obtain the equations for the chemical potential everywhere in the multilayers in the presence of specular and diffuse scattering at the interfaces, and diffuse scattering in the bulk of the layers. The variation of the chemical potential within a mean-free path of the interfaces leads to a breakdown of the resistors-in-series model which is currently used to analyze experimental data. While the resistance of the whole system is found by adding resistances due to the bulk of the layers and resistances due to the interfaces, the interface resistances are not independent of the properties of the bulk of the layers, particularly, of the ratio of the layer thickness to the mean-free path in this layer.

A mechanism of the magnetization switching that is driven by spin-polarized current is studied in noncollinear magnetic multilayers. Even though the transfer of the spin angular momentum between current carriers and local moments occurs near the interface of the magnetic layers, in order to determine the magnitude of the transfer one should calculate the spin transport properties far beyond the interfacial regions. Due to the presence of long longitudinal spin-diffusion lengths, the longitudinal and transverse components of the spin accumulations become intertwined from one layer to the

next, leading to a significant amplification of the spin-torque with respect to the treatments that concentrate on the transport at the interface only, i.e., those that only consider the contribution to the torque from the bare current and neglect that arising from spin accumulation.

Contents

	iii
Acknowledgements	iv
Abstract	v
List of Figures	ix
List of Appendices	xii
1 Introduction	1
1.1 Magnetoresistive effects	1
1.2 Spin-dependent transport in metallic magnetic multilayers and the GMR	6
1.3 Current-induced switching	11
1.4 Problems to be solved	13
1.4.1 Interface resistance	13
1.4.2 Current-induced magnetization switching	15
2 Description of transport in multilayers	19
2.1 Boltzmann equation	20
2.2 Landauer approach - interface resistance.	28
3 Interface resistance in multilayers - theory	32
3.1 General solution of the Boltzmann equation	33
3.2 Boundary conditions at the interface between two layers	34
3.3 Equations for chemical potential profile in a multilayer	36
3.4 Special forms of diffuse scattering	40

4 Interface resistance in multilayers - results	43
4.1 Two layers	45
4.1.1 Same metals	45
4.1.2 Different metals	45
4.1.3 Anticipation of the breakdown of the resistors-in-series model . .	49
4.2 Three and five layers	51
4.3 Co-Cu and Fe-Cr systems	56
5 Spin-torques - theory	65
5.1 Review of formalism	65
5.2 Two ferromagnetic layers	71
5.3 Correction to CPP resistance	79
5.4 Permalloy	80
6 Spin-torques in the thin FM - thick FM - NM structure	83
6.1 Numerical results	84
6.2 Spin current at the interface between ferromagnetic layers	96
6.3 Resistance	98
7 Conclusion	100
Appendices	103
Bibliography	135

List of Figures

1.1	Anisotropic magnetoresistance	2
1.2	Magnetoresistance of Fe/Cr superlattices	3
1.3	Ferromagnetic and antiferromagnetic configuration of a multilayered magnetic metallic structure	4
1.4	Current In Plane of the layers and Current Perpendicular to the Plane of the layers geometries	4
1.5	Density of states for up and down electrons for cobalt	7
1.6	Spin-dependent scattering	8
1.7	Two current model: resistor network analogy	10
1.8	Current-induced magnetization switching	12
1.9	Resistors-in-series model	14
1.10	Chemical potential profile in two semi-infinite metallic layers	15
1.11	Multilayered pillar-like structure used for current induced reversal of a magnetic layer	17
1.12	Exchange splitting	17
2.1	Displacement of the Fermi surface in the momentum space under the influence of the electric field	24
2.2	One-dimensional barrier with the transition coefficient T and reflection coefficient $R = 1 - T$, connected to an external source	29
3.1	Scattering at an interface	34
3.2	System consisting of two layers	37
3.3	Diffuse scattering $S(\theta)$	42
4.1	Chemical potential and interface resistance in two layers of identical metals	46

4.2	Step-like potential experienced by electrons at an interface between two metals	46
4.3	Chemical potential profile in two-layered system with $V_2/V_1 = 2$ for different amount of diffuse scattering at the interface	47
4.4	Effect of the diffuse scattering in the bulk of the layers on the interface resistance in two-layered system	48
4.5	Summary of the results for the two-layered system	50
4.6	Step-like potential experienced by electrons in a multilayered system	52
4.7	Chemical potential profiles in the multilayered systems	53
4.8	Summary of results for the three-layered and five-layered systems	55
4.9	FM-N structures	57
4.10	Step-like potentials experienced by up and down electrons in the Co-Cu and Fe-Cr multilayered structures	58
4.11	Resistances due to the interfaces in the Co-Cu systems	61
4.12	Deviations from the resistors-in-series model in the Co-Cu systems	62
4.13	Resistances due to the interfaces in the Fe-Cr systems	63
4.14	Deviations from the resistors-in-series model in the Fe-Cr systems	64
5.1	Direction of the effective field and spin-torque acting on a thin FM layer background magnetization	71
5.2	System of two thick ferromagnetic layers	72
5.3	Spin accumulation and spin current distribution in two-layered system	77
5.4	Spin-torque and effective field acting on the FM layer in FM-Sp-FM system as a function of the layer thickness	78
6.1	Multilayered pillar-like structure used for current induced reversal of a magnetic layer	84
6.2	Total torque acting on the thin FM layer in the FM-Sp-FM-NM system as a function of the layer thickness for different λ_J and λ_{sdl}^F and zero interface resistance	87
6.3	Total torque acting on the thin FM layer in the FM-Sp-FM-NM system as a function of the layer thickness for different λ_J and λ_{sdl}^F and non-zero interface resistance	88
6.4	Total effective field acting on the thin FM layer in the FM-Sp-FM-NM system as a function of the layer thickness for different λ_J and λ_{sdl}^F and zero interface resistance	89

6.5	Total effective field acting on the thin FM layer in the FM-Sp-FM-NM system as a function of the layer thickness for different λ_J and λ_{sdl}^F and non-zero interface resistance	90
6.6	Spin-accumulation and spin-current distribution in the FM-Sp-FM-NM system with the thin FM layer thickness $t_F = 3$ nm and zero interface resistance	92
6.7	Spin-accumulation and spin-current distribution in the FM-Sp-FM-NM system with the thin FM layer thickness $t_F = 15$ nm and zero interface resistance	93
6.8	Spin-accumulation and spin-current distribution in the FM-Sp-FM-NM system with the thin FM layer thickness $t_F = 3$ nm and non-zero interface resistance	94
6.9	Spin-accumulation and spin-current distribution in the FM-Sp-FM-NM system with the thin FM layer thickness $t_F = 15$ nm and non-zero interface resistance	95
6.10	True spin current at the interface between the thin and the thick ferromagnetic layers in comparison with the bare transverse current as a function of the angle between the magnetization directions in the layers	97
6.11	Normalized resistance of the thick FM-Sp-thin FM-NM structure as a function of the angle between the magnetization directions in the layers	99
A.1	Specular scattering at the potential barrier	108
A.2	Reflection coefficient at the potential barrier as a function of the angle of incidence	111
A.3	System consisting of three layers	111
A.4	System consisting of five layers	115
B.1	Structure of the interface between the ferromagnetic and non-magnetic layers	123
B.2	Three-layered structure used for current induced reversal of a magnetic layer	131

List of Appendices

A Appendices for interface resistance chapters	103
A.1 Calculus related to the problem	103
A.1.1 Dirac delta function in ϵ and v space	103
A.1.2 Angular averaging	104
A.1.3 Diffuse scattering term $F(g)$ in the boundary conditions	105
A.2 Current conservation across an interface	105
A.3 Specular reflection and transmission at the potential step	107
A.4 Equations for chemical potential for three-layered system	110
A.5 Equations for chemical potential for five-layered system	114
A.6 Numerical procedure of solving the Fredholm equation of the second kind	118
A.7 Parameters entering the equations for the chemical potentials for Co-Cu and Fe-Cr systems	119
A.7.1 Electrons Fermi velocities ratios for Co-Cu system	119
A.7.2 The summary of the Fermi velocities ratios entering the equations for the chemical potentials	120
B Appendices for torques chapters	122
B.1 Derivation of the boundary conditions for spin-accumulation and spin-current between the layers	122
B.2 Solution of the diffusion equation for spin-accumulation	131

Chapter 1

Introduction

1.1 Magnetoresistive effects

During the last decade, attention has been focused on a question of magnetically controlled electrical transport. Materials can change their resistance in response to a magnetic field. This phenomena is called magnetoresistance (MR). All metals have an inherent, though small, MR owing to the Lorentz force that a magnetic field exerts on moving electrons. Metallic alloys containing magnetic atoms can have an enhanced MR. For example, an anisotropic magnetoresistance (AMR) measures the change in resistance as the direction of the magnetization changes relative to the direction of the electric current. (Fig. 1.1) If θ is the angle between the magnetization and the current direction, (Fig. 1.1b)), the resistance is the following function of θ :

$$R = R_0 + \Delta R_{AMR} \cos^2 \theta, \quad (1.1)$$

where R_0 is the resistance at $\theta = \pi/2$, and $\Delta R_{AMR}/R_0$ is the AMR ratio. The resistivity is typically smaller if the current direction is perpendicular to the direction of magnetization than in the condition that those are parallel due to the scattering anisotropy of electrons. The AMR ratio is fairly small: a few percent for $\text{Ni}_{0.8}\text{Fe}_{0.2}$ alloy (permalloy) at room temperature, and somewhat larger at lower temperatures. Nevertheless, the phenomenon of anisotropic magnetoresistance has a significant importance for technical applications, such as magnetic sensors. As illustrated in Fig. 1.1c), if a magnet is attached on a rotating disk, an MR sensor can detect the number of rotations or the speed of motion from the resistance change of the MR sensor. It has also been attempted to

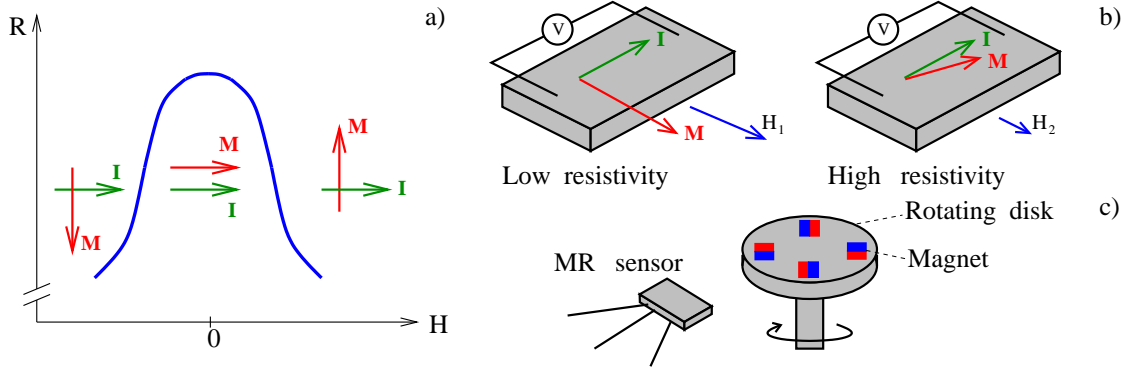


Figure 1.1: Anisotropic magnetoresistance (AMR): a) Resistance as a function of applied field. b) Measurement. V, I, M, H and θ are voltage, current, magnetization, applied field, and the angle between the current and the magnetization. c) Application of AMR sensor. Adapted from Ref. [1]

apply an AMR sensor for a magnetic recording technology, but for ultra-high density recording, a very high sensitivity of reading head is necessary, and thus the high MR ratio is required, which can't be provided by the AMR effect.

Magnetoresistive effects are more pronounced in magnetic layered structures, or magnetic superlattices. They are formed artificially by alternately depositing on a substrate several atomic layers of one element, say, iron, followed by layers of another element, such as chromium. A term Giant Magnetoresistance (GMR) is used to describe the behavior of materials consisting of alternating layers of ferromagnetic and nonmagnetic metals deposited on an insulating substrate. The GMR effect has been observed in 1988 in the resistivity measurements on Fe/Cr multilayers, [2] as shown in Fig. 1.2. At 4.2 K the resistivity of the Fe/Cr multilayer was decreased by almost 50% by applying an external field. At 300 K, the decrease of resistivity reaches 17%, which is significantly larger than MR changes caused by the AMR effect. If θ is the angle between the magnetization directions of the neighboring ferromagnetic layers, the resistance of the system takes the following form:

$$R = R_P + \frac{\Delta R_{GMR}}{2}(1 - \cos \theta), \quad (1.2)$$

where R_P is the resistance of the system when the magnetic moments in the alternating layers are aligned in the same direction, or parallel ($\theta = 0$), and $\Delta R_{GMR} = R_{AP} - R_P$,

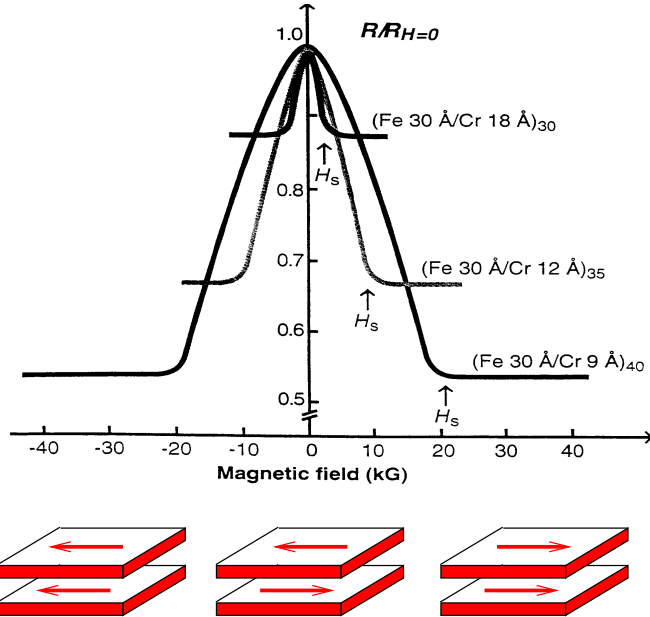


Figure 1.2: Magnetoresistance of three Fe/Cr superlattices at 4.2 K. The current and the applied field are along the same [110] axis in the plane of the layers. Adapted from Ref. [2]

where R_{AP} is the resistance of the system when the magnetic moments of the neighboring layers are oppositely aligned, or antiparallel ($\theta = \pi$). Resistance is the greatest for the antiparallel (AP) configuration of the magnetizations, and smallest for the parallel (P) one (Fig. 1.3). The GMR ratio is defined as $(R_{AP} - R_P)/R_{AP} * 100\%$ or, alternatively, as $(R_{AP} - R_P)/R_P * 100\%$. GMR effects has been obtained in two geometries (Fig. 1.4). In the first one the current is applied in the plane of the layer (Current In Plane, or CIP geometry), while in the second one the current flows perpendicular to the plane of the layers (Current Perpendicular to the Plane, or CPP geometry). The CPP-MR is larger than the CIP-MR, and it exists at much larger thicknesses of the samples.

The mechanism of GMR is attributed to the change of the magnetic structure induced by an external field. The role of external magnetic field is to change the internal magnetic configuration; in cases when it is not possible, the GMR does not appear. It is necessary to separate magnetic regions from one another so as to be able to reorient their magnetization, otherwise layers are too strongly coupled and ordinary fields can

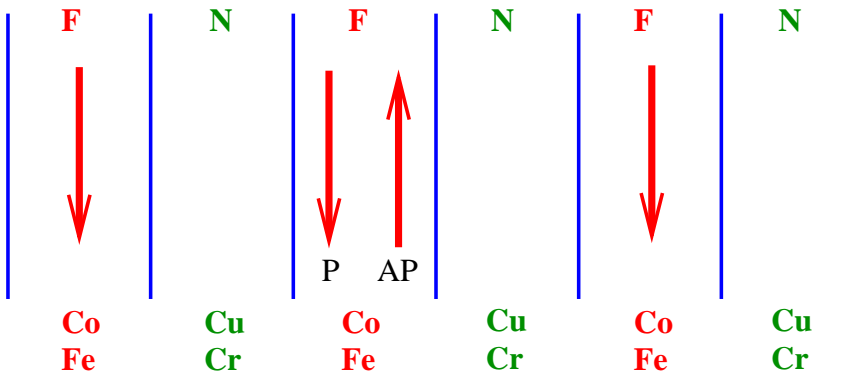


Figure 1.3: Ferromagnetic and antiferromagnetic configuration of a multilayered magnetic metallic structure

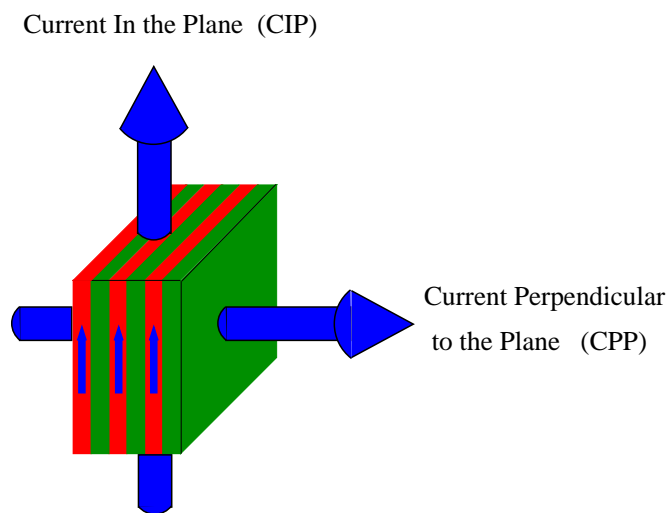


Figure 1.4: Current In Plane of the layers and Current Perpendicular to the Plane of the layers geometries. Adapted from Ref [3]

not rotate magnetic moments in one layer relative to moments in the neighboring layer. The multilayers are designed so that at zero external field the magnetizations of the alternating magnetic layers are aligned opposite to each other. The external magnetic field rotates the magnetization, so that all ferromagnetic layers become aligned in the same direction, and resistance changes. There are several ways to provide the original antiparallel alignment of the neighboring FM layers. The first one involves choosing the metallic interlayer thickness (≈ 1 nm) such that the Ruderman-Kittel-Kasuya-Yoshida (RKKY) coupling between localized moments via the conduction electrons forces the magnetic layers to be antiferromagnetically coupled. The other is to make the successive magnetic layers with different coercivities. Smaller field may switch a layer with the smaller coercivity, while the layer with a bigger one remains in the previous direction; it will rotate at larger field, and there is a range of external fields when the alignment is antiparallel. Finally, a phenomena known as "exchange bias" may be used, when an AF metal in a contact with FM metal pins the magnetization of the later in the direction opposite to the magnetization of the last layer of AF so as to produce zero net magnetization. The second FM layer, separated from the pinned one by the nonmagnetic layer remains free to rotate its magnetization under the influence of the external field.

The primary source of GMR is spin-dependent scattering of conducting electrons, or, more precisely, change in the scattering rate as the magnetic configuration changes by an external magnetic field. In the antiparallel magnetic structure, conduction electrons are much more scattered than in the parallel magnetic structure. Spin-dependent scattering can make a large contribution to the resistivity. In the following section, I will discuss a phenomenon of spin-dependent scattering and its effect on the electron transport.

Similarly to AMR sensors, GMR sensors can also be used to detect rotations and to measure the speed of motion. They have an advantage of the full angular dependence. Whereas for an AMR-type sensor opposite field directions produce the same signal, for a GMR-type sensor parallel and antiparallel magnetization alignments yield different resistivities. High sensitivity of GMR sensors make them attractive as the sensors for magnetic fields, particularly, as read-out heads in hard disk drives in computers. The fact that GMR is mainly an interface effect (see below) allows the sensor to be made thinner, which leads to the improvement of the spatial resolution in read-out. GMR-based hard drives are already being used in computer industry. The magnetic random access memories (MRAMs) based on GMR effect have also been realized, but they are not favorable because of the relatively small resistance of the GMR memory element compared with the current leads connecting it with the processing unit.

Besides metallic multilayer systems, similar phenomena are found in granular sys-

tems where small ferromagnetic clusters are dispersed in non-magnetic matrices. Extremely large MR effect has been found in manganese perovskite oxides and is called the colossal MR (CMR) effect. Another class of structures where high MR ratios has been obtained is the tunneling junctions, where the layers of ferromagnetic metal are separated by a thin insulating barrier; the MR effect in these structures is called tunnel magnetoresistance (TMR).

1.2 Spin-dependent transport in metallic magnetic multilayers and the GMR

The transport in the GMR devices studied to date is *diffusive*. In a macroscopic sample, electron undergoes scattering off a large number of impurities. One is in the regime of diffusive transport when the concentration of impurities requires the averaging of the scattering potential. The averaging leads to the loss of the memory of the electron momentum direction and, hence, to a resistance. The characteristic lengthscale over which electrons retain a memory of their momentum is called the mean free path, λ_{mfp} . Due to the large transverse size of the layered systems, the macroscopic transport equations, such as the Boltzmann equation or diffusion equation, see Sec. 2, can be applied in order to describe electron transport in multilayers, even if the thickness of the layers is of the order or smaller than the mean free path. In the multilayers, the presence of interfaces leads to additional scattering. At the interface between layers of different metals, electrons experience *specular* scattering due to the band mismatch. The direction of the electron momentum changes, but it does so in a predictable and reproducible fashion. Specular scattering at the interface between two metals is treated in detail in Appendix A.3. Roughness of the interfaces leads to an additional, *diffusive* scattering, when the incoming electron unpredictably changes the direction of its momentum, and the information about the electron momentum is lost. Due to the short screening length in metals (typically about 1-3 Å, which is at least an order of magnitude smaller than the layer thicknesses in the structures currently being investigated), a layer by layer treatment of the multilayers is possible, where the macroscopic transport equation is solved in each layer, while the details of the interface scattering are taken into account via the boundary conditions.

In ferromagnetic metals, the transport properties of electrons are *spin-dependent*. This dependency arises from the unbalance of the spin populations at the Fermi level due to the splitting between the up and down spin states (exchange splitting). As illustrated

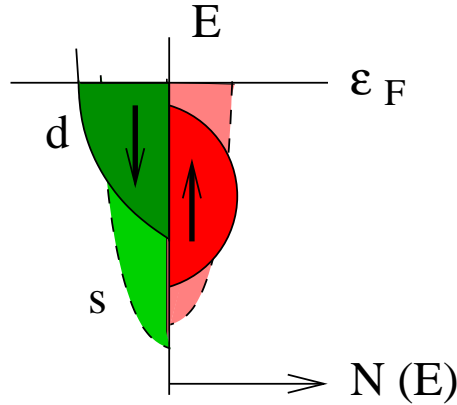


Figure 1.5: Density of states $N(E)$ for up and down s and p electrons for cobalt. ϵ_F is the Fermi energy.

in Fig. 1.5 for cobalt, the majority (spin parallel to the magnetization, or spin-up) d-states are all filled, and the d-electron states at the Fermi level contain entirely minority (spin anti-parallel to the magnetization, or spin-down) electrons. Although there are also s and p electrons at the Fermi level, a significant number of the carriers are the more highly polarized d electrons, which produces a current which is partially spin-polarized. The imbalance of spin-up and spin-down electrons also results in the different probabilities of the s→d transition for majority and minority electrons and consequently in different resistivities.

Spin-dependent scattering occurs both in the bulk of the layers and at the interfaces. In a multilayer, electrons move in the potential which reflects the band mismatch at the interfaces between the magnetic and nonmagnetic layers. The exchange splitting of the up- and down d-bands in the ferromagnetic layers results in different heights of the steps seen by up- and down- conduction electrons (Fig. 1.6a)). In the P configuration, the height of the steps is the same in all layers but different for majority and minority spins. In the AP state, small and large steps alternate for each spin direction. Another contribution to the scattering is due to the presence of impurities in the layers, and due to the roughness at the interfaces. This scattering is also spin-dependent in ferromagnetic metals, and it is stronger for minority electrons (Fig. 1.6b)), resulting in the different resistance in P and AP states and the GMR effect.

A remarkable property of the electron transport in magnetic multilayers is that at low temperatures most of the scattering encountered by the electrons does not flip their

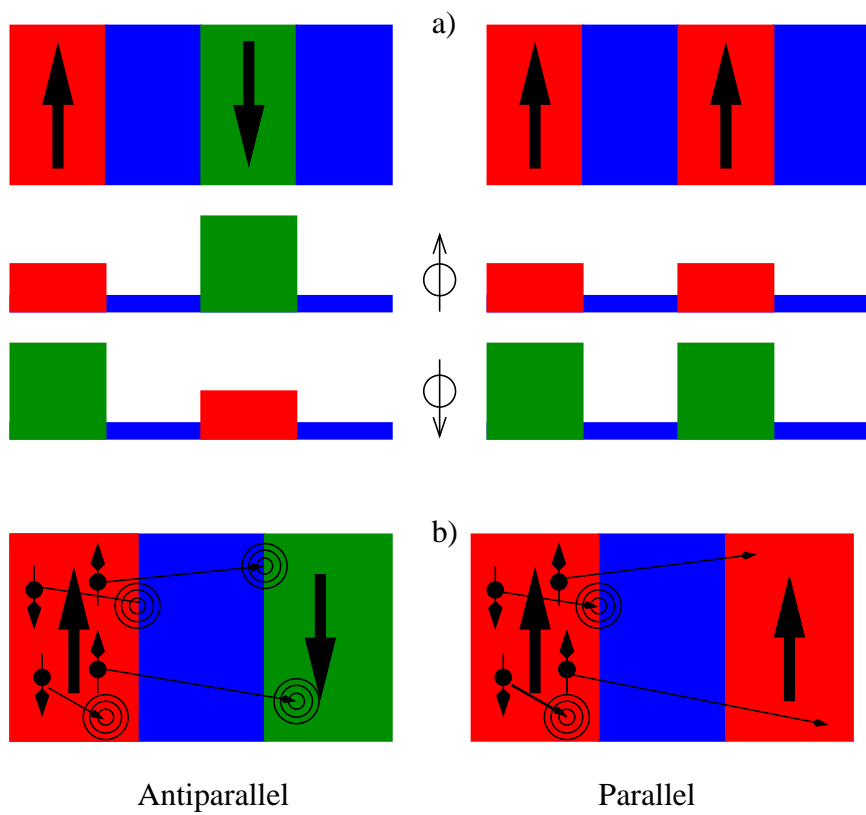


Figure 1.6: a) Spin dependent potentials in a magnetic multilayer for the AP and P configurations for majority and minority electrons. Adapted from Ref. [3]. b) Illustration of spin-dependent electron scattering in GMR multilayers. Adapted from Ref. [4].

spin, as it costs energy. Even though the carrier may undergo many scattering events, the orientation of its spin can be very long-lived. The characteristic time when the electron remembers its spin is the spin-flip time τ_{sf} , and the characteristic length scale is the spin-diffusion length $\lambda_{sdl} = \sqrt{D\tau_{sf}}$, where D is the diffusion constant. The spin-diffusion length is usually of the order of ten times larger than the electron mean-free path. The slow spin relaxation leads to a formation of a steady-state non-equilibrium build-up of magnetic moments, or spin-accumulation, extending over a length λ_{sdl} from the interface between the layers with antiparallel magnetization directions. This magnetization acts as a bottleneck for spin transport across the interface, which in turn hinders the flow of charge and results in the higher resistance in the antiparallel configuration compared with the parallel configuration. [5]

The large spin-diffusion length in ferromagnetic metals means that the current can be considered to be carried by two independent channels of carriers, one for spin-up electrons with a resistivity ρ_{\uparrow} , and the other made of spin-down electrons with a resistivity ρ_{\downarrow} ; this is commonly referred to as the *two current model*. This model allows a simple illustration of how the GMR effect works in CPP structures. If the thickness of the layers is larger than the electron mean free path in the layers, a resistor network analogy is appropriate (Fig. 1.7a)), when the resistivities of each layer for each spin direction are added in series, while those for two channels are added in parallel. Since the resistances of the majority (R_M) and minority (R_m) electrons are different, and $R_M < R_m$, there is a "short-circuit" effect in the parallel configuration, and resistance is smaller in P state than in the AP state, and the GMR effect exists. In the CIP geometry, a simple resistor network analogy yields the same resistances in both P and AP configurations (Fig. 1.7b)), and the absence of the GMR effect. For the CIP-MR to exist, the mean-free-path has to be larger than the thickness of a layer. In this case, electrons, which travel parallel to the interfaces, sample the scattering from different layers, and the current is sensitive to the change of the magnetic configuration of the system. The electron mean-free path is the characteristic length scale for spin-dependent transport in the CIP geometry. In the CPP geometry, where the electric current samples scattering in all layers, the GMR does not depend on λ_{mfp} . The characteristic length scale for the transport in the CPP geometry is the spin-diffusion length λ_{sdl} . Spin-flips limit the distance over which the two spin currents are independent. If the size of a sample is larger than λ_{sdl} , spin-up and spin-down currents are mixed, and the CPP-MR is decreased. In this work, I will only consider the current perpendicular to the plane of the layers geometry.

A CPP-MR model that provides a significant insight into the problem was developed by Valet and Fert. [6] Within this model, the Boltzmann equation, with an additional

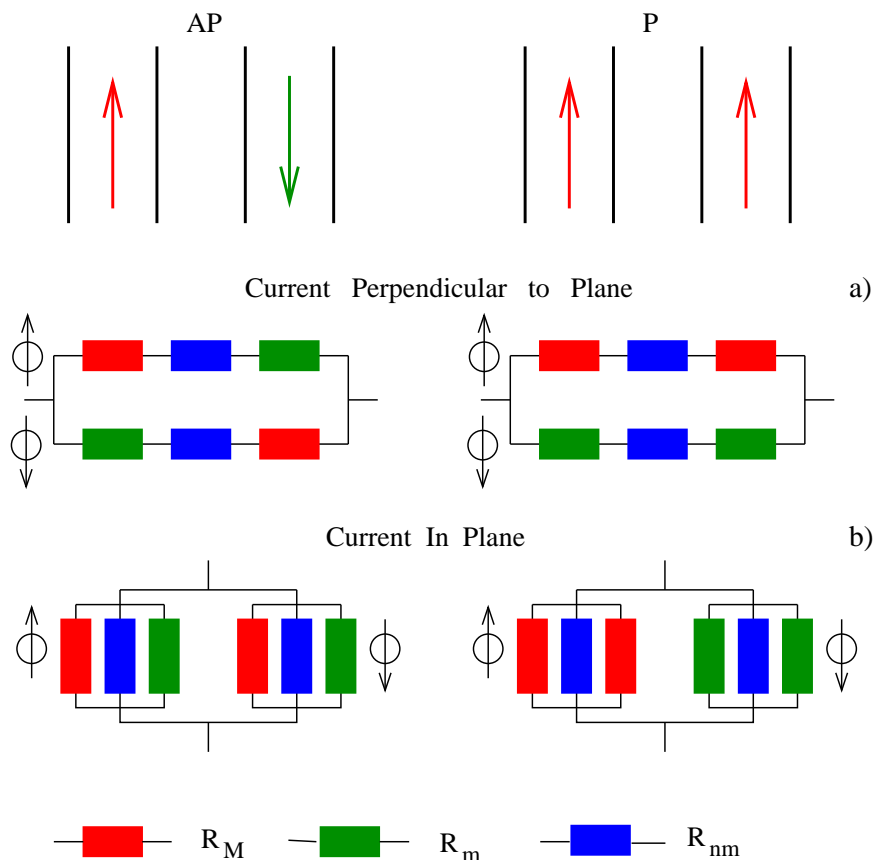


Figure 1.7: Two-current model: resistor network analogy for the CIP and CPP resistances of the ferromagnetic (P) and antiferromagnetic (AP) configurations of the magnetic moments in a multilayer. R_M (red), R_m (green), and R_{nm} (blue) stand for the resistances of the magnetic layers for spin parallel and antiparallel to the local magnetization, and of the non-magnetic layers. Adapted from Ref. [3]

term to account for spin accumulation, is solved at zero temperature. In the case when the mean free path is much smaller than the spin diffusion length, the macroscopic transport equations are obtained that relate the current and the electrochemical potential, so that the resistance of the system can be found. The Valet-Fert model correctly describes the main features of magnetoresistive multilayers, i.e., increase in MR with decreasing temperature, increase with decreasing film thickness and increase with increasing number of layers.

1.3 Current-induced switching

It has been seen from the discussion of the GMR effect that the relative orientation of the magnetic moments of the layers affects the electric current, causing different resistances for different magnetic configurations. The reverse effect, that a spin-polarized current could affect the magnetic moment of a layer, has also been predicted, [7, 8, 9, 10, 11] and experimentally demonstrated. [12, 13, 14] In the perpendicular transport geometry, the spin-polarized currents may transfer angular momentum between the layers, resulting in the current-driven excitations in magnetic multilayers: either reversal of layer magnetization, or generation of spin-waves. [15]

Spin-polarized current exerts a torque on a ferromagnetic layer if that layer's moment is not collinear with the direction of current polarization. The reversal of the magnetization is due to the interaction between the magnetization and the spin accumulation in a direction perpendicular to the magnetization. Fig. 1.8 shows schematically the five-layered structure used to measure current-induced switching, and the directions of the torque acting on the magnetic moment of the thin ferromagnetic layer due to the spin transfer by the current, polarized in the direction of the magnetization of the thick ferromagnetic layer. [12]

The great interest in the phenomenon of the current-driven excitations in magnetic multilayers lies both in trying to understand the underlying physics and in its potential for device use: magnetization reversal for magnetic media and magnetic memories, and spin-wave generation for production of high frequency radiation. In present magnetic devices the moments are reversed via externally generated magnetic fields. The reading/writing processes would be simplified by applying a polarized current through the magnetic layer itself. Practically, though, the magnetization reversal by spin transfer requires high current densities, around 10^7 A/cm², in order to overcome magnetic damping. The current density should be reduced by approximately an order of magnitude so

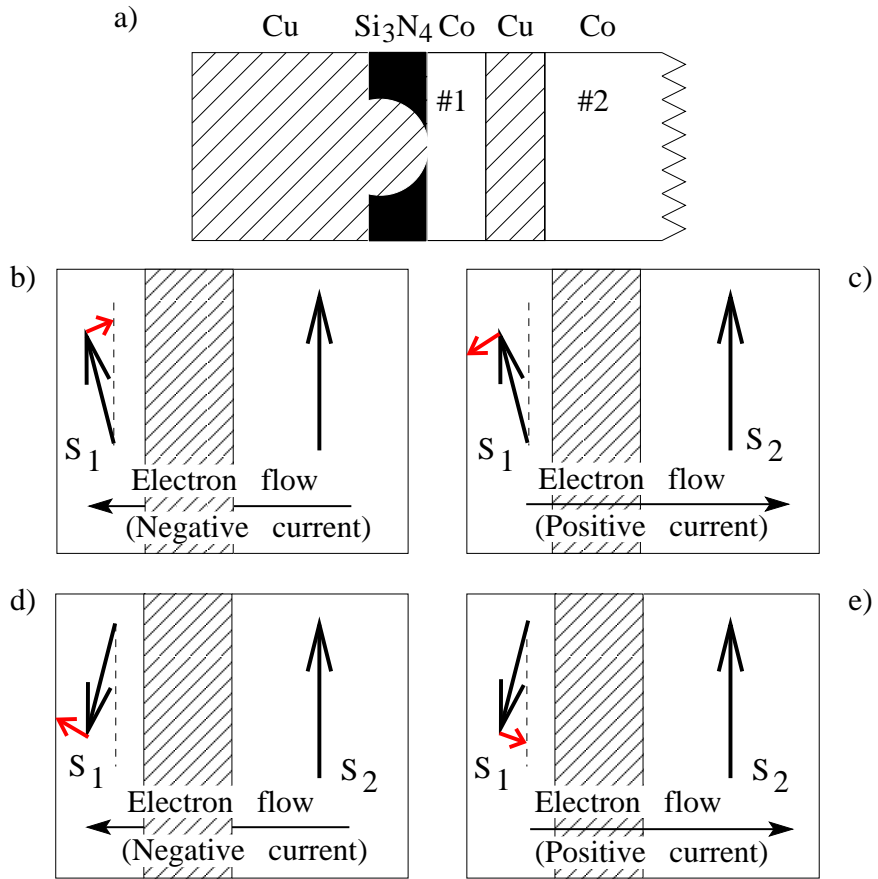


Figure 1.8: a) Schematic representation of the five-layered structure used to measure current-induced switching. The system consists of the thin Co layer of the variable thickness (#1), separated by the 4 nm Cu layer from the the thick (100 nm) Co layer (#2). Another Cu layer contacts the thin Co layer via an opening 5 to 10 nm in diameter in an insulating silicon nitride membrane. b)-e) Directions of torque (red arrows) on the magnetic moments in the thin FM layer due to the spin-polarized current. Adapted from Ref. [12]

that this effect could be considered for applications. [16]

1.4 Problems to be solved

Transport properties of magnetic multilayers in current perpendicular to the plane of the layers geometry are defined by diffusive scattering in the bulk of the layers, and diffusive and ballistic scattering across the interfaces. Electrons scattered at the interfaces may be scattered again in the bulk of the layers, and, in order to better describe transport in the entire structure, the transport in the bulk of the layers and the transport through the interfaces should be treated self-consistently. Embedding the ballistic and diffusive interface scattering in the framework of the diffusive scattering in the bulk of the layers is the unifying idea behind the problems that I address in my work: the problem of finding the interface resistance and the problem of current-induced magnetization switching.

1.4.1 Interface resistance

Chapters 3 and 4 of this work are devoted to the problem of finding resistance due to the interfaces in metallic multilayered structures. The presence of the specular and diffuse scattering at interfaces leads to a finite voltage drop across them, [17, 6, 18, 19] and, hence, to a resistance. An origin of interface resistance, and the procedure of finding a resistance of an interface between two ballistic conductors is discussed in Chap. 2. In the realistic multilayered structure, where transport in the bulk of the layers is diffusive, resistance of the interfaces has to be incorporated into the resistance of the whole system. In order to do that, the resistors-in-series model was developed, and is currently used to analyze experimental data. [20, 21, 22, 23] Within this model, resistance of an interface is treated independently of the resistance of the bulk of the layers, and total resistance of a multilayered system is a sum of the bulk and interface contributions.(Fig. 1.9)

But the assumption that the resistance of the interface and resistance of the bulk are independent is not correct. An electron reflected from the interface can be scattered in the bulk and go back to the interface, not to the reservoir, hence changing the current through the interface. In terms of chemical potentials it means that in addition to an abrupt drop at an interface, there is a gradual change in the chemical potential within a mean-free-path from the interface. [24, 25, 26, 27, 28, 29] Fig. 1.10 shows schematically a chemical potential profile at an interface between two semi-infinite metallic layers. In Fig. 1.10, as well as in the all following pictures of chemical potentials, only the

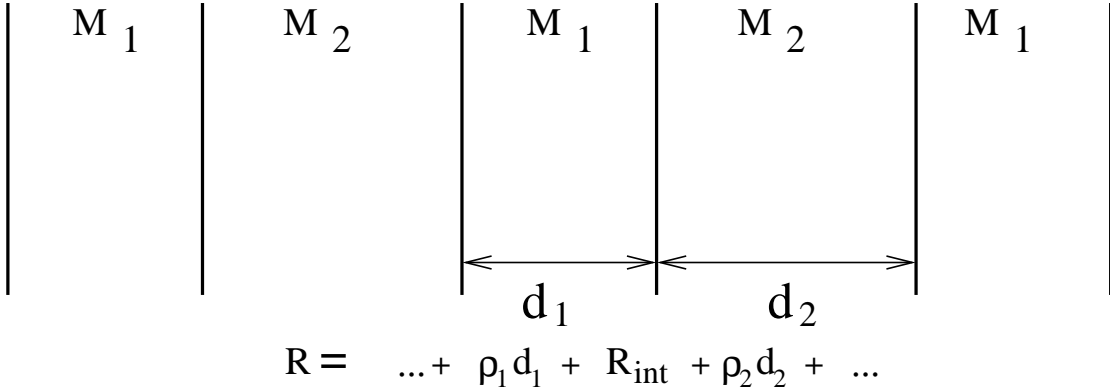


Figure 1.9: Resistors-in-series model. ρ_1 and ρ_2 are resistivities of the metallic layers M_1 and M_2 , d_1 and d_2 are thicknesses of M_1 and M_2 , R_{int} is a resistance of the interface between M_1 and M_2 .

potential drop due to the scattering from the interface is shown; the drop due to the resistivity of the adjacent layers is not shown. The resistance measured far from the interface, R_1 , is different from the one that would be measured in its immediate vicinity, R_0 . In the multilayers with layer thicknesses of the order of electron mean-free path, the chemical potential doesn't reach its asymptotic value within a layer. This leads to a breakdown of the resistors-in-series model. While the resistance of the whole system is still found by adding resistances due to the bulk of the layers and resistances due to the interfaces, interface resistances are not independent of the properties of the bulk of the layers, in particular, of the ratio of the layer thickness to the electron mean-free path in this layer.

In order to determine the contribution of the interfaces to the resistance of the whole multilayered structure with layer thicknesses of the order or less the electron mean-free path, the form of chemical potential everywhere in the system has to be considered, and there was no such study for the systems with both specular and diffuse scattering at interfaces. In Ref.[25] the variation of the chemical potential was studied, however without examining how diffuse scattering at the interface altered its pattern, while in Ref. [30] the interface resistance R_1 (their $R_{A/B}$) coming from the specular reflection at the interface together with diffuse scattering in the bulk of the layers is calculated far from the interface. More recently the change of interface resistance $R_{A/B}$ with diffuse scattering at the interface was calculated in Ref. [31], however only far from the interface. Contrary to the works [25, 30, 31], where ab-initio calculations of the interface

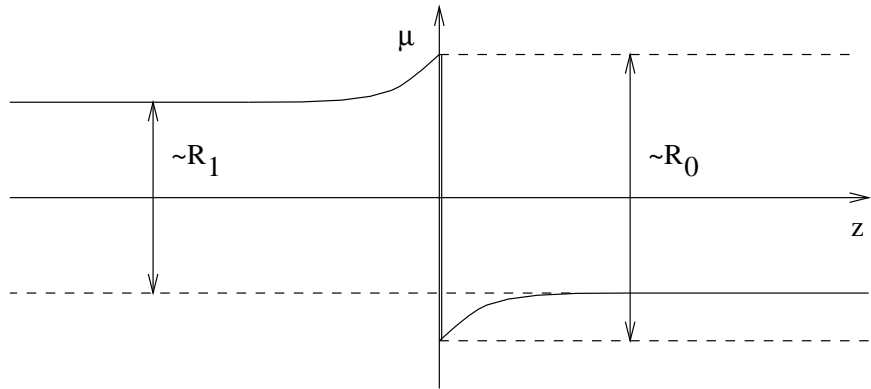


Figure 1.10: Chemical potential profile in two semi-infinite metallic layers. Only the potential drop due to the scattering from the interface is shown; the drop due to the resistivity of the adjacent layers is not shown. R_0 is the resistance measured directly at the interface; R_1 is the resistance measured far from the interface.

resistance due to specular reflections at interfaces are performed, simple free-electron model for reflections at the interfaces is used in this work. In Chap. 3, a procedure allowing one to find a chemical potential profile everywhere in the multilayered structure in CPP geometry, including the close vicinity of the interfaces, and take into account both specular and diffuse scattering at the interfaces will be developed. [32] Results of the calculation of the resistances due to the interfaces in various systems will be presented in Chap. 4.

1.4.2 Current-induced magnetization switching

Chapters 5 and 6 of this work are devoted to the problem of the magnetization switching that is driven by spin-polarized current in noncollinear magnetic multilayers. It is known that the transfer of spin angular momenta between current carriers and local moments occurs near the interface of magnetic layers when their moments are non-collinear. The specular scattering of the current at interfaces between magnetic and nonmagnetic layers that is attendant to ballistic transmission can create spin torque. [7, 8, 9, 10, 11, 33, 34, 35] However, to determine the magnitude of the transfer, one should calculate the spin transport properties far beyond the interface regions. [36] In this work, I consider the effect that the diffuse scattering in the bulk of the magnetic layers and the diffuse scattering at interfaces have on the spin-torque; the spin transfer that occurs at interfaces

is self-consistently determined by embedding it in the globally diffusive transport calculations. [37] The ballistic component of transport can be accommodated within the formalism described below, but this requires the knowledge of the band structure in the layers and is outside the scope of this study. [38]

A model system to calculate the spin torque is a magnetic multilayer whose essential elements consist of a thick magnetic layer, whose primary role is to polarize the current, a thin magnetic layer that is to be switched, a nonmagnetic spacer layer so that there is no interlayer exchange coupling between the thick and thin layers, and a nonmagnetic layer or lead on back of the thin magnetic layer; see Fig. 1.11. The transport in the multilayer is considered as a diffusive process, and the interfaces are taken into account via the boundary conditions. In order to discuss the angular momentum transfer between the spin-polarized current and the magnetic background, one has to consider the exchange interaction between the accumulation and the background, or "sd" interaction, described by the Hamiltonian operator $H_{int} = -J\mathbf{m} \cdot \mathbf{M}_d$. The term $(J/\hbar)\mathbf{m} \times \mathbf{M}_d$ can be shown to exist in the equation of motion of the spin-accumulation by considering the quantum Boltzmann equation for the distribution function which takes the spin of an electron into account. [39] It describes a deterministic or ballistic precession of the accumulation due to the "sd" interaction when the magnetization directions of the spin-accumulation and the local moments are not parallel. The exchange coupling parameter J is the difference between the energies of the spin-up and spin-down electrons for each particular value of the electron momentum, $J(k) = \epsilon_{\uparrow}(k) - \epsilon_{\downarrow}(k)$ (see Fig. 1.12), averaged over the Fermi surface. The value of J can be obtained from the band structure calculations. For cobalt, I use the value of $J = 0.3$ eV. [40] For permalloy, J has been directly measured to be about 0.1 eV. [41]

The exchange interaction leads to the appearance of the component of the spin accumulation transverse to the local magnetization direction. The transverse spin accumulation produces two effects simultaneously: one is to create a magnetic "effective field" acting on a local magnetization in the layer, and the other, the "spin torque", is to increase or decrease the angle between the magnetizations in the ferromagnetic layers. Contrary to the previous treatments, [7, 8, 9, 10, 11] both these effects enter the equation of motion for the local magnetization (the Landau-Lifshitz-Gilbert equation, Eq. (5.8)) on an equal footing.

One of the consequences of the global approach to evaluate the effect the polarized current has on the background magnetization is that due to the presence of the long longitudinal spin diffusion length, longitudinal and transverse components (to the local magnetization direction) of spin accumulations are intertwined from one layer to the

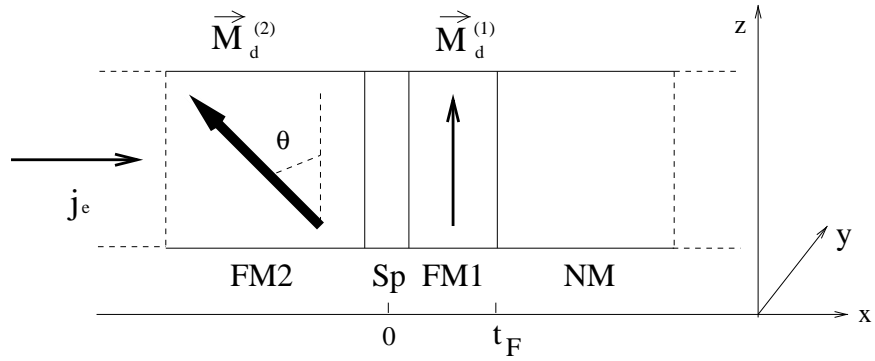


Figure 1.11: Multilayered pillar-like structure used for current induced reversal of a magnetic layer. FM2 is a thick ferromagnetic layer with the thickness exceeding λ_{sd}^F and local magnetization $\mathbf{M}_d^{(2)} = \cos \theta \mathbf{e}_z - \sin \theta \mathbf{e}_y$, Sp is a thin nonmagnetic spacer, FM1 is a thin ferromagnetic layer with the thickness t_F and local magnetization $\mathbf{M}_d^{(1)} = \mathbf{e}_z$, and NM is a nonmagnetic back layer.

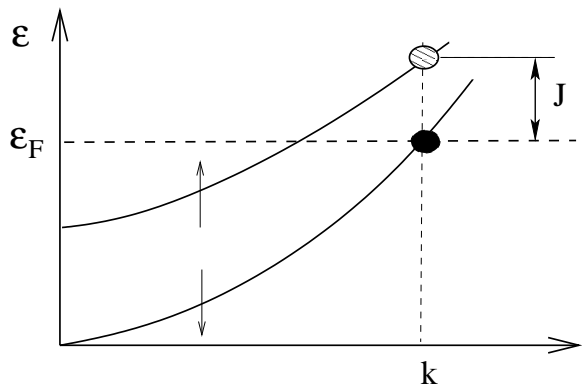


Figure 1.12: Exchange splitting

next. As will be shown in Chap. 6, this leads to a large amplification of the spin torque acting on the free ferromagnetic layer. The angular momentum transferred to a thin layer *far exceeds* the transverse component (to the orientation of the magnetization of the free layer) of the bare portion of the incoming spin polarized current, i.e., the part proportional to the electric field. This, in turn, may lead to the reduction of the critical current necessary to switch spintronics devices (see Sec. 1.3).[16]

The transfer of angular momentum from the polarized current has an effect on the voltage drop across the multilayer being studied. [7] The experimental data on several multilayered structures has confirmed that there are corrections to the simple $\cos^2(\theta/2)$ dependence of the CPP resistance, where θ is the angle between the magnetization directions in the magnetic layers. [42, 43] The formalism described in this work allows to evaluate these corrections.

In Chap. 5, I will present a spin transfer model in which the equation of motion of the spin accumulation (essentially a spin-diffusion equation) is solved in order to describe the effect of the spin-polarized current on the background magnetization. Based on this equation, a simplified system of two thick magnetic layers separated by a non-magnetic spacer, and, in Chap. 6, a realistic multilayered structure depicted in Fig. 1.11 will be studied.

Chapter 2

Description of transport in multilayers

In this chapter, the different formalisms for calculating electrical transport in solids will be reviewed. There are three most widely used ways to describe transport - semiclassical Boltzmann equation approach, Landauer formalism, and Kubo approach.

The semi-classical Boltzmann equation approach combines Newton's law with a probabilistic description of random scattering forces. It can be used to describe transport in the systems where the quantum interference effects do not play a significant role, i.e., the electron mean-free path is large compared to the lattice constant, and small relative to the macroscopic dimensions of the system. The Boltzmann equation approach gives conductivity in terms of classical parameters of electrons - velocity, mean-free path, density. This formalism will be discussed in Sec. 2.1 below in detail as it is the main tool used to obtain results in the present work.

In the Landauer approach, [44, 45] current flow can be viewed as a consequence of the injection of carriers at contacts of a sample, and their probability of reaching the other end. In this approach, a current through a conductor, and conductivity, are expressed in terms of scattering properties of the system, or in terms of the probability that an electron can transmit through a conductor. [46, 47] The Landauer formula for the conductance of a localized scatterer (an interface between two metallic layers, for example) will be derived and discussed below in Sec. 2.2.

The Kubo formalism is a method of calculating the response of a many-particle system to an external potential, for instance, the electrical current in response to an electric field. The external field is treated as a small perturbation on the equilibrium state of the system, eliciting a linear response, whose magnitude measures the corresponding transport coefficient, which is given in terms of the equilibrium properties of the system,

i.e., in zero field. The electrical conductivity tensor for example, may be expressed abstractly by the Kubo formula:[48]

$$\sigma_{\mu\nu} = \frac{1}{kT} \int_0^\infty \langle j_\mu(t) j_\nu(0) \rangle dt.$$

The conductivity depends on the time correlation between a component of the current operator $j_\nu(0)$ at time zero and the component $j_\mu(t)$ at some later time t , integrated over all time and evaluated as the average of the expectation value of the product over the equilibrium ensemble. The direct application of the Kubo formulas can be cumbersome, but they provide an exact basis for various theorems involving the transport coefficients. Fortunately, all three approaches - Boltzmann equation, Kubo, and Lan-dauer (for electrical conductivity) - can be shown to be equivalent, and yield the same results for transport coefficients in some limits. [47]

2.1 Boltzmann equation

The Boltzmann approach assumes the existence of a distribution function $f(\mathbf{k}, \mathbf{r})$, which is a local concentration of carriers in the state \mathbf{k} in the neighborhood d^3r of the point \mathbf{r} in space. The total number of the carriers in the small volume $d^3r d\mathbf{k}$ of the phase space is

$$2 \times (\# \text{ of the allowed } \mathbf{k} \text{ states per unit volume in the momentum space}) \\ \times d\mathbf{k} \times f(\mathbf{k}, \mathbf{r}) d^3r,$$

where the factor of 2 enters because of the spin degeneracy. The number of allowed states per unit volume $d\mathbf{k}$ is inverse of the volume occupied by one state in the momentum space. As follows from the Schrödinger equation for a free electron with periodic boundary conditions in the $L_x \times L_y \times L_z$ box, the allowed \mathbf{k} -states are spaced within $2\pi/L_i$ in each direction, so that the volume in the \mathbf{k} -state per one state is $(2\pi)^3/V$. The total number of carriers in the phase volume $d^3r d\mathbf{k}$ is

$$dN = 2f(\mathbf{k}, \mathbf{r}) \frac{d^3r}{(2\pi)^3} d\mathbf{k}. \quad (2.1)$$

The distribution function can change due to the diffusion of the carriers, under the influence of the external fields, and due to scattering. The Boltzmann equation states

that in a steady state at any point, and for any value of \mathbf{k} , the net rate of change of $f(\mathbf{k}, \mathbf{r})$ is zero, i.e.

$$\left(\frac{\partial f(\mathbf{k}, \mathbf{r})}{\partial t} \right)_{scatt} + \left(\frac{\partial f(\mathbf{k}, \mathbf{r})}{\partial t} \right)_{field} + \left(\frac{\partial f(\mathbf{k}, \mathbf{r})}{\partial t} \right)_{diff} = 0.$$

The rate of the change of the distribution function due to diffusion (the motion of the carriers in and out of the region \mathbf{r}) can be found as follows. Suppose that \mathbf{v}_k is the velocity of a carrier in state k . Then, in an interval t , the carriers in this state move a distance $\mathbf{v}_k t$. Since the volume occupied by particles in phase space remains invariant (Liouville's theorem), the number of carriers in the neighborhood of \mathbf{r} at time t is equal to the number of carriers in the neighborhood of $\mathbf{r} - \mathbf{v}_k t$ at time 0:

$$f(\mathbf{k}, \mathbf{r}, t) = f(\mathbf{k}, \mathbf{r} - \mathbf{v}_k t, 0).$$

This means that the rate of the change of the distribution function due to diffusion is

$$\left(\frac{\partial f(\mathbf{k}, \mathbf{r})}{\partial t} \right)_{diff} = -\mathbf{v}_k \cdot \frac{\partial f(\mathbf{k}, \mathbf{r})}{\partial \mathbf{r}} = -\mathbf{v}_k \cdot \nabla_{\mathbf{r}} f(\mathbf{k}, \mathbf{r}). \quad (2.2)$$

External fields change the \mathbf{k} -vector of each carrier, according to Newton's law, at the rate

$$\dot{\mathbf{k}} = \frac{\mathbf{F}}{\hbar},$$

where \mathbf{F} is the force acting on the carriers due to, for example, an electric field \mathbf{E} , so that $\mathbf{F} = e\mathbf{E}$. According to Liouville's theorem in \mathbf{k} -space, one can write

$$f(\mathbf{k}, \mathbf{r}, t) = f(\mathbf{k} - \dot{\mathbf{k}}t, \mathbf{r}, 0),$$

so that the rate of the distribution function change due to the external fields is

$$\left(\frac{\partial f(\mathbf{k}, \mathbf{r})}{\partial t} \right)_{field} = -\dot{\mathbf{k}} \cdot \frac{\partial f(\mathbf{k}, \mathbf{r})}{\partial \mathbf{k}} = -\frac{e}{\hbar} \mathbf{E} \cdot \nabla_{\mathbf{k}} f(\mathbf{k}, \mathbf{r}). \quad (2.3)$$

The rate of change of $f(\mathbf{k}, \mathbf{r})$ due to scattering is

$$\left(\frac{\partial f(\mathbf{k}, \mathbf{r})}{\partial t} \right)_{scatt} = \int [f(\mathbf{k}', \mathbf{r})(1 - f(\mathbf{k}, \mathbf{r}))P_{\mathbf{k}', \mathbf{k}} - f(\mathbf{k}, \mathbf{r})(1 - f(\mathbf{k}', \mathbf{r}))P_{\mathbf{k}, \mathbf{k}'}] d\mathbf{k}'. \quad (2.4)$$

The process of scattering from \mathbf{k} to \mathbf{k}' decreases $f(\mathbf{k}, \mathbf{r})$. The probability of this process is proportional to the number of carriers in the initial state \mathbf{k} , $f(\mathbf{k}, \mathbf{r})$, and to the number of vacancies in the final state \mathbf{k}' , $1 - f(\mathbf{k}', \mathbf{r})$. It is also proportional to the scattering probability $P_{\mathbf{k}, \mathbf{k}'}$, which measures the rate of transition between the states \mathbf{k} and \mathbf{k}' if the state \mathbf{k} is known to be occupied and the state \mathbf{k}' is known to be empty. There is also the inverse process, the scattering from \mathbf{k}' into \mathbf{k} , which increases $f(\mathbf{k}, \mathbf{r})$. Its probability is proportional to $f(\mathbf{k}', \mathbf{r})(1 - f(\mathbf{k}, \mathbf{r}))$. The transition rate from \mathbf{k}' into \mathbf{k} is $P_{\mathbf{k}', \mathbf{k}}$. The summation over all possible \mathbf{k}' states has to be performed.

Combining the equations (2.2), (2.3), and (2.4), one obtains the Boltzmann equation for the distribution function:

$$\mathbf{v}_\mathbf{k} \cdot \nabla_{\mathbf{r}} f(\mathbf{k}, \mathbf{r}) + \frac{e}{\hbar} \mathbf{E} \cdot \nabla_{\mathbf{k}} f(\mathbf{k}, \mathbf{r}) = \int [f(\mathbf{k}', \mathbf{r})(1 - f(\mathbf{k}, \mathbf{r}))P_{\mathbf{k}', \mathbf{k}} - f(\mathbf{k}, \mathbf{r})(1 - f(\mathbf{k}', \mathbf{r}))P_{\mathbf{k}, \mathbf{k}'}] d\mathbf{k}' \quad (2.5)$$

In this form, the Boltzmann equation is a nonlinear integrodifferential equation. In general, $P_{\mathbf{k}, \mathbf{k}'}$ may depend on the distribution function $f(\mathbf{k}, \mathbf{r})$, and on the distribution of the scatterers. The nonlinearity may be removed provided that the principle of microscopic reversibility is valid, or the symmetry $P_{\mathbf{k}, \mathbf{k}'} = P_{\mathbf{k}', \mathbf{k}}$ exist. This is usually the case if the crystal and scattering potentials are real and invariant under spatial inversion. [49] If the scatterers are sufficiently dilute and the potential describing the interaction between a carrier and a scatterer is sufficiently weak, $P_{\mathbf{k}, \mathbf{k}'}$ is independent of the distribution function $f(\mathbf{k}, \mathbf{r})$.

The Boltzmann equation may be simplified to a linear partial differential equation by the relaxation-time approximation. This approximation assumes that there exist a relaxation time τ such that an electron experiences a collision in an infinitesimal time interval dt with probability dt/τ . In general, the collision rate $1/\tau$ may depend on the position and the momentum of the electron: $\tau = \tau(\mathbf{k}, \mathbf{r})$. The additional assumptions are necessary to express the fact that collisions drive the electronic system toward local equilibrium. First, the distribution of electrons emerging from collisions at any time is assumed not to depend on the structure of the nonequilibrium distribution function $f(\mathbf{r}, \mathbf{k}, t)$ just prior to collision. Second, if the electrons in a region about \mathbf{r} have the equilibrium distribution function

$$f(\mathbf{r}, \mathbf{k}, t) = f^0(\mathbf{r}, \epsilon) = \frac{1}{e^{\frac{\epsilon(\mathbf{k}) - \mu(\mathbf{r})}{k_B T(\mathbf{r})}} + 1}, \quad (2.6)$$

where both the chemical potential μ and the temperature T may depend on the coordinate, the collisions will not alter the form of the distribution function. [50] Assuming a uniform temperature distribution in space, the equilibrium distribution function takes the following form:

$$f(\mathbf{r}, \mathbf{k}, t) = f^0(\epsilon) = \frac{1}{e^{\frac{\epsilon - \epsilon_F}{k_B T}} + 1}, \quad (2.7)$$

where ϵ_F is an electron Fermi energy.

It can be shown [49] that in the relaxation-time approximation the collision term in the Boltzmann equation simplifies to

$$\left(\frac{\partial f(\mathbf{k}, \mathbf{r})}{\partial t} \right)_{scatt} = -\frac{f(\mathbf{k}, \mathbf{r}) - f^0(\epsilon)}{\tau(\mathbf{k}, \mathbf{r})}.$$

This form of the scattering term reflects the fact that the role of the collisions is to bring the system to an equilibrium. The Boltzmann equation in the relaxation-time approximation takes the form

$$\mathbf{v}_k \cdot \nabla_{\mathbf{r}} f(\mathbf{k}, \mathbf{r}) + \frac{e}{\hbar} \mathbf{E} \cdot \nabla_{\mathbf{k}} f(\mathbf{k}, \mathbf{r}) = -\frac{f(\mathbf{k}, \mathbf{r}) - f^0(\epsilon)}{\tau(\mathbf{k}, \mathbf{r})}. \quad (2.8)$$

The relaxation-time approximation provides the same description as the full Boltzmann equation if it is applied to spatially homogeneous disturbances in an isotropic metal with isotropic elastic scattering. [49] In this case, the relaxation time is defined as

$$\frac{1}{\tau(\mathbf{k})} = \int P_{\mathbf{k}, \mathbf{k}'} (1 - \hat{\mathbf{k}} \cdot \hat{\mathbf{k}'}) d\mathbf{k}'.$$

This relaxation time is called the transport relaxation time.

Within the relaxation-time approximation, the Boltzmann equation (2.8) may be solved, and the electrical conductivity, which is the proportionality constant between the electrical current and the field, $\mathbf{j} = \sigma \mathbf{E}$, may be found. In the homogeneous medium kept at constant temperature, the terms proportional to the spacial gradient ∇ are equal to zero, and the distribution function $f(\mathbf{r}, \mathbf{k})$ turns out to be

$$f(\mathbf{k}) = f^0(\epsilon(\mathbf{k})) - \frac{\partial f^0(\epsilon)}{\partial \epsilon} \tau(\mathbf{k}) \mathbf{v}_k \cdot e \mathbf{E}. \quad (2.9)$$

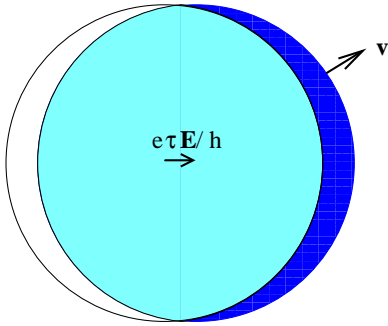


Figure 2.1: Displacement of the Fermi surface in the momentum space under the influence of the electric field

This equation may be written as

$$f(\mathbf{k}, \mathbf{r}) = f^0(\epsilon(\mathbf{k})) - \frac{\partial f^0(\mathbf{k})}{\partial \epsilon(\mathbf{k})} \frac{\partial \epsilon(\mathbf{k})}{\partial \mathbf{k}} \cdot \frac{e\tau(\mathbf{k})}{\hbar} \mathbf{E} = f^0(\epsilon(\mathbf{k}) - \frac{e\tau(\mathbf{k})}{\hbar} \mathbf{E}).$$

Assuming that the electron relaxation time does not depend on its momentum, $\tau(\mathbf{k}) = \tau$, it looks as if the whole Fermi surface had been shifted by the amount $(e\tau/\hbar)\mathbf{E}$ in \mathbf{k} -space (Fig 2.1). But, in fact, only the electrons close to the surface of the Fermi sphere have moved, the ones near the bottom of the conductivity band, deep within the Fermi sphere, are not really affected by the field. One can say that only the electrons with energies close to the Fermi energy, and, hence, the velocities close to the Fermi velocity participate in transport. The conductivity of a metal depends only on the properties of the electrons at the Fermi level, not on the properties of all electrons in the metal.

The electrical current density j is defined as

$$\mathbf{j} = e \int \mathbf{v} f(\mathbf{v}, \mathbf{r}) d\mathbf{v}, \quad (2.10)$$

where $f(\mathbf{v}, \mathbf{r})$ is the density of the carriers in the (\mathbf{r}, \mathbf{v}) space, so that the number of electrons in the volume $d^3 r d\mathbf{v}$ is

$$dN = f(\mathbf{v}, \mathbf{r}) d^3 r d\mathbf{v}.$$

Comparing this expression with the equation (2.1), the following relationship between

$f(\mathbf{v}, \mathbf{r})$ and $f(\mathbf{k}, \mathbf{r})$ may be obtained:

$$f(\mathbf{v}, \mathbf{r}) = \frac{1}{4\pi^3} \left(\frac{m}{\hbar}\right)^3 f(\mathbf{k}, \mathbf{r}), \quad (2.11)$$

where m is the electron mass, and the relation $m\mathbf{v} = \hbar\mathbf{k}$ is used. Considering the case where both \mathbf{j} and \mathbf{E} are in the x -direction, the relaxation time τ is independent of the momentum, and substituting $f(\mathbf{k}, \mathbf{r})$ from the equation (2.9), one obtains the following expression for the conductivity:

$$\sigma = \frac{1}{4\pi^3} \frac{e^2 \tau}{3} \left(\frac{m}{\hbar}\right)^3 \int \left(-\frac{\partial f(\epsilon)}{\partial \epsilon}\right) v^2 d^3 v, \quad (2.12)$$

where the fact that $\int \mathbf{v}_k f^0(\epsilon(\mathbf{k})) d\mathbf{v} = 0$ is used, since $f^0(\epsilon(\mathbf{k}))$ is isotropic in \mathbf{k} . The factor $1/3$ appears in the expression since v_x^2 has been averaged over the Fermi surface, so that $v_x^2 = \frac{1}{3}v^2$. In a metal for the temperature close to 0°K , the function $(-\partial f^0(\epsilon)/\partial \epsilon)$ behaves like a delta-function at the Fermi level, $\delta(\epsilon - \epsilon_F)$, and the expression for the conductivity (2.12) reduces to

$$\sigma = \frac{k_F^3}{3\pi^2} \frac{e^2 \tau}{m} = \frac{n e^2 \tau}{m}, \quad (2.13)$$

where $n = k_F^3/3\pi^2$ is the electron density, and m is the electron mass. Strictly speaking, the above expression for the electrical conductivity is only valid for free electrons. The free-electron description of a metal will be used throughout this work, so the equation (2.13) will be used to calculate the conductivity.

An alternative form of the scattering term in the Boltzmann equation may be obtained as follows. Assuming the rate of transition between the states \mathbf{k} and \mathbf{k}' to be independent of \mathbf{k} and \mathbf{k}' , $P_{\mathbf{k}, \mathbf{k}'} = P_0$, the scattering term Eq. (2.4) may be written as

$$\left(\frac{\partial f}{\partial t}\right)_{scatt} = -\frac{f(\mathbf{r}, \mathbf{k}) - \bar{f}(\mathbf{r})}{\tau},$$

where

$$\begin{aligned} \frac{1}{\tau} &= \int P_0 d\mathbf{k}, \\ \bar{f}(\mathbf{r}) &= \frac{1}{4\pi} \int_{FS} f(\mathbf{r}, \mathbf{k}) d\mathbf{k}. \end{aligned} \quad (2.14)$$

The linearized Boltzmann equation then takes the form

$$ev_{\mathbf{k}} \cdot \mathbf{E} \frac{\partial f^0}{\partial \epsilon} + v_{\mathbf{k}} \cdot \nabla f(\mathbf{r}, \mathbf{k}) = -\frac{f(\mathbf{r}, \mathbf{k}) - \bar{f}(\mathbf{r})}{\tau}. \quad (2.15)$$

Introducing $g(\mathbf{r}, \mathbf{k})$ such that $f(\mathbf{r}, \mathbf{k}) = f^0(\epsilon(\mathbf{k})) - \frac{\partial f^0}{\partial \epsilon} g(\mathbf{r}, \mathbf{k})$, the function $\bar{f}(\mathbf{r})$ may be written as

$$\bar{f}(\mathbf{r}) = f^0(\epsilon(\mathbf{k})) - \frac{\partial f^0}{\partial \epsilon} \frac{1}{4\pi} \int_{FS} g(\mathbf{r}, \mathbf{k}) d\mathbf{k}, \quad (2.16)$$

and the equation for the function $g(\mathbf{r}, \mathbf{k})$ takes the form

$$v_{\mathbf{k}} \cdot \nabla g(\mathbf{r}, \mathbf{k}) + \frac{g(\mathbf{r}, \mathbf{k})}{\tau} = ev_{\mathbf{k}} \cdot \mathbf{E} + \frac{\mu(\mathbf{r})}{\tau}, \quad (2.17)$$

where $\mu(\mathbf{r})$ is defined as

$$\mu(\mathbf{r}) = \frac{1}{4\pi} \int_{FS} g(\mathbf{r}, \mathbf{k}) d\mathbf{k}, \quad (2.18)$$

so that $g(\mathbf{r}, \mathbf{k})$ may be written as

$$g(\mathbf{r}, \mathbf{k}) = \mu(\mathbf{r}) + \tilde{g}(\mathbf{r}, \mathbf{k}),$$

where

$$\int_{FS} \tilde{g}(\mathbf{r}, \mathbf{k}) d\mathbf{k} = 0. \quad (2.19)$$

The function $\mu(\mathbf{r})$ defined in Eq. (2.18) is the non-equilibrium part of the chemical potential, since the distribution function $f(\mathbf{r}, \mathbf{k})$ may be written as

$$f(\mathbf{r}, \mathbf{k}) = f^0(\epsilon(\mathbf{k})) - \frac{\partial f^0}{\partial \epsilon} \mu(\mathbf{r}, \mathbf{k}) - \frac{\partial f^0}{\partial \epsilon} \tilde{g}(\mathbf{r}, \mathbf{k}) \approx \frac{1}{e^{\frac{\epsilon(\mathbf{k}) - (\epsilon_F + \mu(\mathbf{r}))}{k_B T(\mathbf{r})}} + 1} - \frac{\partial f^0}{\partial \epsilon} \tilde{g}(\mathbf{r}, \mathbf{k}) \quad (2.20)$$

Equations (2.17) and (2.18) are the starting point of Chap. 3, where the equations for the chemical potential profile in the multilayered metallic structures are derived.

To conclude the discussion of the Boltzmann approach to the electrical transport in solids, the diffusion equation on the concentration of carriers will be derived below. The *non-stationary* linearized Boltzmann equation takes the following form:

$$\frac{\partial f(x, \mathbf{k}, t)}{\partial t} + v_x \frac{\partial f(x, \mathbf{k}, t)}{\partial x} - e \frac{\partial f^0(x, \epsilon)}{\partial \epsilon} E_x v_x = -\frac{f(x, \mathbf{k}, t) - \bar{f}(x)}{\tau}, \quad (2.21)$$

where, for simplicity, electrical field is assumed to have only one component, E_x , and spacial gradient in x -direction only is considered. Integrating Eq. (2.21) over all \mathbf{v} -space, and using the definitions of the concentration and current density

$$n(\mathbf{r}, t) = \int f(\mathbf{r}, \mathbf{v}, t) d\mathbf{v}, \quad (2.22)$$

and

$$\mathbf{j} = e \int \mathbf{v} f(\mathbf{r}, \mathbf{v}, t) d\mathbf{v}, \quad (2.23)$$

where m is the electron mass, the continuity equation

$$\frac{\partial n(x, t)}{\partial t} + \frac{1}{e} \frac{\partial j_x(x, t)}{\partial x} = 0 \quad (2.24)$$

may be obtained. The term proportional to $\int v_x (\partial \bar{f} / \partial \epsilon) d\mathbf{v}$ can be shown to be zero, and the term proportional to $\int (f - \bar{f}) d\mathbf{v}$ is zero due to the condition (2.19). Multiplying the Boltzmann equation (2.21) by v_x and integrating over all \mathbf{v} -space again, the following equation is obtained:

$$\begin{aligned} \frac{1}{e} \frac{\partial j_x(x, t)}{\partial t} + \int v_x^2 \frac{\partial f(x, \mathbf{v}, t)}{\partial x} d\mathbf{v} &- \frac{1}{4\pi^3} \left(\frac{m}{\hbar} \right)^3 e E_x \int v_x^2 \frac{\partial f^0(x, \epsilon)}{\partial \epsilon} d\mathbf{v} \\ &= -\frac{1}{e} \frac{j_x(x, t)}{\tau}. \end{aligned} \quad (2.25)$$

The term proportional to $\int v_x f^0 d\mathbf{v}$ can be shown to be zero. Assuming the electrical current to be independent of time, and writing the second term, $\int v_x^2 (\partial f / \partial x) d\mathbf{v}$, as $\langle v_x^2 \rangle \frac{\partial}{\partial x} \int f d\mathbf{v} = \frac{1}{3} v_F^2 \frac{\partial}{\partial x} \int f d\mathbf{v}$, the following expression for the current is obtained:

$$j_x(x) = \sigma E_x - e D \frac{\partial n(x)}{\partial x}, \quad (2.26)$$

where $D = \frac{1}{3} v_F^2 \tau$ is the diffusion constant, $\sigma = \frac{k_F^3 e^2 \tau}{3\pi^2 m}$ is the electrical conductivity. Equation (2.26) states that within a linear response model, the current is proportional to the electrical field and the gradient of the carriers concentration with the negative sign. Substituting the equation (2.26) into the continuity equation (2.24), the diffusion equation is obtained:

$$\frac{\partial n(x, t)}{\partial t} = D \frac{\partial^2 n(x, t)}{\partial x^2}. \quad (2.27)$$

Equations (2.24) and (2.26), generalized to the spinor form, are the starting point of Chap. 6, where the equations for the spin-accumulation are obtained.

2.2 Landauer approach - interface resistance.

The conductance G due to elastic scattering of an obstacle, characterized by transmission and reflection coefficients T and R , is given by

$$G = \frac{e^2}{\pi \hbar} \frac{T}{R}, \quad (2.28)$$

where e is electron charge, and \hbar is Plank's constant. At zero temperature T and R are evaluated at the Fermi energy. Equation (2.28) applies to samples of arbitrary shape and structural complexity, and may be used, for example, to calculate the conductance of a planar barrier, such as an interface between two metals. Below, equation (2.28) will be derived within an approximation of a single conductivity channel, [47, 51, 46, 52] which makes a system effectively one-dimensional. Expression (2.28) can be generalized for the case of many independent conducting channels, and for nonzero temperature, [51, 47] but these generalizations won't be covered here.

Consider a barrier connected through ideal 1D wires to some external source (a pair of reservoirs with different chemical potentials μ_1 and μ_2) which drives a current I through the system. The barrier is characterized by its transition coefficient T and reflection coefficient $R = 1 - T$. (Fig. 2.2)

Consider first two reservoirs without a barrier. Left reservoir emits electrons with energies E up to a quasi-Fermi energy (chemical potential) μ_1 , Right reservoir emits electrons with energies E up to the chemical potential μ_2 . Energies are measured relative to equilibrium chemical potential (common for both reservoirs). Current emitted by the left reservoir and going to the right is

$$I^+ = -evn(E - \mu_1) \approx -evn_0(E) + ev \frac{\partial n}{\partial E} \mu_1,$$

where $n(E)$ is electron density per unit length. v is the velocity component along the wire at the Fermi surface. Current emitted by the right reservoir to the left is

$$I^- = evn(E - \mu_2) \approx evn_0(E) - ev \frac{\partial n}{\partial E} \mu_2.$$

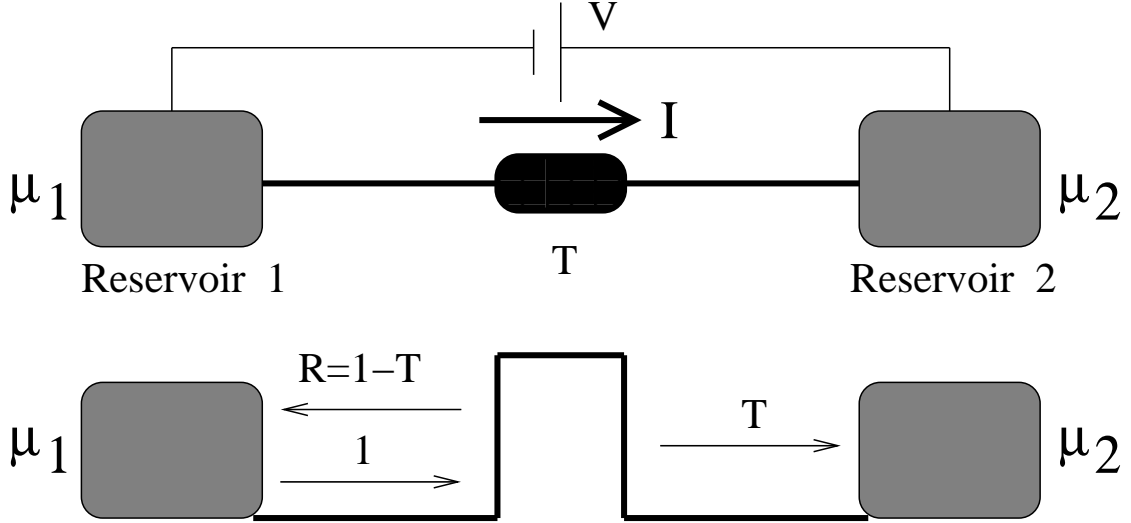


Figure 2.2: One-dimensional barrier with the transition coefficient T and reflection coefficient $R = 1 - T$, connected to an external source (a pair of reservoirs with different chemical potentials μ_1 and μ_2 .)

Then, total current is given by the sum of I^+ and I^- and is equal to

$$I = ev \frac{\partial n}{\partial E} (\mu_1 - \mu_2).$$

$\partial n/\partial E$ is the density of states for two spin directions and for carriers with positive velocity. In one-dimensional case, $\partial n/\partial E = 1/\pi\hbar v$ [53] and

$$I = \frac{e}{\pi\hbar} (\mu_1 - \mu_2).$$

This is the total current emitted by the left reservoir due to the difference in the quasi-Fermi levels. Carriers have a probability T for traversal of the sample and a probability R of being reflected back. Assuming that T and R don't depend on the electron energy in the energy range $\mu_1 > E > \mu_2$, the net current flow may be written as

$$I = \frac{e}{\pi\hbar} T (\mu_1 - \mu_2).$$

The difference in chemical potentials of the two reservoirs $\mu_1 - \mu_2$ can be identified with

the drop of electron potential eV across the source. Conductance, given by $G = I/V$ is

$$G = \frac{I}{(\mu_1 - \mu_2)/e} = \frac{e^2}{\pi\hbar} T,$$

and resistance of the system is

$$G^{-1} = \frac{\pi\hbar}{e^2} \frac{1}{T}. \quad (2.29)$$

Expression (2.29) gives a non-zero resistance in the case of completely transparent barrier, $T = 1$. The resistance in a system consisting only of the ideal wires and reservoirs is a finite quantity

$$G_C^{-1} = \frac{\pi\hbar}{e^2} = 12.9 \text{ } k\Omega. \quad (2.30)$$

This quantity is called the contact resistance. It occurs between a large reservoir with the infinite number of states that an electron can have, and a narrow wire with only one conductivity channel in the same way as traffic jam occurs when 4-lane highway transforms into 2-lane street. If a larger number M of the conductivity channels is allowed to exist in a wire (when the wire is three-dimensional but still very thin, so that the perpendicular motion of an electron is quantized), the contact resistance can be shown to have the form [47]

$$G_c^{-1} = \frac{\pi\hbar}{e^2} \frac{1}{M}.$$

The wider the wire, the larger the number of transverse modes M can propagate in it and the smaller the contact resistance is, and it is negligible for thick contacts.

The resistance of the barrier alone can be calculated by subtracting the contact resistance (equation (2.30)) from the total resistance of the "barrier-contacts-reservoirs" system (equation (2.29)), and is equal to

$$G^{-1} = \frac{\pi\hbar}{e^2} \frac{R}{T}; \quad (2.31)$$

this is equivalent to the expression (2.2) for the conductivity when one uses $1 - T = R$.

Resistance is usually associated with energy loss. In the considered model, scattering both at the barrier and in the wires is perfectly elastic ($R + T = 1$), so that there seems to be no energy loss in this system. Nevertheless, resistance exists. The resistance of the barrier can't be considered without connecting the barrier to the reservoirs. Electrons reflected from the barrier go back to the reservoir. Instead of reissuing the electron that

entered the reservoir, a new one comes out, so that information about the momentum of the electron is lost in a large reservoir, the outcoming electron does not have the same direction of the momentum as the incoming one had. This loss of information is the origin of the resistance of the barrier. [54] The existence of resistance in the Landauer approach requires the presence of the reservoirs, but its magnitude depends only on the elastic events at the barrier.

Chapter 3

Interface resistance in multilayers - theory

The Landauer formula (2.29) is derived for an obstacle connected to the source via ideal scattering-free wires. The purpose of this work, though, is to find a resistance due to interfaces in a realistic multilayered structure consisting of several diffusive metallic layers and interfaces between them. As discussed in Chap. 1, scattering at the interfaces is affected by the presence of the diffuse scattering in the bulk of the layers, and contributions from the bulk of the layers and the interfaces to the total resistance of the structure can't simply be added. In this section, the procedure allowing one to find a chemical potential profile and resistance due to the interfaces in a multilayered metallic structure in CPP geometry that takes into account an interaction of the scattering at the interfaces and scattering in the bulk of that layers will be developed. Transport in the bulk of the layers will be described by semiclassical Boltzmann equation, and interfaces will be taken into account via boundary conditions. Both specular and diffuse scattering at the interfaces will be considered. While Landauer's result for the interface resistance won't be explicitly used in this work, only scattering properties of the interfaces, their reflection and transmission coefficients will be used, which is a signature of the Landauer approach.

First, a general solution of the semiclassical linearized Boltzmann equation in CPP geometry is presented. Next, boundary conditions at an interface between two layers in the presence of both specular and diffuse scattering at the interface will be discussed. Then, a system of integral equations describing a chemical potential profile in two semi-infinite metallic layers will be derived. [32] Integral equations on the chemical poten-

tials in the systems consisting of three and five layers are presented in Appendices A.4 and A.5. This chapter is completed with determining the special form of diffuse scattering such that resistances measured at the interface and far from it are the same for a system consisting of two semi-infinite layers of identical metals and an interface between them. The forms of diffuse scattering for which a prediction can be made as to whether the potential drop at the interface is bigger or smaller than that measured far from it will be indicated.

3.1 General solution of the Boltzmann equation

In the relaxation-time approximation the linearized Boltzmann equation in CPP geometry takes the form (see Eq. (2.17) and $\mu(z)$ denoting the non-equilibrium part of the chemical potential):

$$\frac{\partial g(\theta, z)}{\partial z} + \frac{g(\theta, z)}{v_z \tau} = e E_z + \frac{\mu(z)}{v_z \tau}, \quad (3.1)$$

where e is an electron charge, τ is an electron relaxation rate, v_z and E_z are an electron velocity and an electric field in the direction z perpendicular to the plane of the layers, and θ is the angle that the electron momentum \mathbf{k} makes with z axis which takes values from 0 to π . Chemical potential $\mu(z)$ is the average of $g(\theta, z)$ in momentum space (see Eq. (2.18)):

$$\mu(z) = \frac{1}{2} \int_0^\pi g(\theta, z) \sin \theta d\theta. \quad (3.2)$$

Equation (3.1) is an ordinary first-order differential equation. Since the chemical potential $\mu(z)$ enters the right hand side of this equation, its solution $g(\theta, z)$ in the region between z_1 and z_2 of z axis will depend on $\mu(z)$ via an integral:

$$g(\theta, z) = \int_{z_1}^{z_2} dz' k(\theta, z, z') \mu(z') + y(\theta, z), \quad (3.3)$$

where $k(\theta, z, z')$ and $y(\theta, z)$ are functions defined by the geometry of the problem and the boundary conditions. By using the definition of the chemical potential (3.2), an equation for $\mu(z)$ can be obtained by integrating equation (3.3) over θ :

$$\mu(z) = \int_{z_1}^{z_2} dz' K(z, z') \mu(z') + Y(z), \quad (3.4)$$

where $K(z, z') = \frac{1}{2} \int_0^\pi k(\theta, z, z') \sin \theta d\theta$, $Y(z) = \frac{1}{2} \int_0^\pi y(\theta, z) \sin \theta d\theta$. [55]

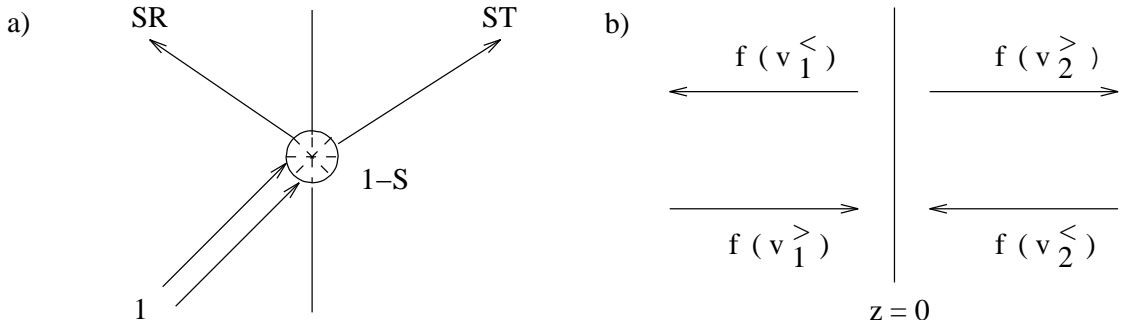


Figure 3.1: Scattering at an interface: a) schematic representation of electron scattering, b) direction of electron fluxes at an interface.

In the structure consisting of several layers (N), boundary conditions connect distribution function in a layer (L_i) with the distribution functions in the adjacent layers (L_j). Equation (3.4) can then be generalized to describe the chemical potential everywhere in the system:

$$\mu_i(z) = \sum_{j=1}^N \int_{L_j} dz' K_{ij}(z, z') \mu_j(z') + Y_i(z). \quad (3.5)$$

The integral equation (3.5) is a system of Fredholm equations of the second kind, which can be numerically solved to obtain the chemical potential profile everywhere in the layered structure. [32, 56] The functions $K_{ij}(z, z')$ and $Y_i(z)$ are defined by the boundary conditions at the interfaces. Numerical procedure of solving the Fredholm equation of the second kind is presented in the Appendix A.6.

3.2 Boundary conditions at the interface between two layers

At the interface between two layers, an incoming electron is scattered via reflection and transmission. There is also diffuse scattering in all directions. In the present work, a simple model for the diffuse scattering will be used, where a single parameter S represents an amount of electrons which are *not* scattered diffusely, so that the specularly reflected and transmitted electron fluxes are scaled by S . $1-S$ is the amount of electrons scattered diffusely. Figure 3.1a) represents schematically how an electron is scattered at an interface.

The boundary conditions for the distribution function f at the interface $z = 0$ between two semi-infinite layers in the presence of diffuse and specular scattering take the following form: [24, 57]

$$\begin{cases} f(v_2^>, 0) = S(v_1, v_2)R_{21}(v_1, v_2)f(v_2^<, 0) + S(v_1, v_2)T_{12}(v_1, v_2)f(v_1^>, 0) \\ \quad + [1 - S(v_1, v_2)]F(f), \\ f(v_1^<, 0) = S(v_1, v_2)R_{12}(v_1, v_2)f(v_1^>, 0) + S(v_1, v_2)T_{21}(v_1, v_2)f(v_2^<, 0) \\ \quad + [1 - S(v_1, v_2)]F(f), \end{cases} \quad (3.6)$$

where

$$\begin{aligned} F(f) &= \frac{1}{\Omega} \int_{FS} d\mathbf{k} [|v_{2z}^<|f(v_2^<, 0) + |v_{1z}^>|f(v_1^>, 0)], \\ \Omega &= \int_{FS} d\mathbf{k} \delta(\epsilon - \epsilon_F) |v_z|, \end{aligned} \quad (3.7)$$

ϵ_F is the electron Fermi energy, v_1 (v_2) is the electron velocity in the layer 1(2), and $v^>$ ($v^<$) refer to $v_z > 0$ ($v_z < 0$). $R_{ij}(v_1, v_2)$ ($T_{ij}(v_1, v_2)$) is the reflection (transmission) coefficient at an interface for an electron travelling from the layer i to the layer j , and $1 - S(v_1, v_2)$ describes the diffuse scattering. As shown at the Fig. 3.1b), an outgoing particle flux $f(v_2^>)$ ($f(v_1^<)$) comes from the specularly reflected particle flux (first term), the specularly transmitted particle flux (second term), and the particle flux from all directions diffusely scattered in the direction of $v_2^>$ ($v_1^<$) (last term).

Similar boundary conditions, but without the last term, were investigated by Hood and Falicov for currents in plane of the layers geometry. [57] In CPP geometry, current conservation requires the presence of the term responsible for the diffuse scattering at an interface in the boundary conditions. The proof of the fact that the boundary conditions (3.6)-(3.7) indeed conserve the current across an interface is presented in Appendix A.2.

At the interface between two metals, reflection and transmission coefficients R_{ij} and T_{ij} have to be found from quantum mechanical considerations, as reflection and transmission coefficients for the quantum mechanical flux. In general, R_{ij} , T_{ij} and S depend on both variables v_1 and v_2 . In the quasi-one-dimensional layered structures, where the component of electron velocity parallel to an interface is conserved, only z component of velocity enters reflection and transmission coefficients. Furthermore, in the case of specular scattering, angle of reflection and angle of transmission are uniquely defined by the angle of incidence, so that R_{ij} and T_{ij} are the functions of the cosine of an

angle that an electron velocity makes with an interface only, $R_{ij}(\cos \theta_i)$ and $T_{ij}(\cos \theta_i)$, where θ_i is the angle of incidence of an electron at the interface in i -th layer. Specular scattering at an interface between two metals is considered in detail in Appendix A.3. In order to simplify the discussion of the effects of the diffuse scattering at an interface on the electron transport in multilayers, diffuse scattering parameter S is assumed to be constant, independent of the electron direction, with one exception, in Sec. 3.4, where the special forms of the diffuse scattering coefficient for which a shape of the chemical potential profile can be predicted analytically are considered. With these simplifications, the boundary conditions on the function g take the following form:

$$\begin{cases} g(v_2^>, 0) = SR_{21}(\theta_2)g(v_2^<, 0) + ST_{12}(\theta_1)g(v_1^>, 0) + (1 - S)F(g), \\ g(v_1^<, 0) = SR_{12}(\theta_1)g(v_1^>, 0) + ST_{21}(\theta_2)g(v_2^<, 0) + (1 - S)F(g), \end{cases} \quad (3.8)$$

where $F(g)$ can be shown (Appendix A.1.3) to have the form:

$$\begin{aligned} F(g) &= \frac{2v_{F1}^2}{v_{F2}^2 + v_{F1}^2} \int_0^{\pi/2} g(v_1^>, 0) \cos \theta \sin \theta d\theta \\ &+ \frac{2v_{F2}^2}{v_{F2}^2 + v_{F1}^2} \int_0^{\pi/2} g(v_2^<, 0) \cos \theta \sin \theta d\theta, \end{aligned} \quad (3.9)$$

where v_{F1} and v_{F2} are the electron Fermi velocities in the first and the second layer correspondingly.

3.3 Equations for chemical potential profile in a multi-layer

In this section, solution of the Boltzmann equation in the system consisting of two semi-infinite metallic layers and interface between them (Fig. 3.2) is presented, and equations on the chemical potential profile are derived. For simplicity, the same electron relaxation time τ is assumed in both layers. Solution of the Boltzmann equation (3.1) for corrections to the distribution function of the electrons moving to the right $g(v_1^>, z)$ and to the left $g(v_1^<, z)$ in the first layer, and electrons moving to the right $g(v_2^>, z)$ and to

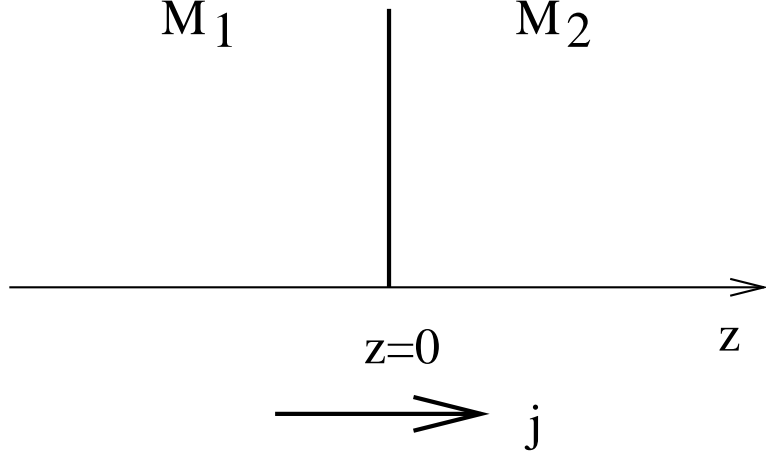


Figure 3.2: System consisting of two layers.

the left $g(v_2^<, z)$ in the second layer take the following form:

$$\left\{ \begin{array}{l} g(v_1^>, z) = \int_{-\infty}^z dz' \exp\left(-\frac{z-z'}{|v_{z1}|\tau}\right) \left(eE_{z1} + \frac{\mu_1(z')}{|v_{z1}|\tau}\right) \\ g(v_1^<, z) = A \exp\left(\frac{z}{|v_{z1}|\tau}\right) + \int_0^z dz' \exp\left(\frac{z-z'}{|v_{z1}|\tau}\right) \left(eE_{z1} - \frac{\mu_1(z')}{|v_{z1}|\tau}\right) \\ g(v_2^>, z) = B \exp\left(-\frac{z}{|v_{z2}|\tau}\right) + \int_0^z dz' \exp\left(-\frac{z-z'}{|v_{z2}|\tau}\right) \left(eE_{z2} + \frac{\mu_2(z')}{|v_{z2}|\tau}\right) \\ g(v_2^<, z) = - \int_z^\infty dz' \exp\left(\frac{z-z'}{|v_{z2}|\tau}\right) \left(eE_{z2} - \frac{\mu_2(z')}{|v_{z2}|\tau}\right), \end{array} \right. \quad (3.10)$$

where $\mu_1(z)$ ($\mu_2(z)$) is the chemical potential in the left (right) layer, E_{z1} (E_{z2}) is an electric field in the left (right) layer, and v_{z1} (v_{z2}) is a component of an electron velocity in the direction z in the left (right) layer. Since only the z component of an electric field is present in CPP geometry, the subscript z will be omitted from E_{z1} and E_{z2} everywhere below. A , B are constants of integration, independent of z . They are defined by the boundary conditions (3.8), and equal to

$$\begin{aligned} A &= SR_{12}(\theta_1)eE_1l_1|\cos\theta_1| - ST_{21}(\theta_2)eE_2l_2|\cos\theta_2| \\ &+ SR_{12}(\theta_1) \int_{-\infty}^0 \exp\left(\frac{\xi'}{\cos\theta_1}\right) \frac{\mu_1(\xi')}{\cos\theta_1} d\xi' \end{aligned} \quad (3.11)$$

$$\begin{aligned}
& + ST_{21}(\theta_2) \int_0^\infty \exp\left(\frac{-\xi'}{\cos \theta_1}\right) \frac{\mu_2(\xi')}{\cos \theta_2} d\xi' + (1-S)F(g) \\
B &= -SR_{21}(\theta_2)eE_2l_2|\cos \theta_2| + ST_{12}(\theta_1)eE_1l_1|\cos \theta_1| \\
& + SR_{21}(\theta_2) \int_0^\infty \exp\left(\frac{-\xi'}{\cos \theta_2}\right) \frac{\mu_2(\xi')}{\cos \theta_2} d\xi' \\
& + ST_{12}(\theta_1) \int_{-\infty}^0 \exp\left(\frac{\xi'}{\cos \theta_2}\right) \frac{\mu_1(\xi')}{\cos \theta_1} d\xi' + (1-S)F(g),
\end{aligned} \tag{3.12}$$

where $l_i = v_{Fi}\tau$ is the electron mean free path in i -th layer, θ_i is an angle that an electron velocity makes with z axis in i -th layer, and a dimensionless variable $\xi = z/l_i$, where $i = 1$ or 2 depending on in which layer the chemical potential is considered, is introduced. Since the boundary conditions connect the distribution functions at both sides of the interface, both angles θ_1 and θ_2 enter the expressions for A and B . From the definition of the chemical potential (3.2) it follows (see Appendix A.1.2) that

$$\begin{cases} 2\mu_1(z) &= \int_0^{\pi/2} (g(v_1^>, z) + g(v_1^<, z)) \sin \theta_1 d\theta_1 \\ 2\mu_2(z) &= \int_0^{\pi/2} (g(v_2^>, z) + g(v_2^<, z)) \sin \theta_2 d\theta_2, \end{cases} \tag{3.13}$$

where the averaging is performed over the electron momentum direction θ_1 and θ_2 in the first or the second layer correspondingly. Hence, the constants of integration A has to be expressed in terms of the angle θ_1 only, $A(\theta_1)$, and B in terms of the angle θ_2 only, $B(\theta_2)$. It can be shown (see Appendix A.3) that angles θ_1 and θ_2 are related; θ_1 can be expressed as a function of θ_2 , $\theta_1(\theta_2)$, and vice versa, $\theta_2(\theta_1)$. It follows from this relation that $T_{12}(\theta_1) = T_{21}(\theta_2)$ and $R_{12}(\theta_1) = R_{21}(\theta_2)$. Note that when calculating the function $F(g)$, change of angles is not required, which reflect the fact that in the process of diffuse scattering angles of incidence, reflection and transmission are not related, so a variable θ will enter the expression for $F(g)$ without the subscript. The electrical fields E_1 and E_2 in the layers are related due to the current conservation, so that $\sigma_i E_i = \text{const}$ throughout the system, where σ_i is the conductivity of the layer i . Since electron relaxation time τ is assumed to be the same in all layers, and the conductivity is inversely proportional to v_F^3 , [53] electrical fields E_1 and E_2 are related via $v_{F1}^2 E_1 l_1 = v_{F2}^2 E_2 l_2$.

The following equations on the chemical potentials in the left and right layers are

obtained from equations (3.10)-(3.13):

$$\begin{aligned}
2\mu_1(\xi) &= eE_1 l_1 \int_0^{\pi/2} \left[(1 + SR_{12}(\theta_1)) \cos \theta_1 - \frac{v_{F1}^2}{v_{F2}^2} ST_{12}(\theta_1) \cos \theta_2(\theta_1) \right] \\
&\times \exp\left(\frac{\xi}{\cos \theta_1}\right) \sin \theta_1 d\theta_1 \\
&+ \int_{-\infty}^0 \mu_1(\xi') d\xi' \\
&\times \int_0^{\pi/2} \left[\exp\left(\frac{-|\xi - \xi'|}{\cos \theta_1}\right) + SR_{12}(\theta_1) \exp\left(\frac{\xi + \xi'}{\cos \theta_1}\right) \right] \tan \theta_1 d\theta_1 \\
&+ \int_0^{\infty} \mu_2(\xi') d\xi' \int_0^{\pi/2} ST_{12}(\theta_1) \exp\left(\frac{-\xi'}{\cos \theta_2(\theta_1)}\right) \exp\left(\frac{\xi}{\cos \theta_1}\right) \frac{\sin \theta_1}{\cos \theta_2(\theta_1)} d\theta_1 \\
&+ \frac{2(1 - S)}{1 + v_{F2}^2/v_{F1}^2} \int_{-\infty}^0 \mu_1(\xi') d\xi' \\
&\times \int_0^{\pi/2} \exp\left(\frac{\xi'}{\cos \theta}\right) \sin \theta d\theta \int_0^{\pi/2} \exp\left(\frac{\xi}{\cos \theta}\right) \sin \theta d\theta \\
&+ \frac{2(1 - S)}{1 + v_{F1}^2/v_{F2}^2} \int_0^{\infty} \mu_2(\xi') d\xi' \\
&\times \int_0^{\pi/2} \exp\left(\frac{-\xi'}{\cos \theta}\right) \sin \theta d\theta \int_0^{\pi/2} \exp\left(\frac{\xi}{\cos \theta}\right) \sin \theta d\theta
\end{aligned} \tag{3.14}$$

$$\begin{aligned}
2\mu_2(\xi) &= -eE_2 l_2 \int_0^{\pi/2} \left[(1 + SR_{21}(\theta_2)) \cos \theta_2 - \frac{v_{F2}^2}{v_{F1}^2} ST_{21}(\theta_2) \cos \theta_1(\theta_2) \right] \\
&\times \exp\left(\frac{-\xi}{\cos \theta_2}\right) \sin \theta_2 d\theta_2 \\
&+ \int_0^{\infty} \mu_2(\xi') d\xi' \\
&\times \int_0^{\pi/2} \left[\exp\left(\frac{-|\xi - \xi'|}{\cos \theta_2}\right) + SR_{21}(\theta_2) \exp\left(\frac{-\xi - \xi'}{\cos \theta_2}\right) \right] \tan \theta_2 d\theta_2 \\
&+ \int_{-\infty}^0 \mu_1(\xi') d\xi' \int_0^{\pi/2} ST_{21}(\theta_1) \exp\left(\frac{\xi'}{\cos \theta_1(\theta_2)}\right) \exp\left(\frac{-\xi}{\cos \theta_2}\right) \frac{\sin \theta_2}{\cos \theta_1(\theta_2)} d\theta_2
\end{aligned}$$

$$\begin{aligned}
& + \frac{2(1-S)}{1+v_{F2}^2/v_{F1}^2} \int_{-\infty}^0 \mu_1(\xi') d\xi' \\
& \times \int_0^{\pi/2} \exp\left(\frac{\xi'}{\cos\theta}\right) \sin\theta d\theta \int_0^{\pi/2} \exp\left(-\frac{\xi}{\cos\theta}\right) \sin\theta d\theta \\
& + \frac{2(1-S)}{1+v_{F1}^2/v_{F2}^2} \int_0^{\infty} \mu_2(\xi') d\xi' \\
& \times \int_0^{\pi/2} \exp\left(\frac{-\xi'}{\cos\theta}\right) \sin\theta d\theta \int_0^{\pi/2} \exp\left(\frac{-\xi}{\cos\theta}\right) \sin\theta d\theta
\end{aligned} \tag{3.15}$$

These equations describe the chemical potential profile everywhere in the system consisting of two semi-infinite metallic layers in the presence of both specular and diffuse scattering at the interface between them. In a similar fashion, equations describing the chemical potential profiles in three- and five-layered systems can be obtained. Because of the tedious calculations required for the derivation, only the final equations are presented in Appendices A.4 and A.5. Even in the simplest structure consisting of two layers of identical metals divided by an interface, the form of the chemical potential can't be found analytically, though in this case a certain prediction can be made. Results of the numerical solution of the equations on the chemical potential in various systems are presented in Chap. 4.

3.4 Special forms of diffuse scattering

In the simple case of identical metals at both sides of an interface, special forms of diffuse scattering $S(\cos\theta)$ can be found, for which the chemical potential remains constant outside the interfacial region, so that the resistance measured at the interface is the same as the resistance measured far from it. In the identical layers, $v_{F1} = v_{F2}$, $\theta_1 = \theta_2$, and chemical potential is antisymmetrical around $z = 0$:

$$\mu_2(\xi) = -\mu_1(-\xi) \tag{3.16}$$

Then, equation 3.14 for the chemical potential in the left layer, $\mu_1(\xi)$ for example, takes the form

$$2\mu_1(\xi) = eE_1 l_1 \int_0^{\pi/2} (1 - S(\theta_1) + 2S(\theta_1)R_{12}(\theta_1)) \exp\left(\frac{\xi}{\cos\theta_1}\right) \sin\theta_1 \cos\theta_1 d\theta$$

$$\begin{aligned}
& + \int_{-\infty}^0 \mu_1(\xi') d\xi' \\
& \times \int_0^{\pi/2} \left(\exp\left(\frac{-|\xi - \xi'|}{\cos \theta_1}\right) + S(\theta_1) (2R_{12}(\theta_1) - 1) \exp\left(\frac{\xi + \xi'}{\cos \theta_1}\right) \right) \tan \theta_1 d\theta_1.
\end{aligned} \tag{3.17}$$

The derivative of the chemical potential $\mu_1(\xi)$ takes the form

$$\begin{aligned}
2\mu'_1(\xi) &= eE_1 l_1 \int_0^{\pi/2} (1 - S(\theta_1) + 2S(\theta_1)R_{12}(\theta_1)) \exp\left(\frac{\xi}{\cos \theta_1}\right) \sin \theta_1 d\theta_1 \\
&+ \int_{-\infty}^0 \mu_1(\xi') d\xi' \\
&\times \int_0^{\pi/2} S(\theta_1) (2R_{12}(\theta_1) - 1) \exp\left(\frac{\xi + \xi'}{\cos \theta_1}\right) \frac{\tan \theta_1}{\cos \theta_1} d\theta_1 \\
&- \int_{-\infty}^{\xi} \mu_1(\xi') d\xi' \int_0^{\pi/2} \exp\left(\frac{-\xi + \xi'}{\cos \theta_1}\right) \frac{\tan \theta_1}{\cos \theta_1} d\theta_1 \\
&+ \int_{\xi}^0 \mu_1(\xi') d\xi' \int_0^{\pi/2} \exp\left(\frac{\xi - \xi'}{\cos \theta_1}\right) \frac{\tan \theta_1}{\cos \theta_1} d\theta_1.
\end{aligned} \tag{3.18}$$

The condition $\mu'_1(\xi) = 0$, so that the chemical potential in the left layer $\mu_1(\xi)$ is constant, can be satisfied when the reflection coefficient $R_{12}(\theta)$ and diffuse scattering parameter $S(\theta)$ are related via

$$S^*(\theta) = \frac{\cos \theta - \beta}{(\cos \theta + \beta)(1 - 2R(\theta))}, \tag{3.19}$$

where β is a constant. Then the chemical potential in the left layer is equal to $\mu_1(z) = \beta e E_1 l_1 = \text{const}$, and in the right layer $\mu_2(z) = -\beta e E_2 l_2 = \text{const}$, where electrical fields E_1 and E_2 , and electron mean-free paths l_1 and l_2 are the same in both layers. The sheet resistance across the interface AR_0 and measured far from it AR_1 (Fig. 1.10) are

$$AR_0 = AR_1 = \frac{\mu_1(z) - \mu_2 z}{ej} = \beta \frac{6\pi^2 \hbar^3}{e^2 m^2 v_F^2},$$

where m is an electron mass, v_F is an electron Fermi velocity, same in both layers.

The special form of diffuse scattering (Eq. (3.19)) which makes $\mu(z)$ constant for $z \neq 0$ can be found for any reflection coefficient. In particular, if an interface between metals is modeled as a sheet delta function potential, so that the reflection coefficient

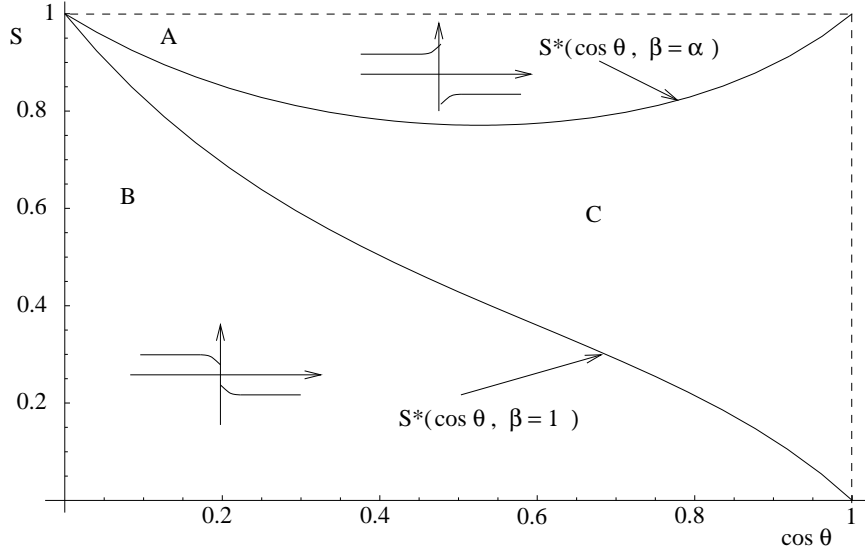


Figure 3.3: Diffuse scattering $S(\theta)$. Region A: potential drop at the interface is bigger than potential drop far from the interface. Region B: potential drop at the interface is smaller than potential drop far from the interface. Region C: region of special forms of diffuse scattering.

takes the form $R(\theta) = \alpha/(\alpha + \cos^2\theta)$, [58] it exists for *any* β from 1 to α . These special forms of S occupy region C in Fig. 3.3. If the function $S(\theta)$ stays above this region for all θ (region A in Fig. 3.3) then the resistance across the interface R_0 is larger than resistance R_s measured far from it. When $S(\theta)$ stays below this region for all θ (region B in Fig. 3.3) then R_0 is smaller than R_1 . For $S(\theta)$ occupying both regions C and A or (and) B, no prediction for the chemical potential shape can be made.

Chapter 4

Interface resistance in multilayers - results

In this chapter, the numerical results for the chemical potential profile and resistance due to the interfaces in the multilayered systems are presented.

The systems consisting of two, three, or five metallic layers, i.e., with 1, 2, or 4 interfaces, in which I consider electrons move across a step-like potential. Energies are referenced to the Fermi level so that $\epsilon_F = 0$, and the effective mass of the electron is assumed to be independent of the material and spin-orientation. In the i -th layer, electrons move in a constant potential $V_i = -mv_{iF}^2/2$, where v_{iF} is the electron Fermi velocity in the i -th layer. The same electron relaxation time τ is assumed in all layers, and an electron mean-free path $l_i = v_{Fi}\tau$ is introduced. Current conservation requires electric fields E_i in the layers to be related by $v_{Fi}^2 E_i l_i = \text{const}$ (see Sec. 3.3). The reflection coefficient at the interface between two metals takes the following form (see Appendix A.3):

$$R_{ij}(\theta_i) = \left| \frac{1 - \sqrt{1 - \frac{1}{\cos^2 \theta_i} + \frac{v_{Fj}^2}{v_{Fi}^2} \frac{1}{\cos^2 \theta_i}}}{1 + \sqrt{1 - \frac{1}{\cos^2 \theta_i} + \frac{v_{Fj}^2}{v_{Fi}^2} \frac{1}{\cos^2 \theta_i}}} \right|^2. \quad (4.1)$$

Besides the specular scattering at the interfaces, diffuse scattering is present, such that the diffuse scattering parameter S (see Chap. 3) is assumed to be independent of the angle of incidence, and the same for all interfaces.

Equations (3.14)-(3.15), (A.15)-(A.19) and (A.20)-(A.28) yield the chemical potentials in each layer of the multilayered system, normalized to the voltage drop within a

mean-free path in this layer $\mu_i(z)/eE_il_i$. Resistance due to the interfaces is proportional to the drop of the chemical potential:

$$AR = \frac{\Delta\mu}{ej}, \quad (4.2)$$

where AR is the sheet resistance due to an interface, e is the electron charge and j is the electric current. In terms of the chemical potential drop normalized to the voltage drop within a mean-free path in the layer $\Delta\mu/eEl$, the interface resistance may be written as

$$AR = \frac{\Delta\mu}{e\sigma E} = \frac{\Delta\mu}{eEl} \frac{l}{\sigma} = \frac{\Delta\mu}{eEl} \frac{6\pi^2\hbar}{e^2k_F^2}. \quad (4.3)$$

The factor $6\pi^2\hbar/e^2k_F^2$, different for each material and each spin-orientation, has to be taken into account when deducing the resistance due to the interfaces from the chemical potential drops obtained by solving the equations for the chemical potential profiles.

R_N , where N is the number of interfaces in the system, $N = 1, 2, 4$, denotes the resistance due to the interfaces, measured far from the interfaces:

$$R_N = [\mu(-\infty) - \mu(+\infty)]/ej.$$

For the two-layered systems, resistance R_0 measured directly at the interface at $z = 0$ (Fig. 1.10) is introduced:

$$R_0 = [\mu(0-) - \mu(0+)]/ej.$$

In this chapter, the systems consisting of two semi-infinite metallic layers are considered. The influence of the diffuse scattering at the interface on the chemical potential profile, and the influence of the diffuse scattering in the bulk of the layers on the interface resistance are investigated. The breakdown of the resistors-in-series model is anticipated. Next, the prediction about the resistors-in-series model breakdown is tested in the systems consisting of three and five layers. The interface resistance dependence on the layers thicknesses relative to the electron mean-free path is obtained for different parameters S of diffuse scattering at the interfaces. Finally, realistic multilayers consisting of two, three and five layers of ferromagnetic and non-magnetic metals (Co-Cu and Fe-Cr systems) are considered. Resistances due to the interfaces R_N are obtained as a function of the layer thicknesses and the amount of the diffuse scattering at the interfaces. I investigate the deviation of the resistance R_N in the three- and five-layered

systems with the layer thicknesses less than the electron mean-free path in the layers from the resistance NR_1 that such systems would have if the interfaces were far enough from each other so that the scattering from the neighboring interfaces would not interfere.

The numerical procedure of solving the integral equations for the chemical potential profile (3.14)-(3.15), (A.15)-(A.19) and (A.20)-(A.28) is discussed in the appendix A.6.

4.1 Two layers

4.1.1 Same metals

Equations (3.16) and (3.17) are solved numerically [32] to obtain the chemical potential profile in the system consisting of two identical metallic layers separated by a delta function potential, so that the reflection coefficient takes the form $R(\theta) = \alpha/(\alpha + \cos^2 \theta)$. [58] Fig. 4.1a) shows how the chemical potential profile changes with the amount of diffuse scattering when S is a constant between 0 (only diffuse scattering is present at an interface) and 1 (only specular scattering is present). Interface resistance grows as the amount of diffuse scattering decreases, [24] and the chemical potential varies within a mean-free path of the boundary. The resistance R_1 measured far from the interface can be larger or smaller than that measured at the interface, R_0 , (see Fig. 1.10), depending on the value of S . Fig. 4.1b) shows the difference between R_0 and R_1 relative to R_1 . This difference can be as large as 18-19%. When there is no diffuse scattering at the interface, $S = 1$, the difference between the resistance R_1 and R_0 , agrees with the results obtained by Penn and Stiles [26].

4.1.2 Different metals

Next, a system consisting of two different metallic layers and an interface between them is considered. [32] Figure 4.2 shows the step-like potential experienced by electrons in such a system. For $z < 0$, electrons move in a constant potential $V_1 = -mv_{F1}^2/2$, and $V_2 = -mv_{F2}^2/2$ for $z > 0$.

Equations (3.14) and (3.15) with the reflection coefficients (4.1) are solved in order to investigate how the chemical potential profile and interface resistance change as the functions of the potential barrier height V_2/V_1 , and the amount of diffuse scattering at the interface. In Fig. 4.3, the forms of the chemical potential for $V_2/V_1 = 2$, and different values of the diffuse scattering parameter S are shown. As in the case of the same metal

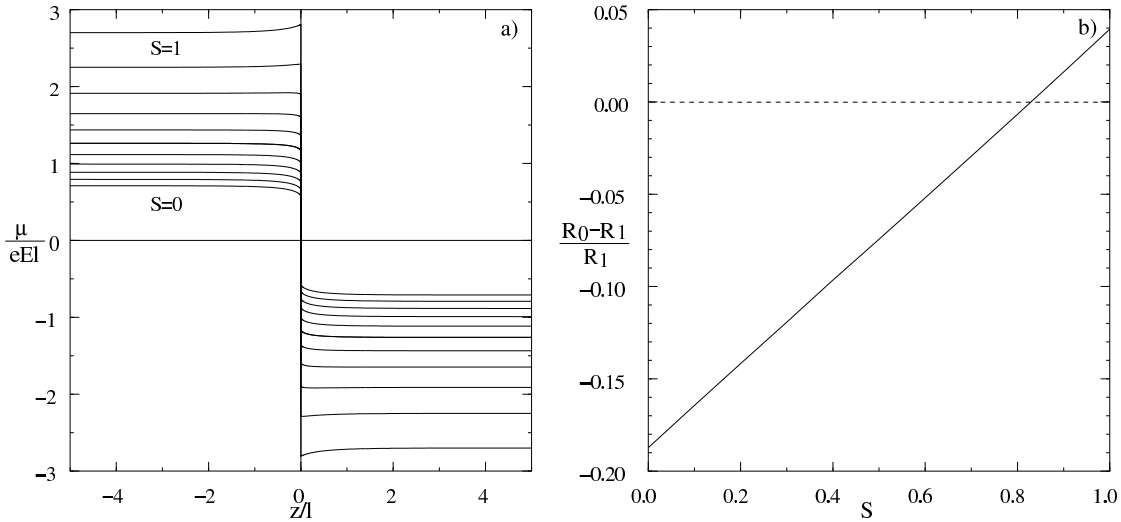


Figure 4.1: Chemical potential and interface resistance in two layers of identical metals:
a) chemical potential profile for $S = 0, 0.1, \dots, 1$, normalized with respect to potential drop eEl within a mean-free path l of the metal, b) the difference between R_0 and R_1 relative to R_1 .

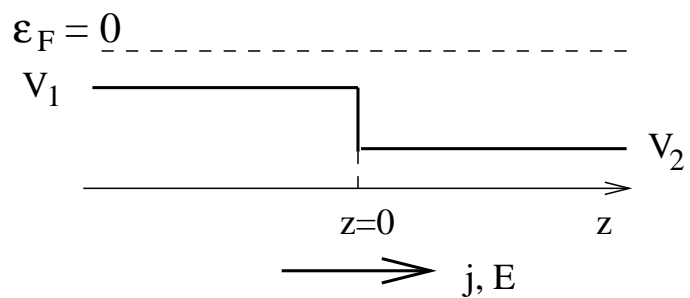


Figure 4.2: Step-like potential experienced by electrons at an interface between two metals.

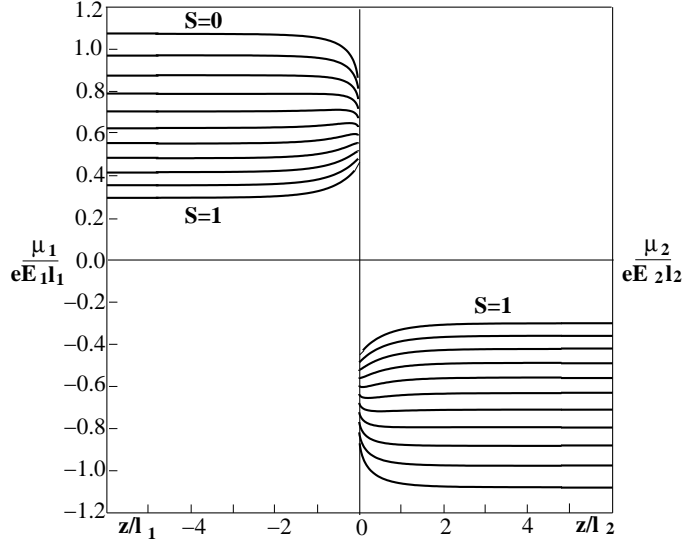


Figure 4.3: Chemical potential profile in two-layered system for different values of diffuse scattering $S = 0, 0.1, \dots, 1$ at the interface, normalized with respect to potential drop $eE_i l_i$ within a mean-free path l_i of each metal, so that the plots are anti-symmetrical around $z = 0$.

on both sides of the boundary, the chemical potential varies within several mean-free paths of the interface. Resistance measured far from the interface, R_1 , is bigger than that measured right at the interface, R_0 , for interfaces where diffuse scattering dominates (S is close to 0). R_1 is smaller than R_0 for the interfaces where specular scattering dominates (S is close to 1). Unlike the case of two identical layers, the resistance of the step-like barrier decreases as the amount of diffuse scattering decreases. [24]

Figure 4.4 demonstrates the effect of diffuse scattering in the bulk of the layers on the interface resistance. In the case of a completely specular interface, $S = 1$, the variation of interface resistance as the function of the barrier height V_2/V_1 is shown in comparison with that obtained by Barnas and Fert in the system of ballistic layers. [18, 19] In the presence of diffuse scattering in the bulk of the layers, both R_0 and R_1 are less than the interface resistance obtained for purely ballistic transport. In the diffusive layer, electrons reflected off the barrier can be scattered back on the barrier, and again have a chance to be transmitted through, making the interface resistance smaller.

Figure 4.5 summarizes the behavior of the interface resistance as the amount of diffuse scattering at the interface, and the height of the potential barrier experienced by

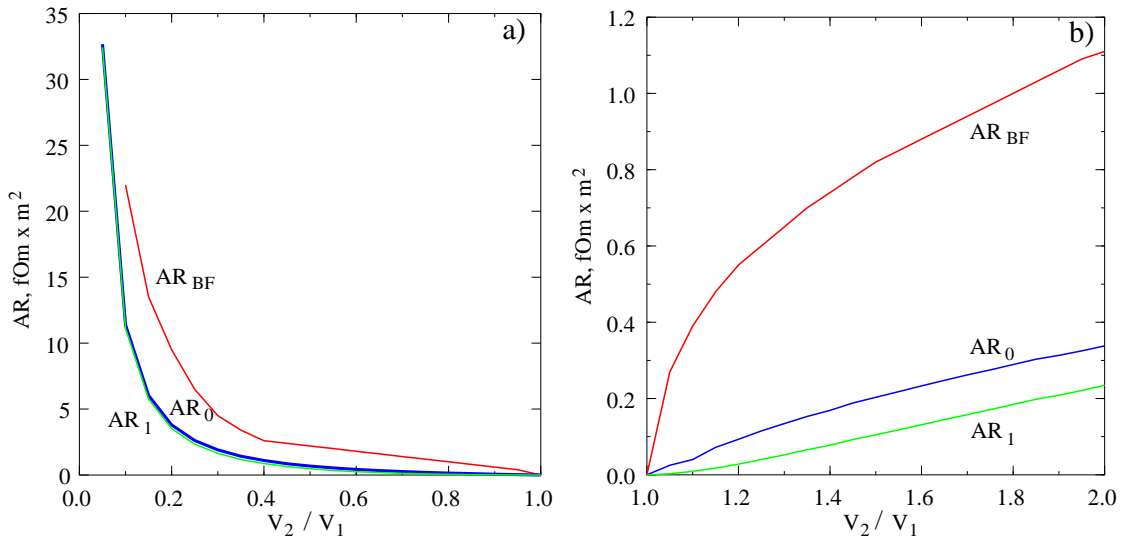


Figure 4.4: Effect of the diffuse scattering in the bulk of the layers on the interface resistance in two-layered system. Red line is the Barnas and Fert result for the sheet interface resistance, AR_{BF} , adapted from Refs. [18, 19], for the ballistic transport in the bulk of the layers and specular scattering at the interface; blue and green lines are resistances AR_0 and AR_1 for diffuse transport in the bulk of the layers and specular scattering at the interface, $S = 1$, as the functions of the electron potentials ratio a) $V_2/V_1 < 1$, b) $V_2/V_1 > 1$.

the electrons at the interface change. Arbitrary units for the resistance are used, since the calculations are performed irrespective of the particular metals. Note that the ratio of the electron Fermi velocities in the layers v_{F2}/v_{F1} is used as a variable, not the ratio of the electron potentials V_2/V_1 , as in the Fig. 4.4. In Figs. 4.5a)-b), the variation of the interface resistance as the function of the amount of diffuse scattering at the interface for the system with $v_{F2}/v_{F1} = 2$ is shown. The resistance R_0 measured directly at the interface is larger than the resistance R_1 measured far from it, and R_0 grows as the interface becomes less diffusive (S approaches 1), while R_1 decreases slightly, so that the absolute value of the difference $R_1 - R_0$ grows, reaching about 70% if calculated relative to R_0 , and 120% if calculated relative to R_1 for a completely specular interface. In Figs. 4.5c)-f), the variation of the interface resistance as the function of v_{F2}/v_{F1} for different values of S is shown. In the absence of the potential barrier ($v_{F2}/v_{F1} = 1$), both R_0 and R_1 increase as the amount of diffuse scattering at the interface increase (S approaches 0), since only diffuse scattering is responsible for the resistance in this case. As the height of the barrier grows (v_{F2}/v_{F1} becoming > 1 or < 1), specular reflection starts to influence the interface resistance, and the values of both R_0 and R_1 are closer to each other for different values of S than they were in the absence of the potential barrier. Values of the potential barrier heights exist where the interface resistance is almost independent of the amount of diffuse scattering at the interface. These values are different for R_0 and R_1 . The percentage difference between R_1 and R_0 shows no variation with the barrier height in the case of completely diffuse interface ($S = 0$), since v_{F2}/v_{F1} only defines the scale of the interface resistance in this case. As the amount of diffuse scattering at the interface decreases, both $(R_1 - R_0)/R_0$ and $(R_1 - R_0)/R_1$ show a strong dependence on the potential barrier height, reaching maximum values of several tens percent for small barriers. This fact is of particular interest, because small barrier heights are realized in Fe-Cr multilayers for minority electrons and Co-Cu multilayers for majority electrons. These systems will be discussed further below.

4.1.3 Anticipation of the breakdown of the resistors-in-series model

The results of the previous section show that the resistance of the interface deduced from the voltage drop measured far from the interface (R_1) should not be interpreted as the interface resistance that would be obtained by measuring the voltage drop directly at the interface (R_0), as they may differ significantly. As seen from Figs. 4.1a) and 4.3, the chemical potential varies within the electron mean-free path from the interface. Hence, in the multilayered system with layers thicknesses of the order or less than the mean-free

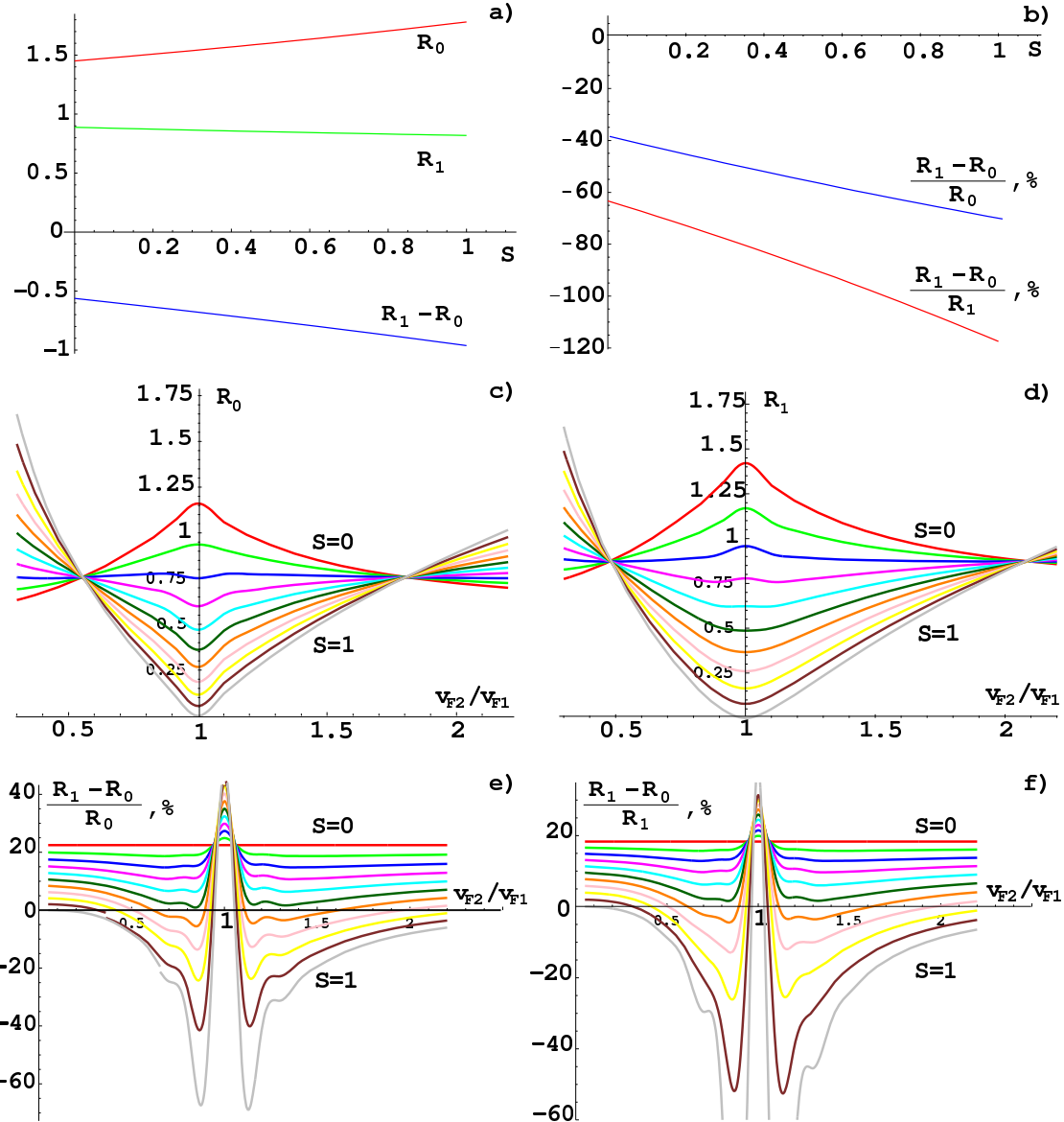


Figure 4.5: Summary of the results for the two-layered system: a) resistances R_0 , R_1 , and the difference $R_1 - R_0$ as the functions of the diffuse scattering S at the interface for $v_{F2}/v_{F1} = 2$, b) percentage differences $R_1 - R_0$ relative to R_0 and R_1 as the functions of S for $v_{F2}/v_{F1} = 2$, c)-d) resistances R_0 and R_1 as the functions of the electrons Fermi velocities ratio v_{F2}/v_{F1} for different values of the diffuse scattering S at the interface. In the plots a)-d), arbitrary units for the resistance are used. e)-f) percentage differences $R_1 - R_0$ relative to R_0 and R_1 as the functions of the electrons Fermi velocities for different values of S .

path, the chemical potential can be expected not to reach its asymptotic value within a layer. The breakdown of the resistors-in-series model can be anticipated, which means that while the resistance of the whole structure still can be found by adding the resistances due to the bulk of the layers and due to the interfaces, neither the resistance R_1 nor R_0 of the interface between the semi-infinite layers should be considered as the resistance of the interface between the layers which are thinner than the mean free path due to the scattering indigenous to them. In other words, even if one maintains the same interface between layers, its contribution to the resistance of a multilayered structures will depend on the thickness of the adjacent layers, or, more precisely, on the ratio of the thickness to the mean-free path. Its contribution will be constant, R_1 , only if the interfaces are far enough from each other for the chemical potential to level off.

In the following section, the prediction about the resistors-in-series model breakdown and interface resistance dependence on the ratio of the layer thickness to the electron mean-free path in this layer will be tested in the systems consisting of three and five layers.

4.2 Three and five layers

In this section, systems consisting of three and five layers of different metals are considered. [56] Figure 4.6 shows the step-like potentials experienced by electrons in such systems. In the three-layered system (Fig. 4.6a)), electrons move in a constant potential $V_1 = -mv_{F1}^2/2$ at $z < -d$ and $z > d$, and $V_2 = -mv_{F2}^2/2$ at $-d < z < d$. In the five-layered system (Fig. 4.6b)), electrons move in a constant potential $V_1 = -mv_{F1}^2/2$ at $z < -3d$, $-d < z < d$, and $z > 3d$, and $V_2 = -mv_{F2}^2/2$ at $-3d < z < -d$ and $d < z < 3d$. The structures with only two possible values of the electron Fermi velocity are chosen for simplicity; further below, when the realistic Fe-Cr and Co-Cu systems will be considered, this restriction will be removed, and the electron Fermi velocity will depend not only on the material but on the magnetization direction in the magnetic layer.

Equations (A.15)-(A.19) and (A.20)-(A.28) with the reflection coefficients (4.1) are solved in order to investigate how the chemical potential profile changes when the thickness of the layers changes and becomes less than the electron mean-free path in the layers. I find the resistance due to the interfaces as the function of the layers thickness relative to the electron mean-free path, for different values of diffuse scattering S at the interfaces, and investigate the deviation from the resistors-in-series model as the barrier

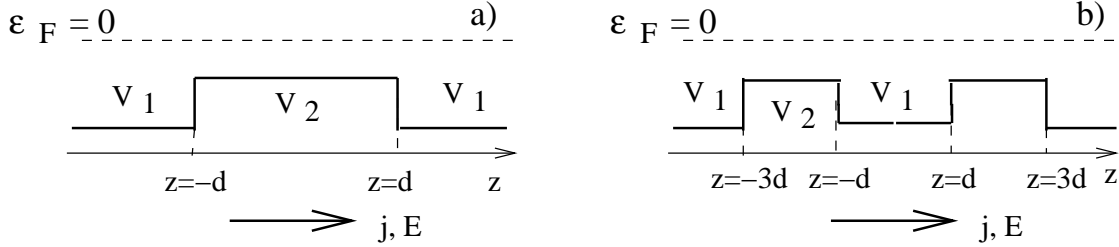


Figure 4.6: Step-like potential experienced by electrons in a) a three-layered system, b) a five-layered system.

height v_{F2}/v_{F1} changes, for different values of S .

Figure 4.7 shows the chemical potential profiles for three- and five-layered systems with $S = 0.5$; this represents interfaces where there is a 50% probability that the electrons are scattered diffusely and 50% specularly. In the case where the thicknesses of the inner layers are much larger than an electron mean free path in these layers (Fig. 4.7a,b)), the chemical potential approaches constant values in the inner layers. This means that the interfaces are independent of each other, and the interface resistance of the N-interface system is found to be N times the resistance of one single interface R_1 , independently of the layer thicknesses as long as they are larger than the mean free path. Because of the diffuse scattering processes in the inner layers electrons lose their memory of the scattering at an interface and come to the next interface as if they were propagating in an infinite layer. In the second case, where the layer thicknesses are much smaller than the electron mean free path (Fig. 4.7c,d)), electrons retain a memory of the scattering from a previous interface; in this case the chemical potential does not approach a constant value, and different interfaces interact with each other, so that the interface resistance depends on the distance between the interfaces.

Figure 4.8 summarizes the behavior of the interface resistance in the multilayers as the thickness of the layers, amount of diffuse scattering at the interfaces, and the height of the potential barriers experienced by electrons at the interfaces change. Arbitrary units for resistance are used, as in the Fig. 4.5, since the calculations are performed irrespective of the particular metals. Figure 4.8a) shows how the resistance due to two interfaces, R_2 , in the trilayer system depends on the thickness $2d$ of the middle layer relative to the electron mean free path l_2 in this layer, for different amounts of diffuse scattering at the interfaces, and in the case where the electron Fermi velocity in the middle layer is twice smaller than the electron Fermi velocity in the outer layers, i.e.,

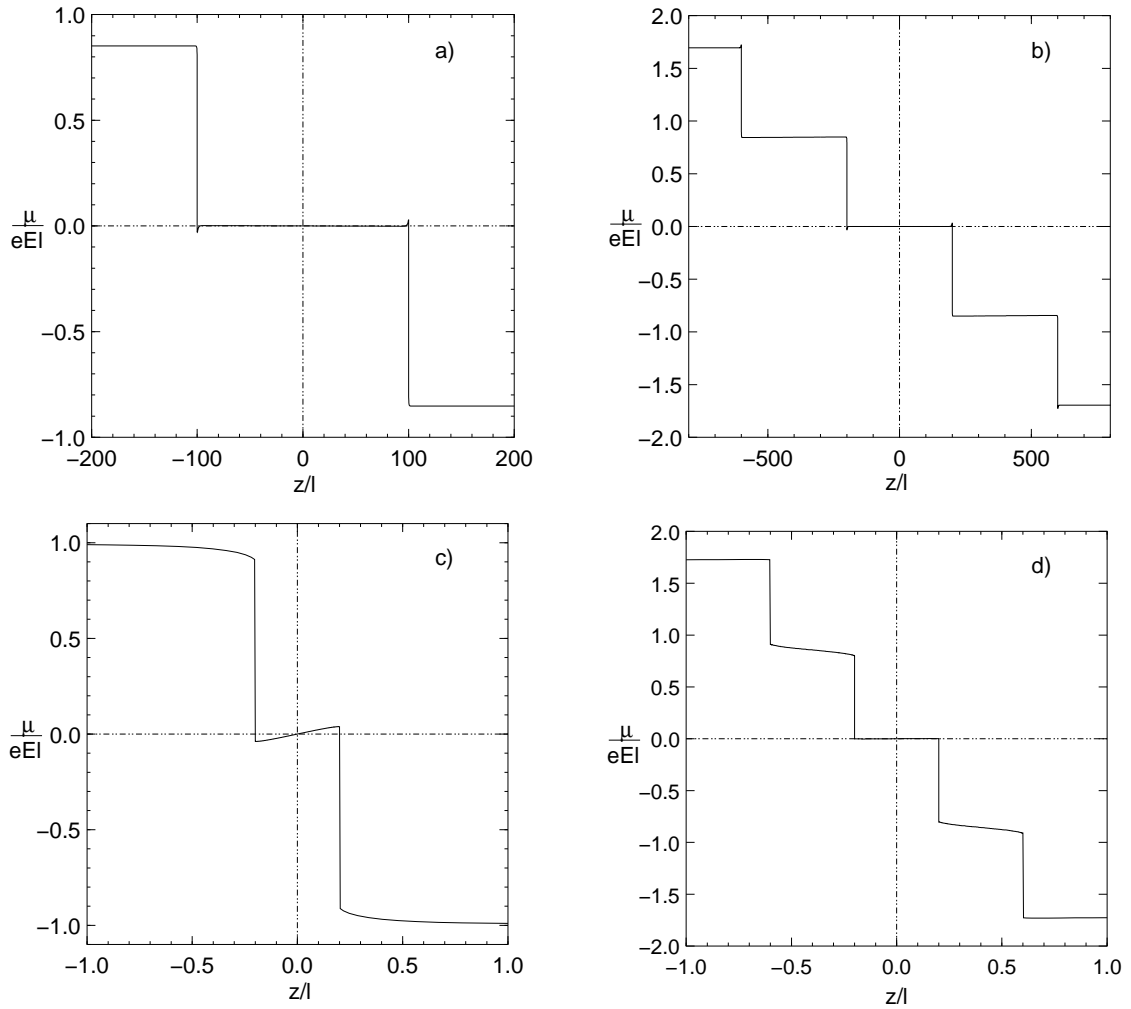


Figure 4.7: Chemical potential profiles for $S = 0.5$, normalized with respect to potential drop eEl within *each* layer: a) in the three-layered system with the middle layer thickness much larger than the electron mean-free path in the layer, b) in the five-layered system with the middle layers thicknesses much larger than the electron mean-free path in the layers, c) in the three-layered system with the middle layer thickness much smaller than the electron mean-free path in the layer, d) in the five-layered system with the middle layers thicknesses much smaller than the electron mean-free path in the layers.

$v_{F1} = 2v_{F2}$. When the thickness of the middle layer is large ($2d/l_2 \gg 1$), R_2 is independent of $2d$, and it is twice the resistance of one single interface R_1 . As the ratio $2d/l_2$ decreases, interface resistance in the trilayer system changes. For completely diffuse interfaces ($S = 0$) interface resistance decreases as $2d/l_2$ decreases. If a small amount of specular scattering is present at the interfaces, interface resistance at first increases significantly as $2d/l_2$ decreases, and then decreases abruptly when $2d/l_2$ becomes less than 0.2. As the amount of specular scattering at the interfaces grows (S reaches 1), the change in the interface resistance as $2d/l_2$ decreases becomes smaller.

In the Fig. 4.8b), the difference between the resistance due to the interfaces in the three-layered system R_2 and twice the resistance of the single interface between two semi-infinite layers $2R_1$ relative to $2R_1$ as a function of the electron Fermi velocities ratio v_{F2}/v_{F1} for different values of S at the interfaces and for $2d/l_2 = 0.4$ is shown. This difference represents the deviation from the resistors-in-series model. In the absence of the barrier ($v_{F2}/v_{F1} = 1$), resistance exists due to diffuse scattering, and $(R_2 - 2R_1)/2R_1 = 0$ for completely specular interfaces only. The deviation from the resistors-in-series model is the largest for the completely specular interfaces ($S = 1$) and $v_{F2}/v_{F1} = 1.4$. The shape of the potential barrier (whether the electrons experience a step up or step down at the interface between the first and the second layers) strongly influences the $(R_2 - 2R_1)/2R_1$ difference, as the plots are asymmetrical around $v_{F2}/v_{F1} = 1$, the ratio of the electron Fermi velocities that represents the absence of the barrier.

Similarly, Fig. 4.8c) shows the resistance due to four interfaces in a five-layered system as a function of the layers thickness $2d$ relative to the electron mean-free path in the second layer l_2 . Unlike in the three-layered system, the variation of the interface resistance with $2d/l_2$ is less pronounced for diffusive interfaces (S approaching 0), and more pronounced for specular interfaces (S approaching 1). Figure 4.8d) shows the deviation from the resistors-in-series model in the five-layered system, the difference between R_4 and $4R_1$ relative to $4R_1$ for different S and $2d/l_2 = 0.4$. As the number of steps experienced by the electrons grows from 2 in the three-layered system to 4 in the five-layered system, the actual shape of the barrier seems to play less important role in defining the $(R_N - NR_1)/NR_1$ difference as a function of v_{F2}/v_{F1} , as the plots for $(R_4 - 4R_1)/4R_1$ look symmetrical around $v_{F2}/v_{F1} = 1$. As in the three-layered system, the maximum deviation from the resistors-in-series model is obtained for completely specular interfaces; it reaches 15% for $v_{F2}/v_{F1} = 1.6$ and $v_{F2}/v_{F1} = 0.6$.

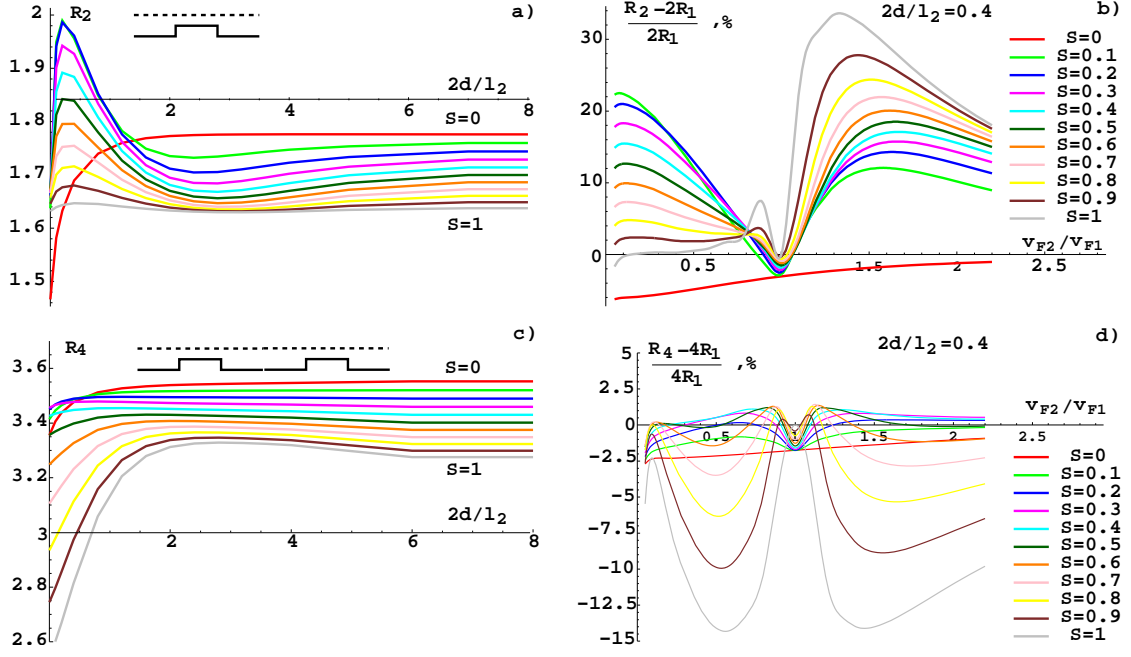


Figure 4.8: Summary of results for the three-layered and five-layered systems: a) resistance due to the interfaces R_2 of the three-layered system as a function of the middle layer thickness to the electron mean-free path in this layer ratio $2d/l_2$ for different values of diffuse scattering S at the interfaces and for the electron Fermi velocities ratio $v_{F2}/v_{F1} = 0.5$, b) percentage difference between R_2 and twice the resistance of the single interface between two semi-infinite layers $2R_1$ relative to $2R_1$ as a function of the electron Fermi velocities ratio v_{F2}/v_{F1} for different values of S at the interfaces and for $2d/l_2 = 0.4$, c) resistance due to the interfaces R_4 of the five-layered system as a function of $2d/l_2$ for different values of S at the interfaces and for $v_{F2}/v_{F1} = 0.5$, d) percentage difference between R_4 and four times the resistance of the single interface between two semi-infinite layers $4R_1$ relative to $4R_1$ as a function of v_{F2}/v_{F1} for different values of S at the interfaces and for $2d/l_2 = 0.4$, In the plots a) and c), arbitrary units for the resistance are used.

4.3 Co-Cu and Fe-Cr systems

In this section the resistance due to the interfaces in the realistic two-, three-, and five-layered Fe-Cr and Co-Cu systems is studied. The following cases are considered: 1) a FM \uparrow -N single interface, 2) FM \uparrow -N-FM $\uparrow(\downarrow)$ - a trilayer with parallel (anti-parallel) magnetization directions in the ferromagnetic layers, and 3) FM \uparrow -N-FM $\uparrow(\downarrow)$ -N-FM \uparrow - a five-layered system with parallel (anti-parallel) magnetization directions in the ferromagnetic layers (see Fig. 4.9). In the case of the five-layered system the thicknesses of the inner layers are taken to be the same, and the magnetization of the middle ferromagnetic layer only is changed. Majority and minority electrons experience different potential steps at the interfaces between magnetic and non-magnetic metals (see Fig. 4.10a)). The ratio of the electron Fermi velocities in the Fe-Cr systems $v_F(Cr)/v_F(Fe)$ is taken to be 0.837 for majority electrons, and 1.003 for minority electrons. [57] In the Co-Cu systems the ratio $v_F(Cu)/v_F(Co)$ is calculated to be 1.05 for majority electrons, and 1.18 for minority electrons (see appendix A.7.1). Interface resistances are calculated by assuming majority and minority channels to be independent, [3] so that the total resistance is the parallel combination of the resistances of up electrons R_{\uparrow} and down electrons R_{\downarrow} :

$$R = \frac{R_{\uparrow}R_{\downarrow}}{R_{\uparrow} + R_{\downarrow}}. \quad (4.4)$$

The step-like potentials experienced by electrons in the two-, three-, and five-layered Co-Cu and Fe-Cr structures are shown schematically in the Fig. 4.10. In order to find the resistances of up and down electrons R_{\uparrow} and R_{\downarrow} in each case a) through j) (see Fig. 4.10), equations (3.14)-(3.15), (A.15)-(A.19), and (A.20)-(A.28) were numerically solved with the reflection coefficients (4.1) and the appropriate parameters v_{F1} , v_{F2} , and v_{F3} . I present the correspondence between R_{\uparrow} , R_{\downarrow} , type of the structure, equations that need to be solved, and parameters v_{F1} , v_{F2} , and v_{F3} entering these equations in the Appendix A.7.2. In order to deduce the interface resistance from the jump of the chemical potential (Eq. (4.3)), the values of the electrons Fermi momentum in the non-magnetic layers are taken to be $k_{FCu} = 1.36A^{-1}$ for copper, and $k_{FCr} = 3.8A^{-1}$ for chromium. [57]

Figures 4.11 and 4.12 summarize the behavior of the resistance due to the interfaces in the Co-Cu multilayers with different magnetization configurations as I change the amount of the diffuse scattering S at the interfaces and the thickness of the layers $2d$ relative to the electron mean-free path l_{mfp} . Figure 4.11a) shows the resistance R_1 measured far from the interface between two semi-infinite layers of Co and Cu, and that

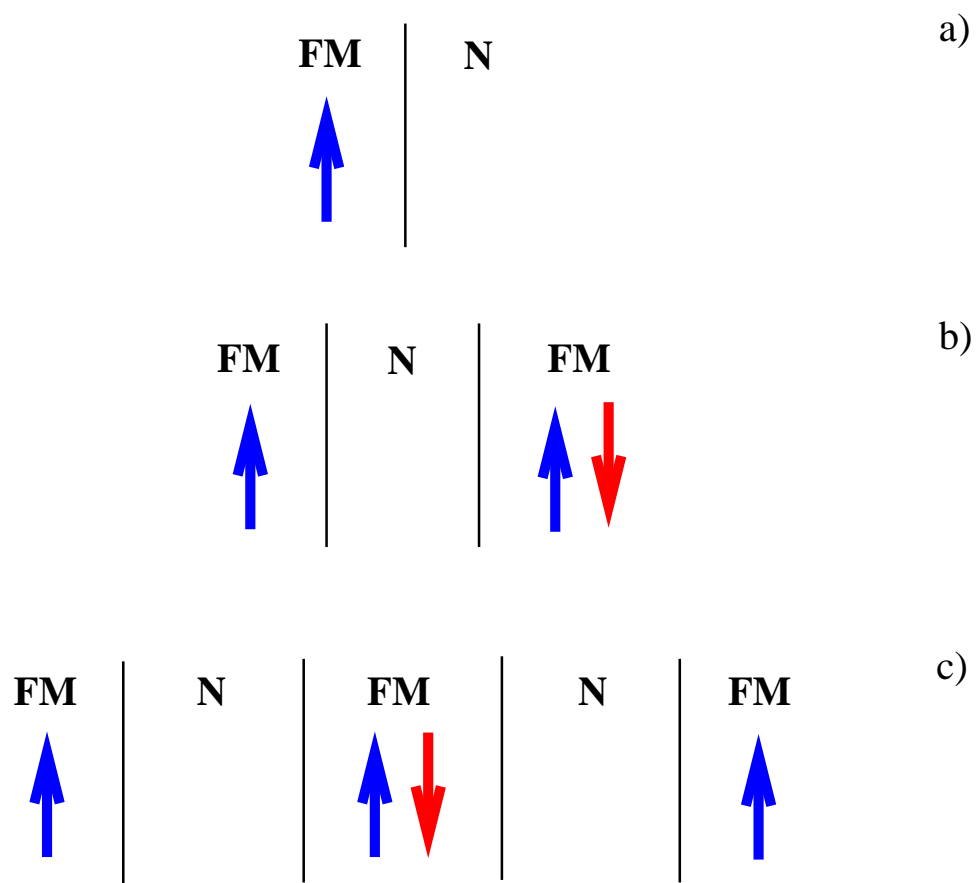


Figure 4.9: a) FM \uparrow -N single interface, b) FM \uparrow -N-FM $\uparrow(\downarrow)$ three-layered system, c) FM \uparrow -N-FM $\uparrow(\downarrow)$ -N-FM \uparrow five-layered system.

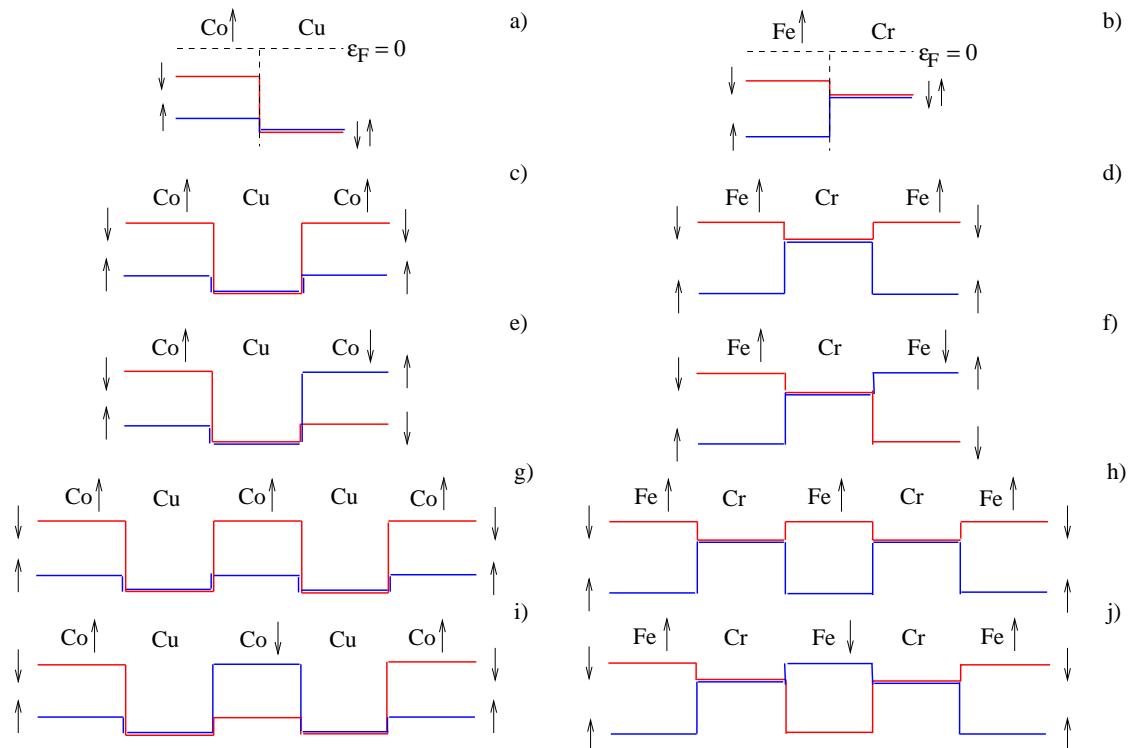


Figure 4.10: Step-like potentials experienced by up (blue) and down (red) electrons in the a)-b) Co-Cu and Fe-Cr structures, c)-d) Co-Cu-Co and Fe-Cr-Fe structures with parallel magnetizations of the ferromagnetic layers, e)-f) Co-Cu-Co and Fe-Cr-Fe structures with anti-parallel magnetizations of the ferromagnetic layers, g)-h) Co-Cu-Co-Cu-Co and Fe-Cr-Fe-Cr-Fe structures with parallel magnetizations, i)-j) Co-Cu-Co-Cu-Co and Fe-Cr-Fe-Cr-Fe structures with anti-parallel magnetizations.

measured right at the interface, R_0 , as the functions of S . For diffuse interfaces (S is close to zero), R_1 is larger than R_0 . Both R_1 and R_0 decrease as the amount of diffuse scattering at the interface decreases (S increases), but R_1 decreases faster, and there exists a value of parameter S when $R_1 = R_0$. The resistance R_0 becomes larger than R_1 for a specular interface. The relative difference between R_1 and R_0 (Fig. 4.11b)) is about 20% for completely diffuse interfaces; as the resistances decrease, this difference may reach more than 100%.

Figures 4.11c)-f) show the resistances due to the interfaces in the multilayers R_2 for three-layered systems and R_4 for five-layered systems as the functions of the layer thicknesses relative to the electron mean-free path for different amounts of diffuse scattering at the interfaces and different magnetization configurations (see Fig. 4.10). In all four geometries, resistance due to the interfaces decreases as the amount of diffuse scattering decreases (S changes from 0 to 1). Interface resistance is very small for completely specular interfaces, due to the very small potential barrier height that the majority electrons experience at the interface between Co and Cu, so that the majority channel shunts the current. As seen from the Figs. 4.11c)-f), resistance due to the interfaces in the multilayers do not depend on the thickness of the layers $2d$ relative to the electron mean-free path l_{mfp} when $2d/l_{mfp}$ is greater than 1, and they are found to be equal to the sum of resistances R_1 of the corresponding number of the independent interfaces, $2R_1$ or $4R_1$. As the thickness of the layers becomes much smaller than the mean-free path, $2d/l_{mfp} \ll 1$, resistances R_2 and R_4 start to deviate from $2R_1$ or $4R_1$, as predicted, indicating the breakdown of the resistors-in-series model.

Figures 4.12a)-d) show the deviations of the actual resistances R_2 and R_4 from the resistors-in-series model results, $2R_1$ or $4R_1$, relative to $2R_1$ or $4R_1$, as the functions of $2d/l_{mfp}$ for different amounts of diffuse scattering at the interfaces and different magnetization configurations. These deviations are not monotonic with $2d/l_{mfp}$. The difference between R_N and NR_1 is especially large for extreme interfaces, almost completely specular, S close to 1, or completely diffuse, S close to 0. (In the three-layered systems the plot for $S = 1$ is not shown, as it has a much larger scale than other plots.) It reaches 10-15% in the three-layered systems, 20% in the five-layered systems with the parallel magnetization directions, and 30% in the five-layered systems with the anti-parallel magnetization directions for completely specular interfaces.

Finally, Figs. 4.12e)-f) show the difference between actual resistance due to interfaces R_N ($N = 1, 2$, and 4) and the resistance that would be obtained assuming interfaces to be independent of each other as a function of the amount of diffuse scattering S at the interfaces. The thickness $2d$ of the non-magnetic layers is taken to be small com-

pared to the electron mean free path in the layers ($2d/l_{mfp}=0.4$). The actual resistance is compared with both the resistance of an independent interface measured right at the interface, NR_0 , and that measured far from the interface, NR_1 . In all geometries, both $(R_N - NR_1)/NR_1$ and $(R_N - NR_0)/NR_0$ are significant for either completely diffuse or completely specular interfaces. For the realistic interfaces where an equal amount of specular and diffuse scattering is present, $S = 0.5$, the difference between the interface resistance one could measure and the resistance of independent interfaces measured right at the interfaces, NR_0 , reaches 10%, which is comparable with the experimental error for the interface resistance. [23]

Figures 4.13 and 4.14 show the same information as the figures 4.11 and 4.12 for Fe-Cr systems. Similarly to the resistances in the Co-Cu systems, R_1 is larger than R_0 at small S , both R_0 and R_1 decrease as the interface becomes more specular (S approaching 1), R_1 decreasing faster (see Fig. 4.13a)). The difference with Co-Cu systems is that R_1 becomes equal to R_0 for S closer to 1. The relative difference between R_0 and R_1 is between 12 and 18% for S up to 0.9, (Fig. 4.13b)), after that the difference grows significantly (not shown). Resistances R_2 and R_4 for different magnetization configurations decrease as the amount of diffuse scattering at the interfaces decreases. In the case of the parallel magnetization directions both in the three- and five-layered structures, resistances of the completely specular interfaces are not shown, because they are small compared to the resistances for $S \neq 1$, due to the very small potential barrier experienced by minority electrons at the interface between Fe and Cr (smaller than that for majority electrons at the interface between Co and Cu). Resistance due to the interfaces depend on the thickness of the layers relative to the electron mean-free path, $2d/l_{mfp}$, as it becomes of the order or less then 1 (Fig. 4.13c)-f)). As it is for the Co-Cu systems, the deviation from the resistors-in-series model for Fe-Cr structures is substantial for extreme interfaces, with S close to 0 or 1 (Fig. 4.14a)-d)), but for the interfaces with $S = 0.5$, the difference between R_N and NR_0 reaches 20% for the systems with parallel magnetic configuration and more then 15% for the systems with anti-parallel magnetic configuration (Fig. 4.13e)). This exceeds experimental error, which is about 10% for the interface resistance and about 15% for the bulk resistance [23].

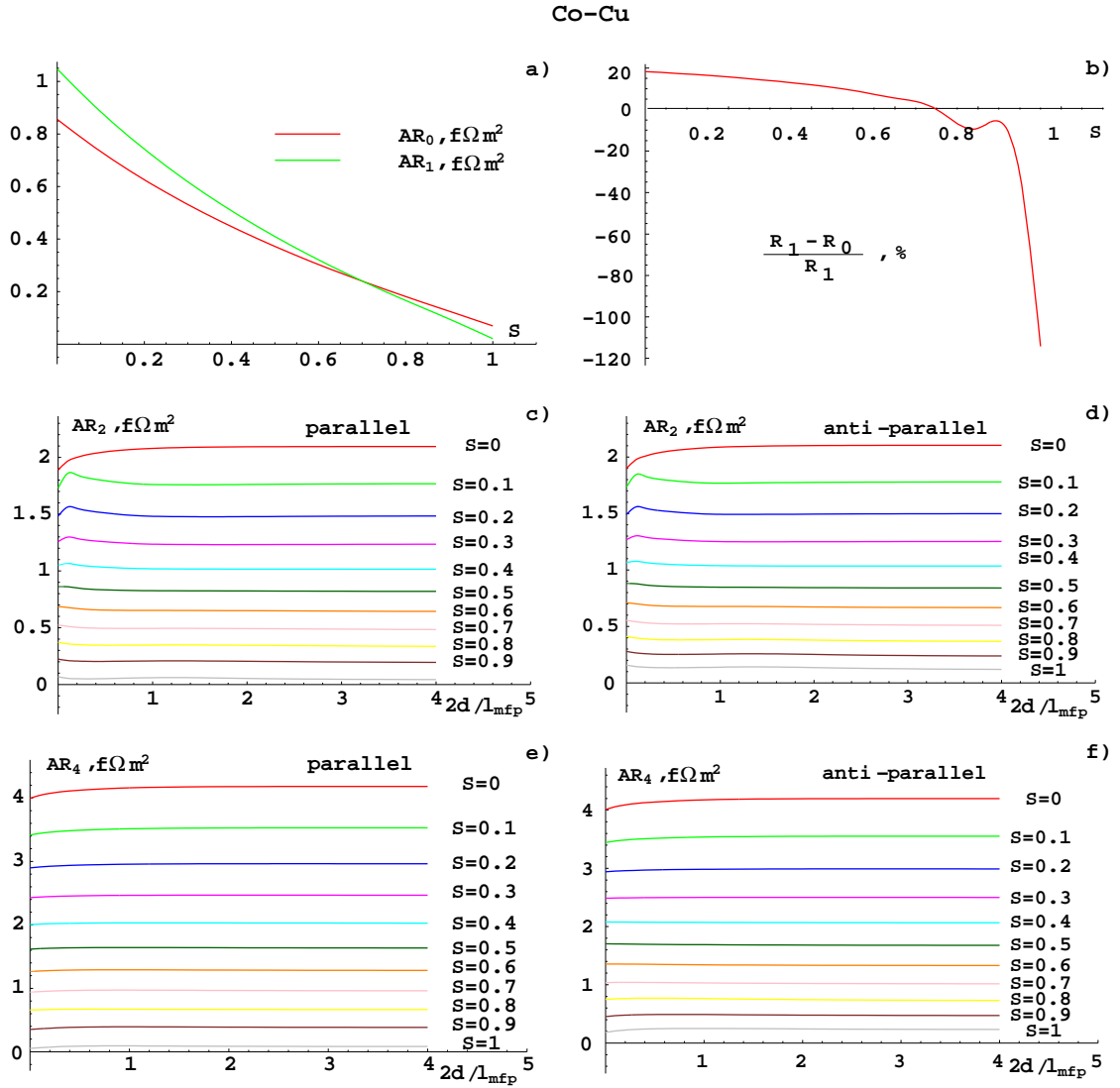


Figure 4.11: Resistances due to the interfaces in the Co-Cu systems: a) sheet resistance measured far from the interface, AR_1 , and that measured at the interface, AR_0 , in the two-layered systems as the functions of the amount of diffuse scattering S at the interface, b) the difference between R_1 and R_0 relative to R_1 in the two-layered systems as a function of S , c)-d) resistance R_2 as a function of the inner layer thickness relative to the mean-free path in the three-layered systems for different values of the diffuse scattering S and different magnetization configurations, e)-f) resistance R_4 as a function of the inner layers thicknesses relative to the mean-free path in the five-layered systems for different values of S and different magnetization configurations.

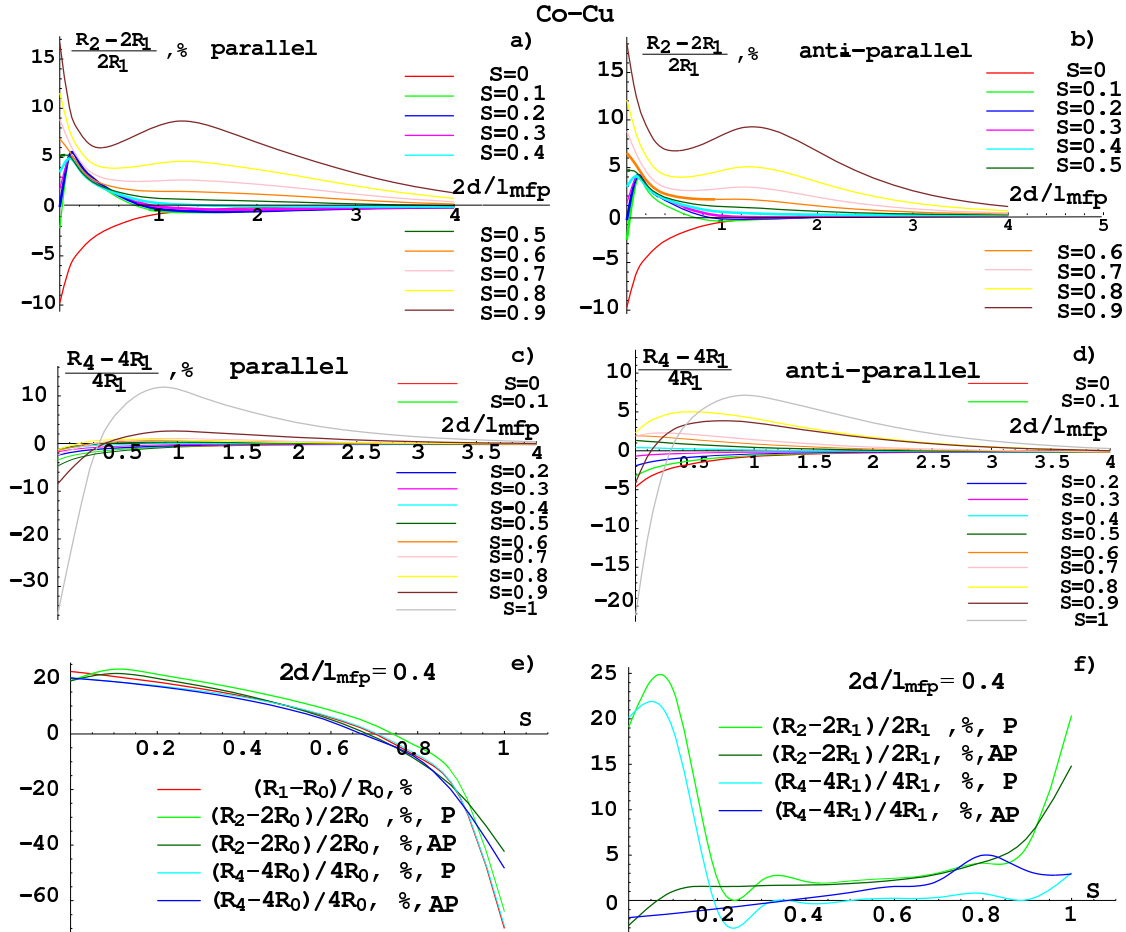


Figure 4.12: Deviations from the resistors-in-series model in the Co-Cu systems: a)-b) the difference between the resistance R_2 and twice the resistance of a single interface $2R_1$ relative to $2R_1$ as a function of the inner layer thickness $2d$ relative to the mean-free path l_{mfp} in the three-layered system for different values of S and different magnetization configurations, c)-d) the difference between the resistance R_4 and four times the resistance of a single interface, $4R_1$, relative to $4R_1$ as a function of $2d$ relative to l_{mfp} in the five-layered system for different values of S and different magnetization configurations, e) the difference between the resistances R_N , with $N = 1, 2, 4$ and N times the resistance R_0 , NR_0 , of a single independent interface measured right at the interface, relative to NR_0 , in the multilayers with $2d \ll l_{mfp}$ as a function of S for different magnetization configurations, f) the difference between the resistances R_N , with $N = 2, 4$ and N times the resistance R_1 of a single independent interface measured far from the interface, NR_1 , relative to NR_1 , in the multilayers with $2d \ll l_{mfp}$ as a function of S for different magnetization configurations.

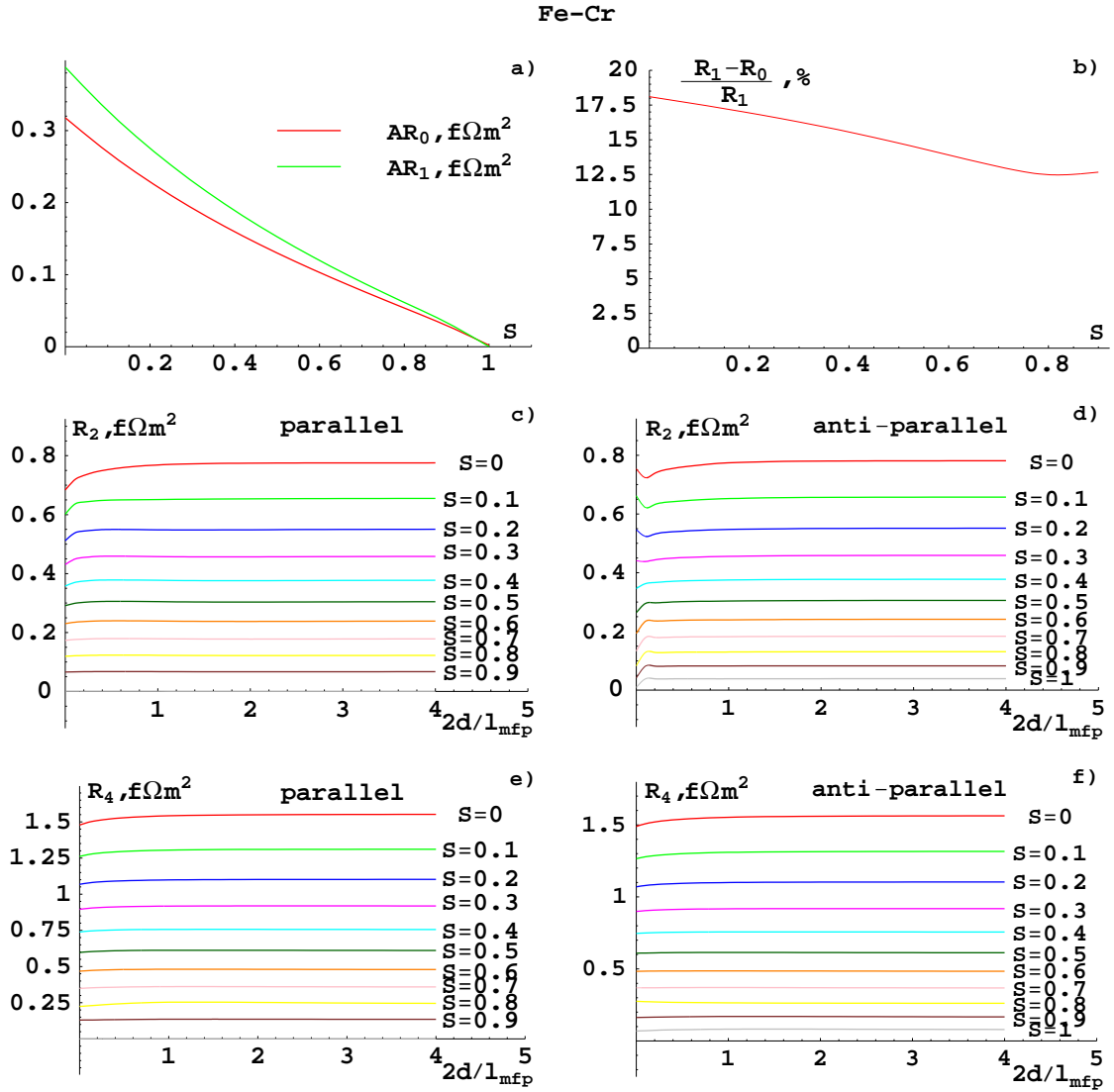


Figure 4.13: Resistances due to the interfaces in the Fe-Cr systems: a) sheet resistance measured far from the interface, AR_1 , and that measured at the interface, AR_0 , in the two-layered systems as the functions of the amount of diffuse scattering S at the interface, b) the difference between R_1 and R_0 relative to R_0 in the two-layered systems as a function of S (note the different S -axis limit), c)-d) resistance R_2 as a function of the inner layer thickness relative to the mean-free path in the three-layered systems for different values of the diffuse scattering S and different magnetization configurations, e)-f) resistance R_4 as a function of the inner layers thicknesses relative to the mean-free path in the five-layered systems for different values of S and different magnetization configurations.

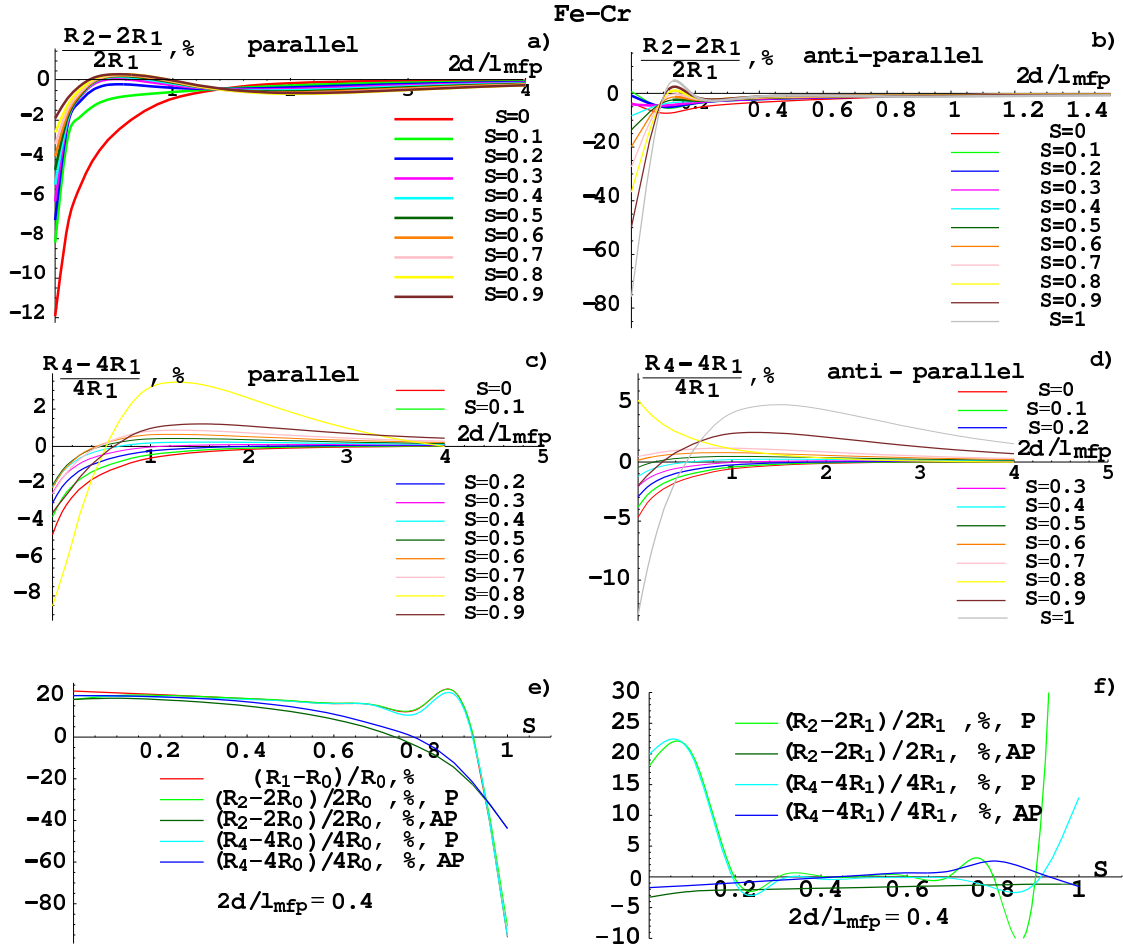


Figure 4.14: Deviations from the resistors-in-series model in the Fe-Cr systems: a)-b) the difference between the resistance R_2 and twice the resistance of a single interface $2R_1$ relative to $2R_1$ as a function of the inner layer thickness $2d$ relative to the mean-free path l_{mfp} in the three-layered system for different values of S and different magnetization configurations, c)-d) the difference between the resistance R_4 and four times the resistance of a single interface, $4R_1$, relative to $4R_1$ as a function of $2d$ relative to l_{mfp} in the five-layered system for different values of S and different magnetization configurations, e) the difference between the resistances R_N , with $N = 1, 2, 4$ and N times the resistance R_0 of a single independent interface measured right at the interface, NR_0 , relative to NR_0 , in the multilayers with $2d \ll l_{mfp}$ as a function of S for different magnetization configurations, f) the difference between the resistances R_N , with $N = 2, 4$ and N times the resistance R_1 of a single independent interface measured far from the interface, NR_1 , relative to NR_1 , in the multilayers with $2d \ll l_{mfp}$ as a function of S for different magnetization configurations.

Chapter 5

Spin-torques - theory

In the following two chapters, a mechanism of the magnetization switching of magnetic multilayers driven by a spin-polarized current is studied. First, I present a spin transfer model in which the equation of motion of the spin accumulation is solved in order to derive the torque acting on the background magnetization. Next, a system of two thick magnetic layers separated by a non-magnetic spacer is considered. The analytical expressions for the spin-current and spin-accumulation distributions in the system, and spin-torque and effective field acting on the local magnetization in the ferromagnetic layers are obtained, and I discuss the significance of the result for the spin-current at the interface between layers in the system with magnetization directions close to anti-parallel. Finally, the correction to the CPP magnetoresistance due to the interaction of the electron spins and background magnetization is calculated. In the next chapter, I present the results for a realistic multilayered structure.

5.1 Review of formalism

The linear response of the current to the electric field in the x -direction for diffusive transport, Eq. (2.26), can be written in a spinor form as [36]

$$\hat{j}(x) = \hat{C}E(x) - \hat{D}\frac{\partial \hat{n}}{\partial x}, \quad (5.1)$$

where $E(x)$ is the electric field, \hat{j} , \hat{C} , \hat{D} , and \hat{n} are the 2×2 matrices representing the current, the conductivity, the diffusion constant, and the charge and spin accumulations

at a given position. The diffusion constant and the conductivity are related via the Einstein relation $\hat{C} = e^2 \hat{N}(\epsilon_F) \hat{D}$ for a degenerate metal, where $\hat{N}(\epsilon_F)$ is the density of states at the Fermi level. In general, these matrices can be expressed in terms of the Pauli spin matrix σ as

$$\begin{cases} \hat{C} = C_0 \hat{I} + \sigma \cdot \mathbf{C}, \\ \hat{D} = D_0 \hat{I} + \sigma \cdot \mathbf{D}, \\ \hat{N} = N_0 \hat{I} + \sigma \cdot \mathbf{N}, \\ \hat{n} = n_0 \hat{I} + \sigma \cdot \mathbf{m}, \\ \hat{j} = j_e \hat{I} + \sigma \cdot \mathbf{j}_m, \end{cases} \quad (5.2)$$

where $2n_0$ is the charge accumulation, $2n_0 = n_\uparrow + n_\downarrow$, and \mathbf{m} is the spin-accumulation, $2|\mathbf{m}| = n_\uparrow - n_\downarrow$, n_\uparrow is the number of electrons with the spins parallel to the principal quantization axis, n_\downarrow is the number of electrons with the spins anti-parallel to the principal quantization axis, and, similarly, electric current $2j_e = j_\uparrow + j_\downarrow$, magnetization current $2|\mathbf{j}_m| = j_\uparrow - j_\downarrow$. Inserting Eqs. (5.2) in Eq. (5.1), the electric current j_e and magnetization current \mathbf{j}_m can be written as

$$j_e \equiv \text{Re}(\text{Tr} \hat{j}) = 2C_0 E(x) - 2D_0 \frac{\partial n_0}{\partial x} - 2\mathbf{D} \cdot \frac{\partial \mathbf{m}}{\partial x}, \quad (5.3)$$

$$\mathbf{j}_m \equiv \text{Re}(\text{Tr}(\sigma \hat{j})) = 2\mathbf{C}E(x) - 2\mathbf{D} \frac{\partial n_0}{\partial x} - 2D_0 \frac{\partial \mathbf{m}}{\partial x}, \quad (5.4)$$

where the units $e = \mu_B = 1$ are chosen for the notation convenience. The first term on the right hand side of Eq. (5.4) is the contribution to the spin polarized current from the electric field, the third term is the contribution from the spin accumulation, which is present in a magnetically inhomogeneous structure. The second term, the contribution coming from the charge accumulation, will be neglected, since its characteristic length-scale, of the order of several angstroms, is of the order of magnitude smaller than other relevant lengthscales. As will be shown below, in magnetic multilayers the contribution of the third term to the spin current can dominate over the first. Comparing Eq. (5.3) with the expression (2.26) for the electric current, the parameters C_0 and D_0 can be identified with $C_0 = \frac{1}{2}\sigma = \frac{k_F^3}{6\pi^2} \frac{e^2\tau}{m}$, $D_0 = \frac{1}{2}D = \frac{1}{6}v_F^2\tau = \frac{1}{6}v_F\lambda_{mfp}$, where $\lambda_{mfp} \equiv v_F\tau$ is the electron mean-free path.

For a transition metal ferromagnet, the spin-polarization parameter for the conductivity β , the diffusion constant β' , and for the density of states β'' can be defined as $\mathbf{C} = \beta C_0 \mathbf{M}_d$, $\mathbf{D} = \beta' D_0 \mathbf{M}_d$, and $\mathbf{N} = \beta'' N_0 \mathbf{M}_d$, where \mathbf{M}_d is the unit vector to represent the direction of the local (background) magnetization. Similarly to the spin-

polarization parameters for the interface, γ , γ' , and γ'' , introduced in the Appendix B.1, spin-polarization parameters for the bulk are related as $\beta' = (\beta - \beta'')/(1 - \beta\beta'')$ (compare with Eq. (B.34)). The experimental value for β can be found in the Ref. [23], and the value of β'' can be found from the bulk densities of states of up and down electrons, N_\uparrow and N_\downarrow , as $\beta'' = (N_\uparrow - N_\downarrow)/(N_\uparrow + N_\downarrow)$. Inserting the expressions for \mathbf{C} and \mathbf{D} in Eqs. (5.3) and (5.4), and eliminating the electric field and charge density, the following expression for the spin-current is obtained:

$$\mathbf{j}_m = \beta j_e \mathbf{M}_d - 2D_0 \left[\frac{\partial \mathbf{m}}{\partial x} - \beta \beta' \mathbf{M}_d (\mathbf{M}_d \cdot \frac{\partial \mathbf{m}}{\partial x}) \right]. \quad (5.5)$$

The equation of motion for the spin accumulation may be obtained by generalizing the continuity equation (2.24) to the systems with both spin-up and spin-down electrons, and including the possibility of spin-flip scattering. The continuity equation for the spin-up electrons density n_\uparrow (spin-down electrons density n_\downarrow) has the form

$$\frac{\partial n_{\uparrow(\downarrow)}}{\partial t} + \frac{\partial j_{\uparrow(\downarrow)}}{\partial x} = -\frac{n_{\uparrow(\downarrow)} - n_{\downarrow(\uparrow)}}{\tau_{sf}},$$

where τ_{sf} is the spin-flip relaxation time of the conduction electrons, and, for the spin-accumulation,

$$\frac{\partial |\mathbf{m}|}{\partial t} + \frac{\partial |\mathbf{j}_m|}{\partial x} = -\frac{2|\mathbf{m}|}{\tau_{sf}}.$$

Introducing the term $J/\hbar \mathbf{m} \times \mathbf{M}_d$ (see Chap. 1), the equation of motion for \mathbf{m} may be written as

$$\frac{\partial \mathbf{m}}{\partial t} + \frac{\partial \mathbf{j}_m}{\partial x} + \frac{J}{\hbar} \mathbf{m} \times \mathbf{M}_d = -\frac{2\mathbf{m}}{\tau_{sf}}. \quad (5.6)$$

Upon placing the expression for the magnetization current Eq. (5.5) in Eq. (5.6) one finds the following equation of motion for the spin-accumulation vector:

$$\begin{aligned} \frac{1}{2D_0} \frac{\partial \mathbf{m}}{\partial t} - \frac{\partial^2 \mathbf{m}}{\partial x^2} + \beta \beta' \mathbf{M}_d \left(\mathbf{M}_d \cdot \frac{\partial^2 \mathbf{m}}{\partial x^2} \right) &+ \frac{\mathbf{m}}{\lambda_{sf}^2} + \frac{\mathbf{m} \times \mathbf{M}_d}{\lambda_J^2} \\ &= -\frac{1}{2D_0} \frac{\partial}{\partial x} (\beta j_e \mathbf{M}_d), \end{aligned} \quad (5.7)$$

where $\lambda_{sf} \equiv \sqrt{D_0 \tau_{sf}}$ and $\lambda_J \equiv \sqrt{2\hbar D_0/J}$. The term on the right hand side of the

time dependent diffusion equation Eq. (5.7) for the spin accumulation is the source term; it is this term that drives the accumulation. [59] Following the conventional treatment of magnetic multilayers for current perpendicular to the plane of the layers, one can assume that the magnetization is uniform throughout a layer, and changes discontinuously between the layers. [60, 6] If one looks for the steady-state solutions of the equation (5.7), the first term on the left-hand side is zero, and the electric current j_e is constant throughout the multilayer; therefore one can see that the source term is confined to interfaces between the layers, and can be taken into account by appropriate boundary conditions. The boundary conditions at the diffusive interfaces between two layers with noncollinear magnetizations are addressed in detail in Appendix B.1. It is shown that while the spin-accumulation experiences a jump at the interfaces, proportional to the interface resistance, the spin-current is continuous across the diffusive interface, and no spin-torque is created at the interface. The specular scattering at the interfaces can also be taken into account within the semiclassical framework presented in this work, as it is done, for example, in Chap. 3; this involves considering each \mathbf{k} vector separately which for a noncollinear multilayer is a cumbersome problem, and it will not be addressed here. Below, the equations for the spin-accumulation and the effect of the spin-accumulation on the local magnetization in the bulk of the layers are discussed.

The equation of motion for the local magnetization \mathbf{M}_d is the Landau-Lifshitz-Gilbert equation

$$\frac{d\mathbf{M}_d}{dt} = -\gamma_0 \mathbf{M}_d \times (\mathbf{H}_e + J\mathbf{m}) + \alpha \mathbf{M}_d \times \frac{d\mathbf{M}_d}{dt}, \quad (5.8)$$

where γ_0 is the gyromagnetic ratio, \mathbf{H}_e is the magnetic field including the contributions from the external field, anisotropy and magnetostatic field, the additional effective field $J\mathbf{m}$ is due to coupling between the local moments and the spin accumulation, and the last term is the Gilbert damping term. Note that the characteristic time scale for the local moment is $\gamma_0^{-1} H_e$, of the order of nanoseconds for a magnetic field of 0.1 T, while the time scale of the spin accumulation is of the order of τ_{sf} and h/J , i.e., of the order of picoseconds. Therefore, the background magnetization can be assumed to be fixed on the time scale of the spin accumulation, and the steady state solution of the equation (5.7) can be considered.

By separating the spin accumulation into longitudinal (parallel to the *local* moment) and transverse (perpendicular to the *local* moment) modes, \mathbf{m}_{\parallel} and \mathbf{m}_{\perp} , and looking for

the steady state solutions, equation (5.7) can be written as

$$\frac{\partial^2 \mathbf{m}_{||}}{\partial x^2} - \frac{\mathbf{m}_{||}}{\lambda_{sdl}^2} = 0, \quad (5.9)$$

where $\lambda_{sdl} = \sqrt{1 - \beta\beta'}\lambda_{sf}$, and

$$\frac{\partial^2 \mathbf{m}_{\perp}}{\partial x^2} - \frac{\mathbf{m}_{\perp}}{\lambda_{sf}^2} - \frac{\mathbf{m}_{\perp} \times \mathbf{M}_d}{\lambda_J^2} = 0. \quad (5.10)$$

Note that the terms longitudinal and transverse refer to the magnetization in the individual layers, i.e., they are *locally* defined and have no global meaning throughout a noncollinear multilayer.

The longitudinal accumulation $\mathbf{m}_{||}$ decays at the length scale of the spin diffusion length λ_{sdl} , while the transverse spin accumulation \mathbf{m}_{\perp} decays as λ_J if one assumes $\lambda_J \ll \lambda_{sf}$. This assumption is valid for cobalt, for example. where the spin-diffusion length λ_{sdl} has been measured to be about 60 nm, β is 0.5, λ_{mfp} is about 6 nm, [23] $v_F = 0.6 \cdot 10^6$ m/s, $J = 0.3$ eV.[40] I estimate β' to be about 0.9 using the bulk densities of states for up and down electrons of 2.42 states/(atom Ry) and 13.42 states/(atom Ry) [61], so that $\lambda_{sf} = 80$ nm, $\lambda_J = 2$ nm, $\lambda_J \ll \lambda_{sf}$, and the transverse spin accumulation has a much shorter length scale compared to the longitudinal one. However, for permalloy, λ_{sdl} has been measured to be about 5 nm, β is 0.7, [23] β' is estimated to be about 0.95 using the bulk densities of states for up and down electrons of 2.4 states/Ry and 15 states/Ry [62, 63], so that λ_{sf} is about 9 nm. Taking the typical diffusion constant of a metal to be $D_0 = 10^{-3}$ m²/s, and $J = 0.1$ eV, [41], λ_J can be estimated to be 4 nm, comparable with λ_{sf} . The majority of the results presented in this work are obtained in the limit $\lambda_J \ll \lambda_{sf}$, so that they are applicable to cobalt. The structure consisting of two semi-infinite permalloy layers divided by a nonmagnetic spacer is considered separately below.

As seen from Eq. (5.8), the longitudinal spin accumulation has no effect on the local moment; therefore, one can re-write Eq. (5.8) in terms of the transverse spin accumulation only by replacing \mathbf{m} by \mathbf{m}_{\perp} :

$$\frac{d\mathbf{M}_d}{dt} = -\gamma_0 \mathbf{M}_d \times (\mathbf{H}_e + J\mathbf{m}_{\perp}) + \alpha \mathbf{M}_d \times \frac{d\mathbf{M}_d}{dt}. \quad (5.11)$$

In order to describe the transverse accumulation, it is convenient to introduce an aux-

iliary vector \mathbf{A} such that $J\mathbf{m}_\perp = \mathbf{A} \times \mathbf{M}_d$. [36] If one considers a system with two noncollinear ferromagnetic layers, the spin accumulation in one layer depends on the orientation of the other. Supposing that the above equation is used for the layer F1 (see Fig. 1.11), the local magnetization of this layer is labeled as $\mathbf{M}_d^{(1)}$, and the magnetization of the other layer is labeled as $\mathbf{M}_d^{(2)}$. Without loss of generality, the vector \mathbf{A} can be written as a linear combination of the vector $\mathbf{M}_d^{(2)}$, and the vector perpendicular to $\mathbf{M}_d^{(2)}$, for example, $\mathbf{A} = a\mathbf{M}_d^{(2)} - b\mathbf{M}_d^{(2)} \times \mathbf{M}_d^{(1)}$, so that the two components of the accumulation in the plane perpendicular to $\mathbf{M}_d^{(1)}$ are written as

$$J\mathbf{m}_\perp = a\mathbf{M}_d^{(2)} \times \mathbf{M}_d^{(1)} + b\mathbf{M}_d^{(1)} \times (\mathbf{M}_d^{(2)} \times \mathbf{M}_d^{(1)}), \quad (5.12)$$

where a and b are determined by geometric details of the multilayer. By placing this form of the accumulation in the equation of motion for the background magnetization, Eq. (5.11), one finds the following equation of motion for $\mathbf{M}_d^{(1)}$:

$$\frac{d\mathbf{M}_d^{(1)}}{dt} = -\gamma_0 \mathbf{M}_d^{(1)} \times (\mathbf{H}_e + b\mathbf{M}_d^{(2)}) - \gamma_0 a \mathbf{M}_d^{(1)} \times (\mathbf{M}_d^{(2)} \times \mathbf{M}_d^{(1)}) + \alpha \mathbf{M}_d \times \frac{d\mathbf{M}_d}{dt}. \quad (5.13)$$

Thus the transverse spin accumulation produces two effects simultaneously: the term $b\mathbf{M}_d^{(1)} \times \mathbf{M}_d^{(2)}$ is the torque due to an "effective field" $b\mathbf{M}_d^{(2)}$, and the other is $a\mathbf{M}_d^{(1)} \times (\mathbf{M}_d^{(2)} \times \mathbf{M}_d^{(1)})$ is called the "spin torque" predicted in the Refs. [7, 8, 9, 10, 11]. The first term produces a precessional motion about $\mathbf{M}_d^{(1)}$; in this sense it acts *as if* the spin current creates a magnetic field on $\mathbf{M}_d^{(1)}$ (see Fig. 5.1). The second term acts so as to increase or decrease the angle between $\mathbf{M}_d^{(1)}$ and $\mathbf{M}_d^{(2)}$; also, it acts so as to assist or oppose the damping term in Eq. (5.8). Note that both the spin-torque and effective field terms appear on an equal footing in the equation (5.13), as both are related to the transverse spin accumulation.

The torque transmitted by the current to the background may also be determined from the following considerations. The torque τ acting on the background angular momentum \mathbf{M}_d is the time derivative of \mathbf{M}_d , $\tau = d\mathbf{M}_d/dt$. The *total* angular momentum of the system, which is the sum of the electron angular momentum \mathbf{m} and the background angular momentum \mathbf{M}_d is conserved, so that $\mathbf{m} + \mathbf{M}_d = \text{const}$. The torque acting on the background magnetization can be written in terms of the electron spin accumulation and spin current as

$$\tau = -\frac{d\mathbf{m}}{dt} = -\frac{\partial \mathbf{m}}{\partial t} - \frac{\partial \mathbf{j}_m}{\partial x},$$

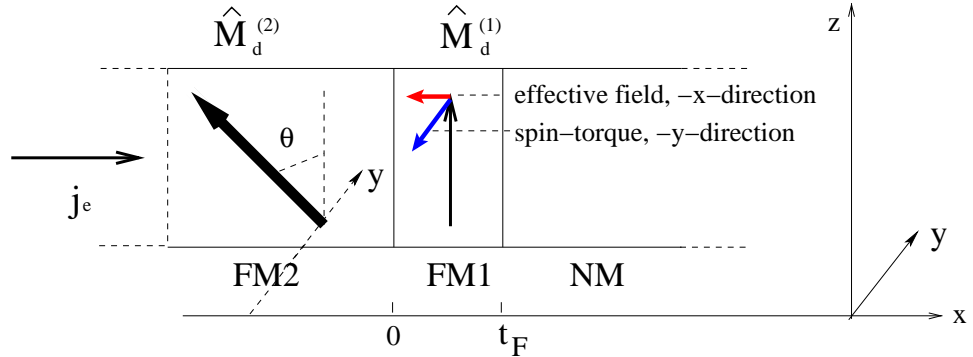


Figure 5.1: Direction of the effective field (red vector) and spin-torque (blue vector) acting on a thin FM layer background magnetization $\hat{\mathbf{M}}_d^{(1)} = \mathbf{e}_z$, if the magnetization of the thick layer is $\hat{\mathbf{M}}_d^{(2)} = \cos \theta \mathbf{e}_z - \sin \theta \mathbf{e}_y$.

so that the torque transmitted by a steady-state current is given by the *gradient* of the spin current. Integrating this over a layer with the thickness d which absorbs the momentum, one finds

$$\Delta\tau = - \int_0^d \frac{\partial \mathbf{j}_m}{\partial x} dx = \mathbf{j}_m(0) - \mathbf{j}_m(d). \quad (5.14)$$

The total torque absorbed by the layer is the difference between the spin current values at the boundaries of the layer.

5.2 Two ferromagnetic layers

In order to illustrate the method developed in Sec. 5.1 to determine the effective field and spin-torque acting on the ferromagnetic layer, I choose a simplified system where I can analytically derive the spin accumulation, spin-current, effective field, and spin-torque. I consider a system consisting of two thick ferromagnetic layers with the magnetizations $\hat{\mathbf{M}}_d^{(1)} = \cos \theta \mathbf{e}_z + \sin \theta \mathbf{e}_y$ and $\hat{\mathbf{M}}_d^{(2)} = \cos \theta \mathbf{e}_z - \sin \theta \mathbf{e}_y$, where x is the direction of the electric current (see Fig. 5.2), separated by a nonmagnetic spacer layer so that there is no exchange coupling between ferromagnetic layers, and backed by nonmagnetic layers, or leads. The nonmagnetic spacer layer thickness is considered to be small compared to the spin-diffusion length in the nonmagnetic metal ($\lambda_{sdl}^N \sim 600$ nm), so that both spin accumulation and spin current are constant in the spacer, and I will use both terms "spacer" and "interface between magnetic layers" interchangeably. The thickness of

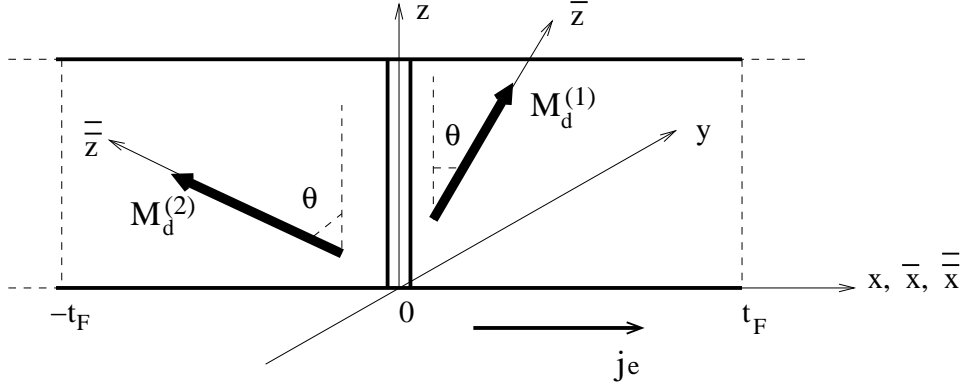


Figure 5.2: System of two thick ferromagnetic layers separated by a spacer layer and backed by nonmagnetic layers, or leads. Magnetization of the first (right) layer is $\mathbf{M}_d^{(1)} = \cos \theta \mathbf{e}_z + \sin \theta \mathbf{e}_y$, magnetization of the left (second) layer is $\mathbf{M}_d^{(2)} = \cos \theta \mathbf{e}_z - \sin \theta \mathbf{e}_y$. (x, y, z) is the global coordinate system, $(\bar{x}, \bar{y}, \bar{z})$ and $(\tilde{x}, \tilde{y}, \tilde{z})$ are the local coordinate systems connected to the local magnetizations in the first and second layers.

the ferromagnetic layers t_F is large enough so that one can neglect the reflections from the outer boundaries of the layers. The difference between this system and the system considered in the Ref. [36] is that in the latter, the second layer is assumed to be half metallic, so that the current is fully spin-polarized, while here this approximation is abandoned.

I solve Eqs. (5.9) and (5.10) to find the longitudinal and transverse spin accumulation in both ferromagnetic layers, and use Eq. (5.5) to find the spin-current. In the local coordinate system $(\bar{x}, \bar{y}, \bar{z})$ connected to the local magnetization of the right layer, the spin-accumulation and spin current take the following form:

$$\begin{cases} m_{\bar{z}}^{(1)} = G_1 \exp(-x/\lambda_{sdl}) \\ m_{\bar{x}}^{(1)} = 2\text{Re}(G_2 \exp(-x/l_+)) \\ m_{\bar{y}}^{(1)} = 2\text{Im}(G_2 \exp(-x/l_+)), \end{cases} \quad (5.15)$$

$$\begin{cases} j_{m,\bar{z}}^{(1)} = \beta j_e + \frac{2D_0(1-\beta\beta')}{\lambda_{sdl}} G_1 \exp(-x/\lambda_{sdl}) \\ j_{m,\bar{x}}^{(1)} = 4D_0 \operatorname{Re} \left(G_2 \frac{\exp(-x/l_+)}{l_+} \right) \\ j_{m,\bar{y}}^{(1)} = 4D_0 \operatorname{Im} \left(G_2 \frac{\exp(-x/l_+)}{l_+} \right), \end{cases} \quad (5.16)$$

where G_1 and G_2 are constants of integration, and

$$\frac{1}{l_+} = \sqrt{\frac{1}{\lambda_{sf}^2} - \frac{i}{\lambda_J^2}} \approx \frac{1-i}{\sqrt{2}\lambda_J} \quad (5.17)$$

when $\lambda_J \ll \lambda_{sf}$. Similar expressions for the local spin-accumulation and spin-current are written for the second layer.

To determine the constants of integration, the boundary conditions at the interface between two ferromagnetic layers have to be invoked. The boundary conditions are discussed in detail in Appendix B.1. At a diffusive interface, the spin-current is conserved, and the spin-accumulations to the left and to the right of the interface in the global (x, y, z) coordinate system are related as follows:

$$\begin{cases} m_x(0-) - m_x(0+) = 2j_{m,x}(0)r\frac{\lambda_J}{\sqrt{2}D_0} \\ m_y(0-) - m_y(0+) = 2j_{m,x}(0) \left(\cos^2 \theta + \frac{\sin^2 \theta}{(1-\gamma\gamma')} \right) r\frac{\lambda_J}{\sqrt{2}D_0} \\ m_z(0-) - m_z(0+) = -\gamma j_e \cos \theta r\frac{\lambda_J}{\sqrt{2}(1-\gamma\gamma')D_0} + 2j_{m,x}(0) \left(\sin^2 \theta + \frac{\cos^2 \theta}{(1-\gamma\gamma')} \right) r\frac{\lambda_J}{\sqrt{2}D_0}, \end{cases}$$

where r is proportional to the interface resistance AR_I (see Eq. (B.35)), γ and γ' are the spin polarization parameters for the conductivity and the diffusion constant at the interface (see Eq. (B.5)). Note that the spin-accumulation is conserved across the interface if there is no diffuse scattering at the interface ($AR_I = 0$). Vectors in the local and global coordinate systems are related via the rotation matrix (see Eq.(B.20)), and the constants of integration are

$$G_1 = -\frac{\beta j_e}{\sqrt{2}\lambda_J J} \frac{\hbar a_0^3}{e\mu_B} \times \frac{\sin^2 \theta (1 + \bar{r}) + \frac{\bar{r}(1-\gamma/\beta)}{1-\gamma\gamma'} \cos^2 \theta}{\cos^2 \theta (1 + \frac{\bar{r}\lambda}{1-\gamma\gamma'}) + \lambda \sin^2 \theta (1 + \bar{r})} \quad (5.18)$$

$$G_2 = \frac{\beta j_e}{2\sqrt{2}\lambda_J J} \frac{\hbar a_0^3}{e\mu_B} \times \frac{(1 + \bar{r}t\lambda) \sin 2\theta}{\cos^2 \theta (1 + \frac{\bar{r}\lambda}{1 - \gamma\gamma'}) + \lambda \sin^2 \theta (1 + \bar{r})} (1 - i), \quad (5.19)$$

where $\lambda = (1 - \beta\beta')\lambda_J/\sqrt{2}\lambda_{sdl}$, $t = \gamma/\beta(1 - \gamma\gamma')$, $\bar{r} = \sqrt{2}AR_I e^2 N_0^I(\epsilon_F) D_0(1 - \gamma''^2)/\lambda_J(1 - \gamma\gamma')$, AR_I is the resistance of the interface between two ferromagnetic layers, β , β' are spin-polarization parameters for conductivity and diffusion constant in the bulk of the layers, γ , γ' , γ'' are spin-polarization parameters for conductivity, diffusion constant, and electron density of states at the interface; $N_0^I(\epsilon_F)$ is the density of states at the interface at Fermi energy (see Appendix B.1). The expressions for the spin-accumulation in the right layer are

$$\begin{cases} m_x^{(1)} = 2e^{-\frac{x}{\sqrt{2}\lambda_J}} \operatorname{Re} G_2 [\cos \frac{x}{\sqrt{2}\lambda_J} + \sin \frac{x}{\sqrt{2}\lambda_J}] \\ m_y^{(1)} = -2e^{-\frac{x}{\sqrt{2}\lambda_J}} \operatorname{Re} G_2 [\cos \frac{x}{\sqrt{2}\lambda_J} - \sin \frac{x}{\sqrt{2}\lambda_J}] \cos \theta + G_1 e^{-\frac{x}{\lambda_{sdl}}} \sin \theta \\ m_z^{(1)} = 2e^{-\frac{x}{\sqrt{2}\lambda_J}} \operatorname{Re} G_2 [\cos \frac{x}{\sqrt{2}\lambda_J} - \sin \frac{x}{\sqrt{2}\lambda_J}] \sin \theta + G_1 e^{-\frac{x}{\lambda_{sdl}}} \cos \theta. \end{cases} \quad (5.20)$$

In the left layer they are

$$\begin{cases} m_x^{(2)}(x) = m_x^{(1)}(-x) \\ m_y^{(2)}(x) = m_y^{(1)}(-x) \\ m_z^{(2)}(x) = -m_z^{(1)}(-x). \end{cases}$$

The spin-current in the layers can be found from Eq. (5.5). The expressions for the components of \mathbf{j}_m are complicated, and I will only present the values of the x -, y -, and z -components of \mathbf{j}_m at $x = 0$, in the nonmagnetic spacer, in the absence of the scattering at the interface. Due to the symmetry of the problem, only the z -component is non zero, so that

$$\mathbf{j}_m(x = 0) = \frac{\beta j_e \cos \theta}{\cos^2 \theta + \lambda \sin^2 \theta} \mathbf{e}_z, \quad (5.21)$$

where $\lambda = \sqrt{1 - \beta\beta'}\lambda_J/\sqrt{2}\lambda_{sf}$, and it is of the order of 0.02 for cobalt. The spin current at the interface reaches its maximum value of

$$j_{m,max}(x = 0) = \frac{\beta j_e \cos \theta^*}{2\lambda} \quad (5.22)$$

when the angle between the local magnetizations is $2\theta^*$, where

$$\cos 2\theta^* = -\frac{1-3\lambda}{1-\lambda}, \quad (5.23)$$

and $2\theta^*$ is close to π when $\lambda \ll 1$. The magnitude of the spin-current is enhanced by a large factor of λ^{-1} compared to the bare spin-current $\beta j_e \cos \theta$. This enhancement comes from the interplay between longitudinal and transverse accumulations; it is the result of the global nature of the spin-current even though the transverse components of the spin current and accumulation are absorbed within a region of several λ_J of the interface. While the total spin torque acting on a symmetric two-layered structure is zero, the result of Eq. (5.21) can serve as an indication that in the non-symmetric structure when one layer is pinned and the other free; the spin-torque acting on the free layer, and, hence, the angular momentum transferred to it, exceeds the transverse component of the bare portion of the incoming spin-current by $1/2\lambda$. This prediction will be tested in the next chapter, where the non-symmetric three-layered system is discussed.

The spin-torque a_1 and the effective field b_1 acting on the ferromagnetic layer can be found from the following considerations. From Eq. (5.15), the transverse spin-accumulation in the right layer can be written as

$$\mathbf{m}_\perp^{(1)} = \mathbf{m}_{\bar{x}}^{(1)} \mathbf{e}_{\bar{x}} + \mathbf{m}_{\bar{y}}^{(1)} \mathbf{e}_{\bar{y}} = 2\text{Re}(G_2 \exp(-x/l_+)) \mathbf{e}_{\bar{x}} + 2\text{Im}(G_2 \exp(-x/l_+)) \mathbf{e}_{\bar{y}}, \quad (5.24)$$

where $\mathbf{e}_{\bar{x}}$ and $\mathbf{e}_{\bar{y}}$ are unit vectors in the *local* coordinate system. By noticing that G_2 can be written as $\tilde{G}_2 \sin 2\theta$, $\mathbf{M}_d^{(2)} \times \mathbf{M}_d^{(1)} = -\sin 2\theta \mathbf{e}_{\bar{x}}$, $\mathbf{M}_d^{(1)} \times (\mathbf{M}_d^{(2)} \times \mathbf{M}_d^{(1)}) = -\sin 2\theta \mathbf{e}_{\bar{y}}$, one can write $\mathbf{m}_\perp^{(1)}$ as

$$\begin{aligned} \mathbf{m}_\perp^{(1)} &= -2\text{Re}(\tilde{G}_2 \exp(-x/l_+)) \mathbf{M}_d^{(2)} \times \mathbf{M}_d^{(1)} \\ &\quad - 2\text{Im}(\tilde{G}_2 \exp(-x/l_+)) \mathbf{M}_d^{(1)} \times (\mathbf{M}_d^{(2)} \times \mathbf{M}_d^{(1)}). \end{aligned} \quad (5.25)$$

One can see that the form of the transverse spin-accumulation given by Eq. (5.25) is exactly the form used in the definition of a and b (Eq.(5.12)):

$$J\mathbf{m}_\perp = a\mathbf{M}_d^{(2)} \times \mathbf{M}_d^{(1)} + b\mathbf{M}_d^{(1)} \times (\mathbf{M}_d^{(2)} \times \mathbf{M}_d^{(1)}). \quad (5.26)$$

To obtain the coefficients a and b , one averages the spin-accumulation (5.25) over the thickness t_F of the right layer. The spin-torque and effective field *per unit length* acting

on the ferromagnetic layer take the form

$$a_1 = -\frac{\beta j_e}{2\sqrt{2}\lambda_J} \frac{\hbar a_0^3}{e\mu_B} \times \frac{1 - \cos(\frac{t_F}{\sqrt{2}\lambda_J}) e^{-\frac{t_F}{\sqrt{2}\lambda_J}}}{t_F/(\sqrt{2}\lambda_J)} \times \frac{(1 + \bar{r}t\lambda)}{\cos^2 \theta(1 + \frac{\bar{r}\lambda}{1-\gamma\gamma'}) + \lambda \sin^2 \theta(1 + \bar{r})}, \quad (5.27)$$

$$b_1 = \frac{\beta j_e}{2\sqrt{2}\lambda_J} \frac{\hbar a_0^3}{e\mu_B} \times \frac{\sin(\frac{t_F}{\sqrt{2}\lambda_J}) e^{-\frac{t_F}{\sqrt{2}\lambda_J}}}{t_F/(\sqrt{2}\lambda_J)} \times \frac{(1 + \bar{r}t\lambda)}{\cos^2 \theta(1 + \frac{\bar{r}\lambda}{1-\gamma\gamma'}) + \lambda \sin^2 \theta(1 + \bar{r})}. \quad (5.28)$$

Note that in order to get the true torque and field acting on the ferromagnetic layers, the coefficients a and b has to be multiplied by $\sin 2\theta$ (see Eq. (5.26)).

Both spin-torque $a \sin 2\theta$ and effective field $b \sin 2\theta$ reach their maximum value when $\theta = \theta^{**}$ where

$$\cos 2\theta^{**} = -\frac{1 - \lambda}{1 + \lambda} \quad (5.29)$$

in the absence of the interface resistance; we see that θ^{**} is close to 90° .

In the second layer, the spin-torque a_2 is equal to $-a_1$, and the effective field b_2 is equal to $-b_1$ due to the symmetry of the problem.

In Fig. 5.3 I present the spin accumulation and spin current distribution in the FM-Sp-FM structure with $\lambda_J = 4$ nm, $\lambda_{sdl} = 60$ nm in the presence of the interface resistance $AR_I = 0.5$ f Ω \cdot m 2 ; [23] the diffusion constant is taken to be 10^{-3} m 2 /s. Both \mathbf{m} and \mathbf{j}_m are constant in the spacer, so I don't show the spacer in these plots. As follows from Eq. (5.20), the characteristic length scale of the x-component of the accumulation, perpendicular to the plane of the layer magnetizations, is λ_J . *Global* y- and z-components of spin accumulation are defined by both transverse and longitudinal *local* components of the accumulation, so for them, two length scales may be distinguished: one of the order of λ_J for a more rapid change of the spin accumulation, and the longer one, of the order of the spin-diffusion length λ_{sdl} . Only the z-component of the spin accumulation is discontinuous in the presence of the interface resistance due to the symmetry of the problem. Far from the interfaces, $x \gg \lambda_J$ and $x \ll -\lambda_J$, the spin current is collinear with background magnetization $\mathbf{M}_d^{(1)}$ or $\mathbf{M}_d^{(2)}$, approaching its bare values $\mathbf{j}_m = \beta j_e \mathbf{M}_d^{(1)}$ or $\mathbf{j}_m = \beta j_e \mathbf{M}_d^{(2)}$. As follows from the equation (5.21), a large amplification of z-component of the spin-current occurs within a distance of several λ_J from the interface.

In Fig. 5.4 I show the spin-torque and effective field per unit length acting on the first ferromagnetic layer as a function of the thickness of the layers t_F relative to $\sqrt{2}\lambda_J$.

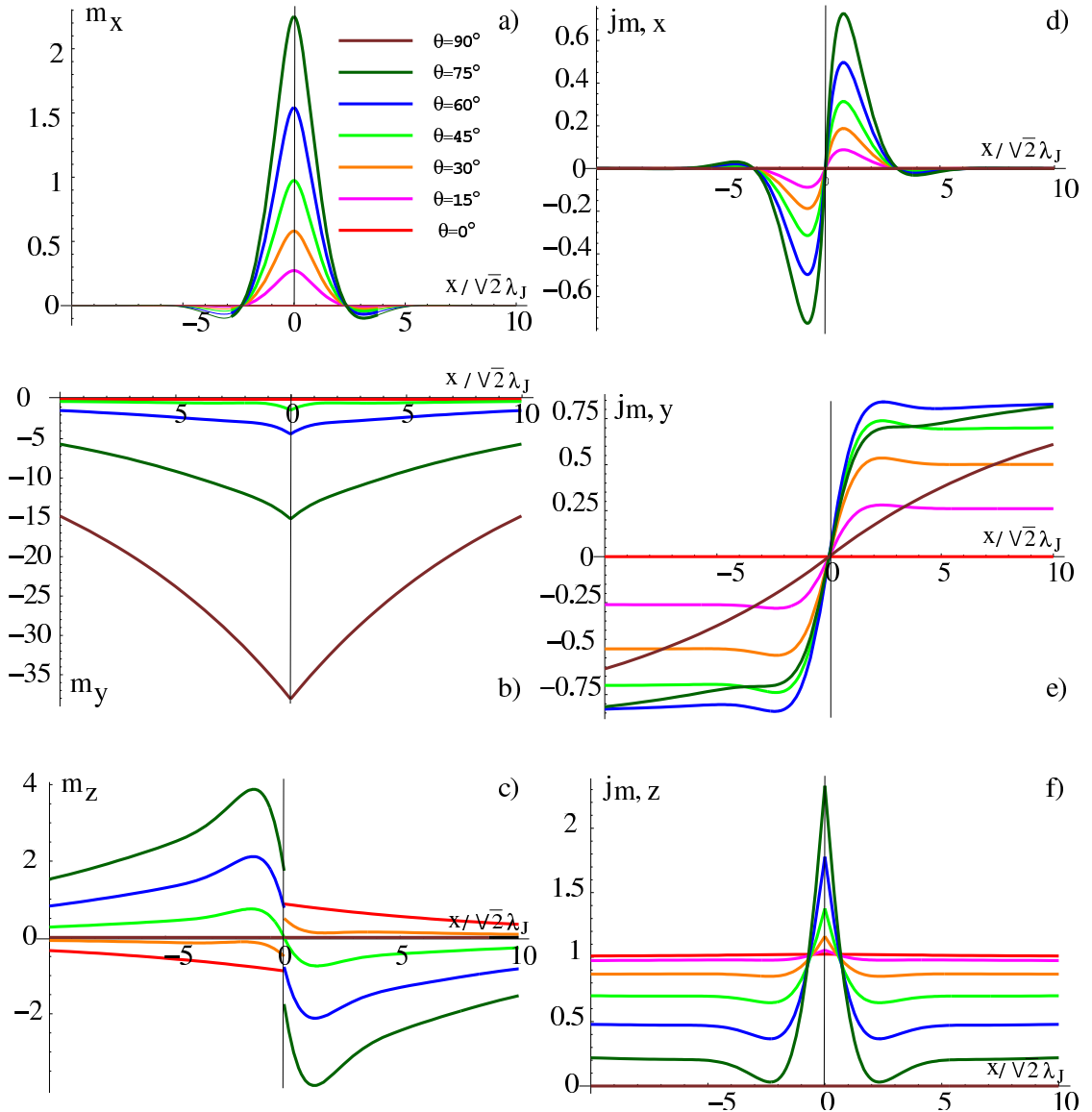


Figure 5.3: x -, y -, and z -components of the spin-accumulation $\mathbf{m}/(\beta j_e/\sqrt{2}\lambda_J J)(\hbar a_0^3/e\mu_B)$ (a-c) and spin-current $\mathbf{j}_m/\beta j_e$ (d-f) distribution in FM-Sp-FM system in the presence of interface resistance for $\lambda_J = 4$ nm, $\lambda_{sdl} = 60$ nm and different angles θ .

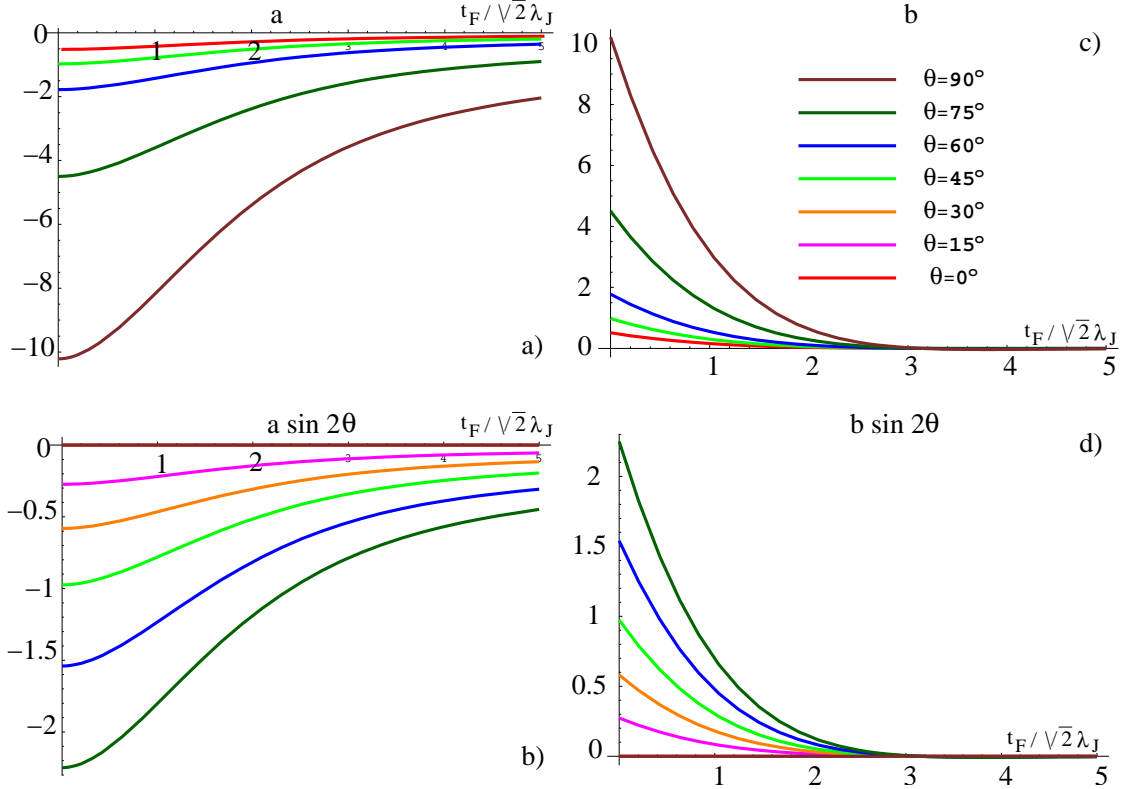


Figure 5.4: Spin-torque $a/\beta j_e(\hbar a_0^3/e\mu_B)$ and (b) $a \sin 2\theta/\beta j_e(\hbar a_0^3/e\mu_B)$, (c) effective field $b/\beta j_e(\hbar a_0^3/e\mu_B)$ and (d) $b \sin 2\theta/\beta j_e(\hbar a_0^3/e\mu_B)$ acting on the FM layer in FM-Sp-FM system as a function of $t_F/\sqrt{2}\lambda_J$ in the presence of interface resistance for $\lambda_J = 4$ nm, $\lambda_{sdl} = 60$ nm and different angles θ .

One can see that while the torque and field terms a and b (Fig. 5.4a) and c)) are largest for $\theta = 90^\circ$, they don't act on the background magnetization, since $\sin 2\theta = 0$. The true torque and field $a \sin 2\theta$ and $b \sin 2\theta$ (Fig. 5.4b) and d)) are largest for θ close to 90° (see Eq. (5.29)). It is worth noting that while the effective field decreases much faster than the spin torque as the thickness of the layers increases, at their maximum, they have the same magnitude, so they indeed have to appear on an equal footing in the equation of motion for the local magnetization.

5.3 Correction to CPP resistance

The normalized angular dependence of the resistance can be defined as [43]

$$R_{norm} = \frac{R(2\theta) - R(0)}{R(2\pi) - R(0)}, \quad (5.30)$$

and the data was fit to

$$R_{norm} = \frac{1 - \cos^2(\theta)}{1 + \chi \cos^2(\theta)}. \quad (5.31)$$

I calculate the angular dependence of the CPP resistance based on the spin currents that are found using the diffusion equation for the spin accumulation in noncollinear structures as follows.

The resistivity of a system is a proportionality coefficient between electric field and electric current, $E = \rho j_e$. From Eq. (5.3), electric current can be written in terms of the longitudinal spin accumulation $\mathbf{m}_{||}$ as

$$j_e = 2C_0 E - 2D_0 \beta' \frac{\partial m_{||}}{\partial x}, \quad (5.32)$$

where in the right layer $m_{||} \equiv m_{\bar{z}} = G_1 \exp(-x/\lambda_{sdl})$, in the left layer $m_{||} \equiv m_{\bar{z}} = -G_1 \exp(x/\lambda_{sdl})$ (see Eq. (5.15)), G_1 is defined by Eq. (5.18). The resistivity of the first (right) and the second (left) layers then takes the form:

$$\rho_{1,2} = \frac{1 - \frac{2D_0\beta'}{\lambda_{sdl}} \frac{G_1}{j_e} \exp(\mp x/\lambda_{sdl})}{2C_0}. \quad (5.33)$$

The sheet resistance of the whole system can be found by integrating the resistivity over the x -coordinate from $-t_F$ to t_F , and adding the interface resistance AR_I ; I find

$$AR(\theta) = \frac{t_F}{C_0} \left(1 + \frac{\beta\beta'\lambda}{(1 - \beta\beta')} \frac{(1 + \bar{r})(1 - \gamma\gamma') \sin^2 \theta + \bar{r}(1 - \gamma/\beta) \cos^2 \theta}{(1 - \gamma\gamma' + \bar{r}\lambda) \cos^2 \theta + \lambda(1 + \bar{r})(1 - \gamma\gamma') \sin^2 \theta} \right) + AR_I, \quad (5.34)$$

where θ is half of the angle between magnetizations. The parameter χ then takes the following form:

$$\chi = -1 + \frac{1}{\lambda(1 + \bar{r})} + \frac{\bar{r}}{(1 + \bar{r})(1 - \gamma\gamma')}, \quad (5.35)$$

where $\lambda = (1 - \beta\beta')\lambda_J/(\sqrt{2}\lambda_{sdl})$, $\bar{r} = \sqrt{2}AR_Ie^2N_0^I(\epsilon_F)D_0(1 - \gamma''^2)/\lambda_J(1 - \gamma\gamma')$, e is the electron charge, N_0^I is the density of states at the interface, D_0 is the diffusion constant in the bulk, γ , γ' , γ'' are the spin-polarization parameters for the conductivity, diffusion constant, and density of states at the interface (see Appendix B.1). For cobalt, I estimate χ to be about 60 if I take $\lambda_J = 2$ nm, $\lambda_{sdl} = 60$ nm, $D_0 = 10^{-3}$ m²/s, $\beta = 0.5$, $\gamma = 0.75$, $N_\uparrow = 2.42$ states/(atom Ry), $N_\downarrow = 13.42$ states/(atom Ry) for the bulk, $N_\uparrow = 1.83$ states/(atom Ry), $N_\downarrow = 17.75$ states/(atom Ry) for the interface (with Cu), so that $\beta' = 0.9$, $\gamma' = 0.97$, $N_0^I(\epsilon_F) = 6.5 \cdot 10^{28}$ states/m³eV. To my knowledge, there is no experimental data for the value of χ for cobalt, so my result can not be compared with the experimental one. Below, I present a calculation for permalloy, for which an experimental value of χ exists.[43]

5.4 Permalloy

For permalloy, the approximation $\lambda_J \ll \lambda_{sf}$ is not valid, so one has to use the exact expression for l_+ (see Eq. (5.17)),

$$\frac{1}{l_+} = \sqrt{\frac{1}{\lambda_{sf}^2} - \frac{i}{\lambda_J^2}} = \frac{c - id}{\sqrt{2}\lambda_J} \quad (5.36)$$

where $c = \sqrt{(\lambda_J/\lambda_{sf})^2 + \sqrt{(\lambda_J/\lambda_{sf})^4 + 1}}$, $d = \sqrt{-(\lambda_J/\lambda_{sf})^2 + \sqrt{(\lambda_J/\lambda_{sf})^4 + 1}}$. Note that for cobalt $c \approx d \approx 1$. In the absence of the interface resistance, I obtain the following analytical expressions for spin-accumulation distribution, spin-torque, and effective field:

$$\begin{cases} m_x^{(1)} = 2e^{-\frac{cx}{\sqrt{2}\lambda_J}} [\text{Re}G_2 \cos \frac{dx}{\sqrt{2}\lambda_J} - \text{Im}G_2 \sin \frac{dx}{\sqrt{2}\lambda_J}] \\ m_y^{(1)} = -2e^{-\frac{cx}{\sqrt{2}\lambda_J}} [\text{Re}G_2 \cos \frac{dx}{\sqrt{2}\lambda_J} + \text{Im}G_2 \sin \frac{dx}{\sqrt{2}\lambda_J}] \cos \theta + G_1 e^{-\frac{x}{\lambda_{sdl}}} \sin \theta \\ m_z^{(1)} = 2e^{-\frac{cx}{\sqrt{2}\lambda_J}} [\text{Re}G_2 \cos \frac{dx}{\sqrt{2}\lambda_J} + \text{Im}G_2 \sin \frac{dx}{\sqrt{2}\lambda_J}] \sin \theta + G_1 e^{-\frac{x}{\lambda_{sdl}}} \cos \theta, \\ a = -\frac{J}{c^2 + d^2} \frac{1 - \cos(\frac{dt_F}{\sqrt{2}\lambda_J})e^{-\frac{ct_F}{\sqrt{2}\lambda_J}}}{t_F/(\sqrt{2}\lambda_J)} (c\text{Re}\tilde{G}_2 - d\text{Im}\tilde{G}_2) \end{cases}$$

$$- \frac{J}{c^2 + d^2} \frac{\sin(\frac{dt_F}{\sqrt{2}\lambda_J}) e^{-\frac{ct_F}{\sqrt{2}\lambda_J}}}{t_F/(\sqrt{2}\lambda_J)} (d \operatorname{Re}\tilde{G}_2 + c \operatorname{Im}\tilde{G}_2), \quad (5.37)$$

$$\begin{aligned} b &= \frac{J}{c^2 + d^2} (c \operatorname{Re}\tilde{G}_2 - d \operatorname{Im}\tilde{G}_2) \frac{\sin(\frac{t_F}{\sqrt{2}\lambda_J}) e^{-\frac{t_F}{\sqrt{2}\lambda_J}}}{t_F/(\sqrt{2}\lambda_J)} \\ &- \frac{J}{c^2 + d^2} (d \operatorname{Re}\tilde{G}_2 + c \operatorname{Im}\tilde{G}_2) \frac{1 - \cos(\frac{dt_F}{\sqrt{2}\lambda_J}) e^{-\frac{ct_F}{\sqrt{2}\lambda_J}}}{t_F/(\sqrt{2}\lambda_J)}, \end{aligned} \quad (5.38)$$

where

$$G_1 = -\frac{\beta j_e \sqrt{2} \hbar a_0^3}{\lambda_J J e \mu_B} \times \frac{c \sin^2 \theta}{(c^2 + d^2) \cos^2 \theta + 2c\lambda \sin^2 \theta} \quad (5.39)$$

$$G_2 = \tilde{G}_2 \sin 2\theta = -\frac{\beta j_e}{\sqrt{2}\lambda_J J e \mu_B} \frac{\hbar a_0^3}{\sin 2\theta} \times \frac{(d - ic) \sin 2\theta}{(c^2 + d^2) \cos^2 \theta + 2c\lambda \sin^2 \theta}. \quad (5.40)$$

The parameter χ (Eq. 5.31) for permalloy takes the form

$$\chi = -1 + \frac{c^2 + d^2}{2c\lambda}, \quad (5.41)$$

where

$$\begin{aligned} c &= \sqrt{(\lambda_J/\lambda_{sf})^2 + \sqrt{(\lambda_J/\lambda_{sf})^4 + 1}} \\ &= \sqrt{(1 - \beta\beta')(\lambda_J/\lambda_{sdl})^2 + \sqrt{(1 - \beta\beta')^2(\lambda_J/\lambda_{sdl})^4 + 1}}, \\ c^2 + d^2 &= 2\sqrt{(\lambda_J/\lambda_{sf})^4 + 1} = 2\sqrt{(1 - \beta\beta')^2(\lambda_J/\lambda_{sdl})^4 + 1}, \\ \lambda &= \frac{(1 - \beta\beta')}{\sqrt{2}} \frac{\lambda_J}{\lambda_{sdl}}. \end{aligned}$$

Taking λ_J to be 4 nm, λ_{sdl} to be 5 nm, $\beta = 0.7$, $\beta' = 0.95$ (see Sec. 5.1), I estimate χ to be about 3.8. This number has to be compared with the experimentally obtained $\chi = 1.17$. [43] While the theoretical value of χ is more than three times larger than the experimental one, it is calculated without taking into account the resistance of the interface between permalloy layers; the presence of the interface resistance leads to a

smaller value of χ (see Eq. (5.35)).

Chapter 6

Spin-torques in the thin FM - thick FM - NM structure

In this chapter, I consider a realistic pillar-like multilayered structure used for current induced reversal of a magnetic layer [64, 65, 66] consisting of a thick ferromagnetic layer, whose primary role is to polarize the current, and whose magnetization is pinned, a thin ferromagnetic layer that is to be switched, a nonmagnetic spacer layer so that there is no interlayer exchange coupling between the thick and thin layers, and nonmagnetic layer or lead in the back of the thin magnetic layer, Fig. 6.1. The lead in the back of the thick magnetic layer does not have to be considered, because the thickness of the left ferromagnetic layer is taken to exceed the spin diffusion length λ_{sdl} in this layer; the spin polarization of the current is dictated by the thick magnetic layer. As in the symmetrical structure considered in the previous chapter, the thickness of the nonmagnetic spacer layer t_{Sp} is taken to be small compared to the spin-diffusion length in the nonmagnetic metal ($\lambda_{sdl}^N \sim 600$ nm), so that both spin accumulation and spin current are constant in the spacer, and all the results are obtained in the approximation that $t_{Sp} = 0$. The majority of the results for the spin-current, spin-accumulation, spin-torque, and effective field acting on the local magnetization in the thin magnetic layer are obtained numerically using the MathematicaTM software, [67] and presented in Sec. 6.1. Next, I derive an analytical expression for the transverse spin-current at the interface between two ferromagnetic layers within an approximation that the thickness of the thin FM layer t_F is much smaller than the spin-flip length λ_{sf} , but much larger than the characteristic length scale of the transverse spin accumulation λ_J . Finally, I study the angular dependence of the resistance of the structure described above.

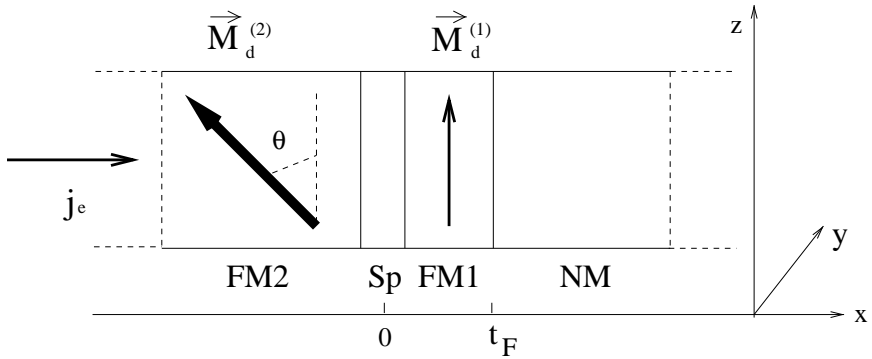


Figure 6.1: Multilayered pillar-like structure used for current induced reversal of a magnetic layer. FM2 is a thick ferromagnetic layer with the thickness exceeding λ_{sdl}^F and local magnetization $\vec{M}_d^{(2)} = \cos \theta \mathbf{e}_z - \sin \theta \mathbf{e}_y$, Sp is a thin nonmagnetic spacer, FM1 is a thin ferromagnetic layer with the thickness t_F and local magnetization $\vec{M}_d^{(1)} = \mathbf{e}_z$, and NM is a nonmagnetic back layer.

6.1 Numerical results

In order to find the spin accumulation and spin current distributions in the structure depicted in Fig 6.1, I solve Eqs. (5.9) and (5.10) in the thick ferromagnetic layer, thin ferromagnetic layer, and nonmagnetic back layer, and find the spin current using Eq. (5.5) (see appendix B.2). In Appendices B.1 and B.2 I derive the boundary conditions on the accumulation and current at the interface between the thick and thin ferromagnetic layers, and at the interface between the thin magnetic layer and the nonmagnetic layer; with these one can determine the spin current across the entire structure, and consequently the spin torque and effective field acting on the thin magnetic layer. In the absence of specular scattering at the interfaces, spin current is continuous across the whole system; the spin accumulation is discontinuous across the diffusive interfaces, the discontinuity being proportional to the interface resistance, and continuous across the interface with zero resistance. I assume that there is neither specular nor diffuse scattering at the interface between the thin ferromagnetic layer and nonmagnetic layer, and that there is no specular scattering at the interface between ferromagnetic layers. I obtain all the results both in the absence and in the presence of the diffuse scattering at this interface. Without further simplifications I am unable to give analytic expressions for the accumulation and current across the multilayer, and I present the numerical results for these quantities

as well as the torque and field they create. In all the plots below, the diffusion constant is taken to be 10^{-3} m²/s in the magnetic layers, and $5 \cdot 10^{-3}$ m²/s in the nonmagnetic layers, and the spin diffusion length in the nonmagnetic layers λ_{sdl}^N is taken to be 600 nm. The amount of diffuse scattering at the interface AR_I , the spin polarization parameters for the conductivity γ at the interface and β in the bulk of magnetic layers β are taken from the experimental data on CPP-MR, $AR_I(1 - \gamma^2) = 0.5$ fO $\text{m} \cdot \text{m}^2$, $\gamma = 0.75$, $\beta = 0.5$. [23] Other spin polarization parameters are obtained using the results of the *ab-initio* calculations of the density of states for up and down electrons. [61]

In Figs. 6.2-6.5 I show the *total* (not per unit length as in the previous chapter for a symmetrical structure) spin torque $a \sin \theta t_F$ and effective field $b \sin \theta t_F$ as a function of the thickness of the thin magnetic layer t_F which is being switched for different combinations of λ_J , λ_{sdl} , AR_I , and for different angles θ between the magnetization directions in the layers. Two values of λ_J are chosen for illustration, $\lambda_J = 4$ nm, which is comparable to the mean free path $\lambda_{mfp} = 6$ nm, and a smaller value of $\lambda_J = 1$ nm; λ_{sdl} is taken to be 60 nm and 30 nm. One can see that while the spin torque rapidly increases for small but finite $t_F \approx \lambda_J$ and then gradually levels off (Figs. 6.2-6.3), the effective field is largest about $t_F \approx 0.5\lambda_J$ and then decreases toward zero with t_F (Figs. 6.4-6.5); this can be understood as follows. When the thickness of the thin layer t_F is much smaller than λ_J , the spin accumulation in the thin layer is the same as that of the thick layer at the interface, and its direction is parallel to that of the magnetization of the thick layer $\mathbf{M}_d^{(2)}$ (note that I do not consider torques created directly at the interface between the ferromagnetic layers); therefore, as follows from the definition of a and b , $J\mathbf{m}_\perp = a\mathbf{M}_d^{(2)} \times \mathbf{M}_d^{(1)} + b\mathbf{M}_d^{(1)} \times (\mathbf{M}_d^{(2)} \times \mathbf{M}_d^{(1)})$ (Eq. (5.12)), only the effective field b can exist, since only the second term has a component along $\mathbf{M}_d^{(2)}$. As t_F increases, the spin accumulation in the thin magnetic layer rotates away from $\mathbf{M}_d^{(2)}$ and develops a transverse component, parallel to $\mathbf{M}_d^{(2)} \times \mathbf{M}_d^{(1)}$, i.e., a spin torque a develops. When t_F becomes larger than λ_J , the spin accumulation is further rotated in the thin layer, out of the plane of $\mathbf{M}_d^{(2)}$ and $\mathbf{M}_d^{(1)}$, and thus the component of the spin accumulation in the plane of the magnetizations decreases rapidly, i.e., the effective field diminishes faster than the torque. As t_F increases further there are no additional contributions to either the field and torque because they represent effects that are centered at the interface with the spacer layer and averaged over the entire thickness of the thin magnetic layer. Although the effective field is negligible compared to the torque in the limit of large t_F , it is noteworthy that at its maximum the field b is at least as large as a , so that both spin torque and effective field should enter the equation of motion of the background

magnetization, Eq. (5.8). One also notes that while the torque and field terms a and b are largest for $\theta = 180^\circ$ and 0° , they do not act on the background magnetization because $\sin \theta = 0$. The largest effects are found for θ close to 180° (see below). Comparing the figures 6.2 and 6.3, 6.4 and 6.5, one can see that interface resistance decreases both spin torque and effective field, and causes the spin torque to achieve saturation for slightly smaller t_F . Comparing the diagrams a) and c), b) and d) at each of the Figs. 6.2-6.5, one notices that when the spin diffusion length is reduced from $\lambda_{sdl} = 60$ nm to $\lambda_{sdl} = 30$ nm, the spin torque and effective field are reduced. Comparing the diagrams a) and b), c) and d) at each of the Figs. 6.2-6.5, one can see that when the spin transfer length is reduced from $\lambda_J = 4$ nm to $\lambda_J = 1$ nm, the spin torque achieves saturation for smaller t_F and the effective field is increased and peaks for lower t_F .

In Figs. 6.6-6.9 I show the spin accumulation and spin current distribution in the thick FM-thin FM-NM system both in the absence and in the presence of the interface resistance for $\lambda_J = 4$ nm, $\lambda_{sdl} = 60$ nm, for different angles θ between magnetization directions in the layers, and for two different thicknesses t_F of the thin ferromagnetic layer. I choose $t_F = 3$ nm, smaller than λ_J , but where the spin torque $a \sin \theta t_F$ starts to saturate, and $t_F = 15$ nm, much larger than λ_J , but smaller than λ_{sdl} . The magnetization in the thin layer $\mathbf{M}_d^{(1)}$ is taken as the global z axis; the current is along the x axis which is along the growth direction of the multilayer, and the y direction is perpendicular to the other two. In these global axes, longitudinal and transverse in the thin magnetic layer refers to the directions z and $x - y$; however for the thick layer, whose magnetization $\mathbf{M}_d^{(2)}$ is at an angle θ relative to $\mathbf{M}_d^{(1)}$, the global y and z axes do not define what is meant by longitudinal and transverse in this layer.

Comparing the figures 6.6 and 6.8, 6.7 and 6.9, one notices that the diffuse scattering at the interface between the ferromagnetic layers produces sizable discontinuities in the accumulation at the interface (see Appendices B.1 and B.2), but it does not lead to an increased spin torque (see Figs. 6.2-6.5); this result is different from the ones obtained within other models.

One can see that far from the interface $x \ll -\lambda_J$ the accumulation and current in the thick layer are collinear with background magnetization $\mathbf{M}_d^{(2)}$, i.e., referred to its local axes they are longitudinal with no transverse components, and the spin current approaches its bare value $\mathbf{j}_m \rightarrow \beta j_e \mathbf{M}_d^{(2)}$ (see Eq. (5.5)), as one expects in the bulk of a ferromagnet. Even though one still has a longitudinal spin accumulation in the region $-\lambda_{sdl} \ll x \ll -\lambda_J$ its gradient is small compared to that of the transverse accumulation which makes large contributions to the spin current in the region $x > -\lambda_J$. This is clear from the plots for m_x and $j_{m,x}$ which go to zero, while $m_y \rightarrow m \sin \theta$, $j_{m,y} \rightarrow \beta j_e \sin \theta$,

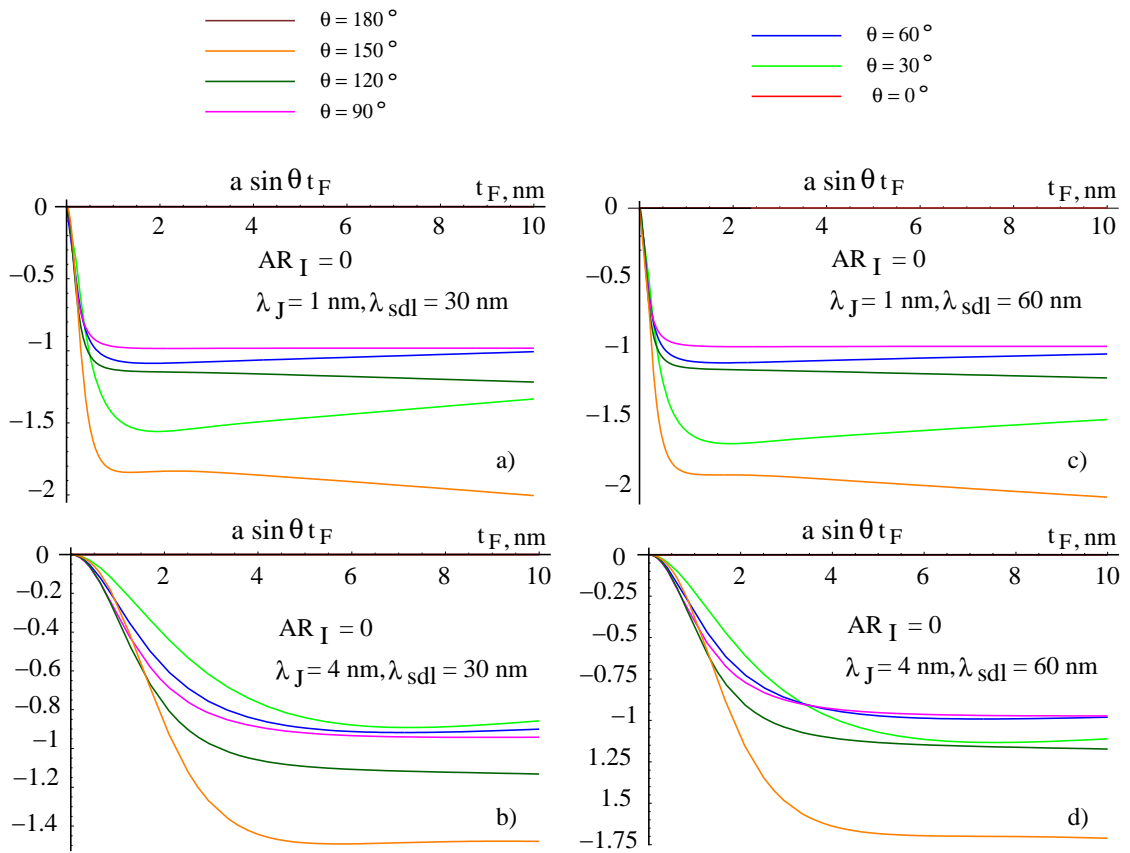


Figure 6.2: Total torque $a \sin \theta t_F / \beta j_e (\hbar a_0^3 / e \mu_B)$ acting on the thin FM layer in the FM-Sp-FM-NM system as a function of the layer thickness for different λ_J and λ_{sdl} and zero interface resistance.

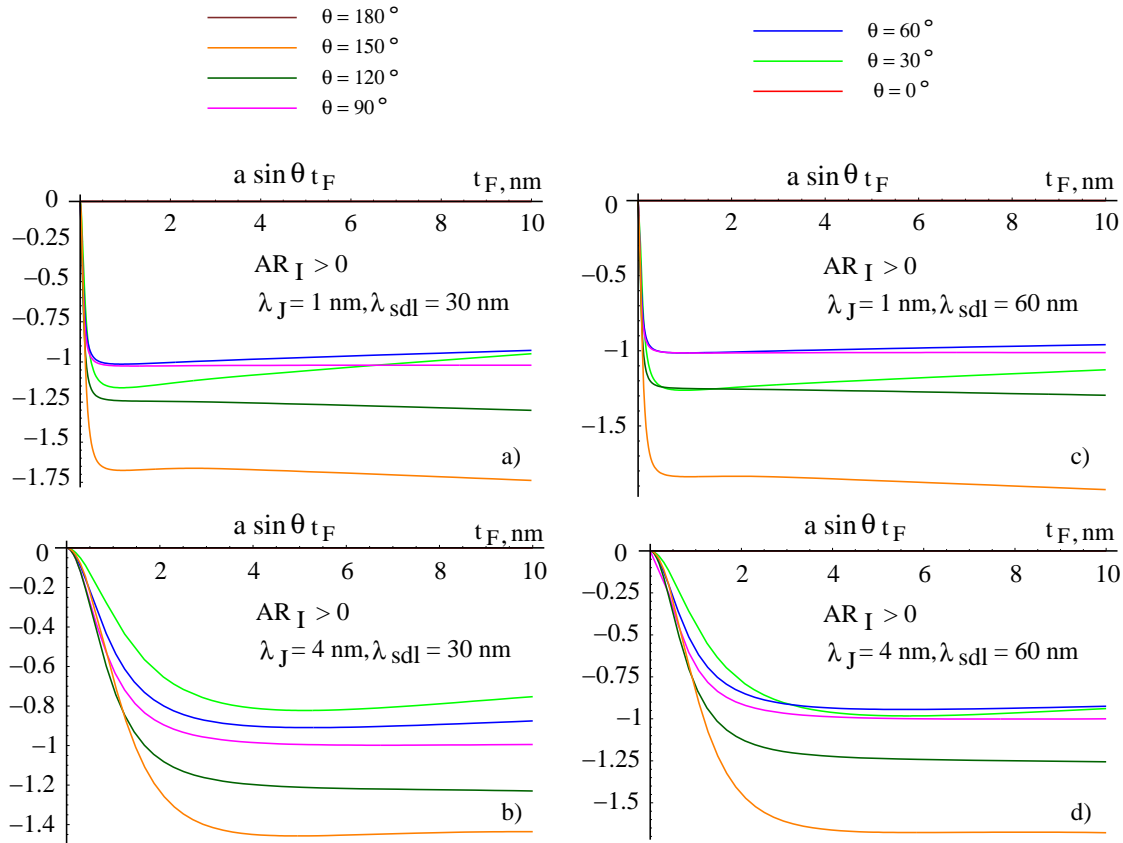


Figure 6.3: Total torque $a \sin \theta t_F / \beta j_e (\hbar a_0^3 / e \mu_B)$ acting on the thin FM layer in the FM-Sp-FM-NM system as a function of the layer thickness for different λ_J and λ_{sdl} and non-zero interface resistance.

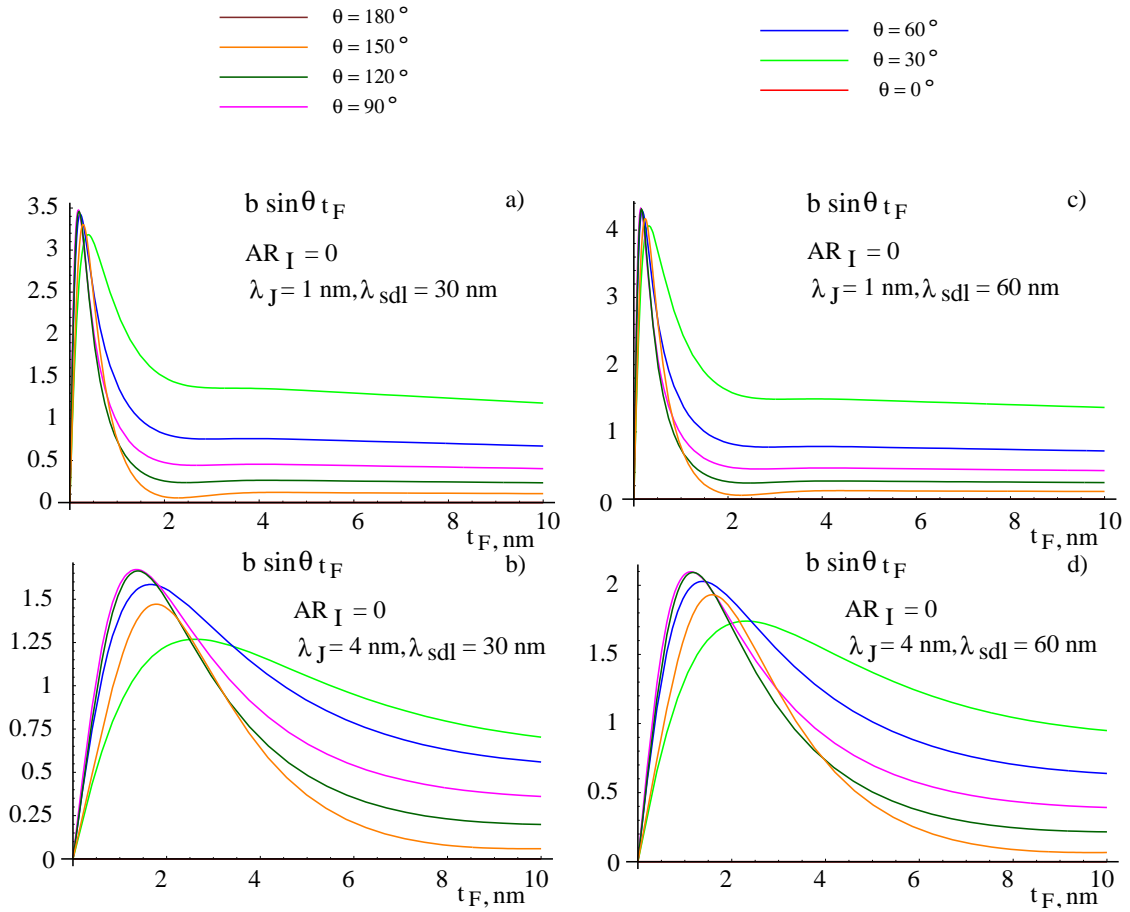


Figure 6.4: Total effective field $b \sin \theta t_F / \beta j_e (\hbar a_0^3 / e \mu_B)$ acting on the thin FM layer in the FM-Sp-FM-NM system as a function of the layer thickness for different λ_J and λ_{sdl} and zero interface resistance.

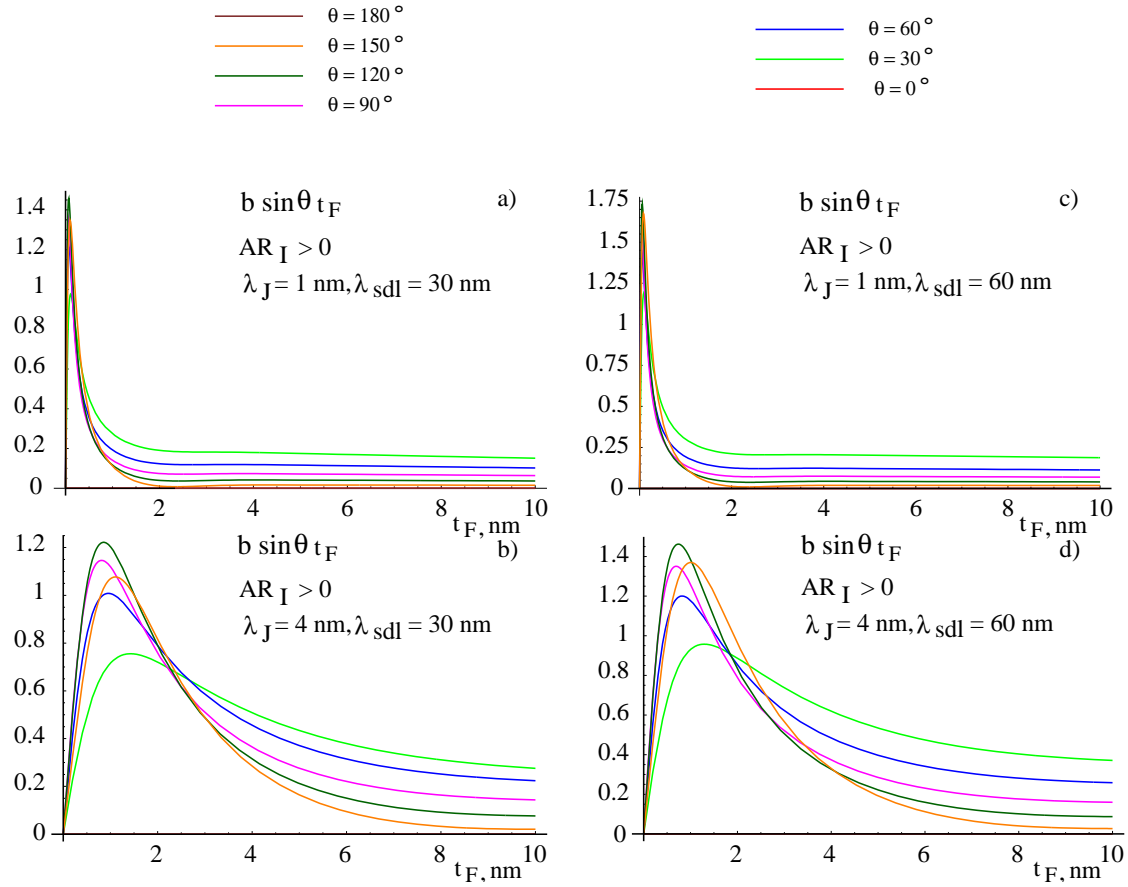


Figure 6.5: Total effective field $b \sin \theta t_F / \beta j_e (\hbar a_0^3 / e \mu_B)$ acting on the thin FM layer in the FM-Sp-FM-NM system as a function of the layer thickness for different λ_J and λ_{sdl} and non-zero interface resistance.

$m_z \rightarrow m \cos \theta$, and $j_{m,z} \rightarrow \beta j_e \cos \theta$. For example, for $\theta = 90^\circ$, $j_{m,y} \rightarrow 1$, in units of βj_e , while $j_{m,z} \rightarrow 0$ in the thick ferromagnetic layer far from the interface. In the nonmagnetic layer to the right, $x > t_F$, the spin current is polarized along the magnetization direction in the thin magnetic layer $\mathbf{M}_d^{(1)}$, and there is no, or very little, spin current in the $x - y$ direction.

Surprisingly, there is a huge enhancement of the transverse ($x - y$) components of the spin current in the region about $x = 0$ (diagrams d) and e) in Figs. 6.6-6.9). Since the torque transmitted to the thin magnetic layer is the difference between the transverse component of the spin current at the boundaries of this layer (see Eq. (5.14)), it is greatly amplified compared to what one would find neglecting the spin accumulation. The thick magnetic layer to the left $x < 0$ is pinned so that the enhanced torques acting in the region of the interface do not produce any rotation. The z or longitudinal component of the incoming spin current is not absorbed by the thin magnetic layer as there is no transfer of spin angular momentum along this direction ($t_F \ll \lambda_{sdl}$), see the diagram f) in Figs. 6.6-6.9. The slight decrease in $j_{m,z}$ is due to the spin flip scattering in the magnetic layer which is characterized by $\lambda_{sdl} = 60$ nm. The much slower decrease in $j_{m,z}$ in the nonmagnetic layer, $x > t_F$, comes from the spin flip scattering in the nonmagnetic layer whose $\lambda_{sdl}^N = 600$ nm.

The large enhancement of the transverse spin currents can be understood as follows. At the interface between the thick and thin ferromagnetic layers, the spin accumulation has to adjust to the new magnetization direction. Both the longitudinal and transverse components of \mathbf{m} have to experience the change of the same order, but the distance over which the transverse component is absorbed, λ_J , is much smaller than that for the longitudinal accumulation, λ_{sdl} . Therefore the gradient of the transverse accumulation about $x = 0$ is large and as it is the gradient that contributes to the spin current, Eq. (5.5), one finds an amplification of the transverse components of the spin current at the interface. In the next section I present a quantitative estimate for the enhancement.

It is worth noting that since the transport in the spin transfer region is assumed to be diffusive (see Chap. 1), so that the length scale of \mathbf{m}_\perp and $\mathbf{j}_{m\perp}$ is λ_J , the transverse component of the spin current is absorbed over the *entire* thin layer, if its thickness is comparable with λ_J (diagrams d) and e) in Figs. 6.6 and 6.8). For larger thicknesses t_F (Figs. 6.7 and 6.9), the transverse spin current in the thin magnetic layer indeed goes to zero before reaching the interface with the nonmagnetic back layer $x = t_F$. The reason for the different behavior in the thin layer arises from its confined geometry, i.e., the reflections from the thin magnetic/nonmagnetic back layer interface create the patterns observed for the transverse spin currents.

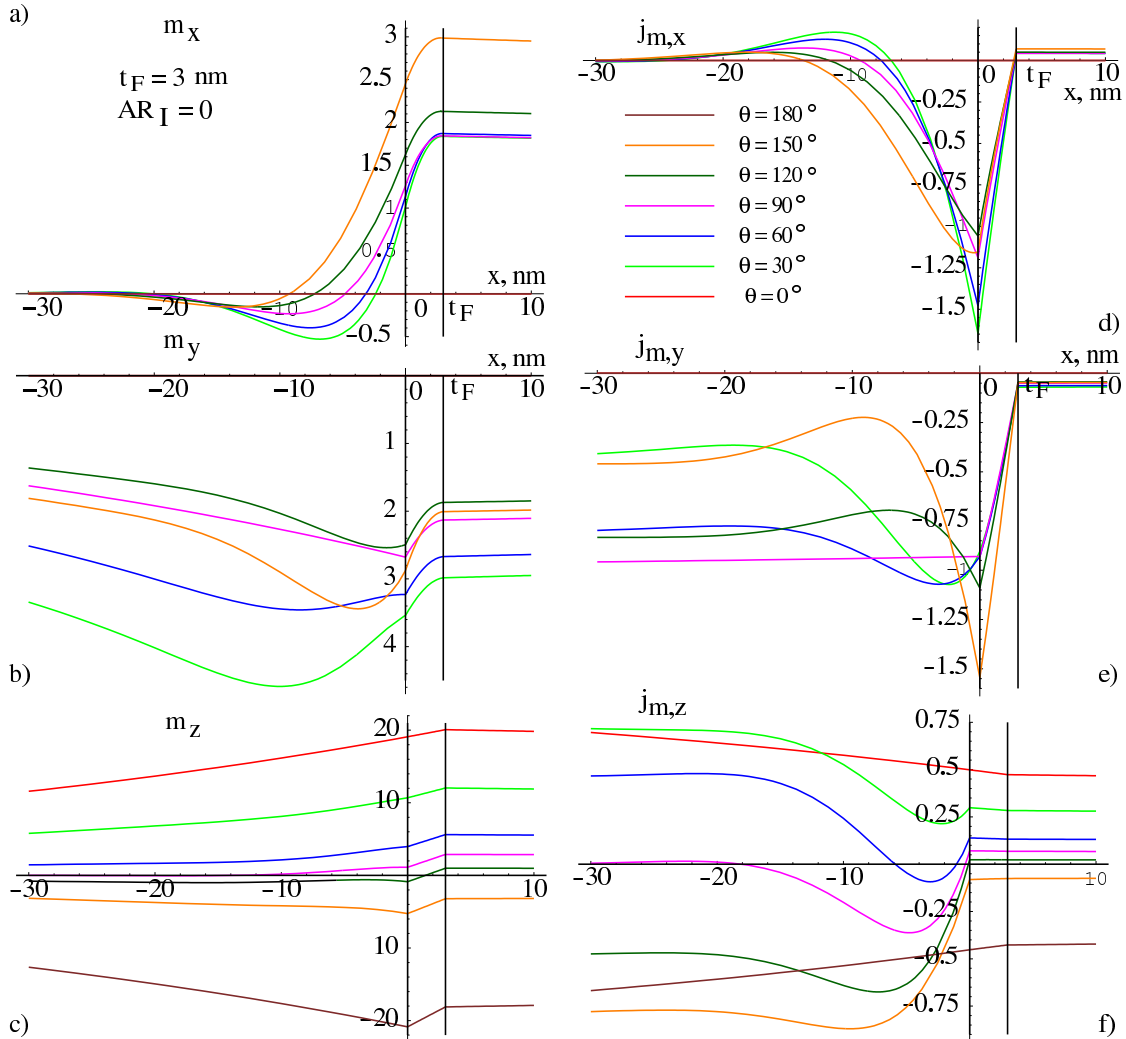


Figure 6.6: x -, y -, and z -components of the spin-accumulation $\mathbf{m}/(\beta j_e/\sqrt{2}\lambda_J J)(\hbar a_0^3/e\mu_B)$ (a-c) and spin-current $\mathbf{j}_m/\beta j_e$ (d-f) distribution in the FM-Sp-FM-NM system with $\lambda_J = 4 \text{ nm}$, $\lambda_{sdl} = 60 \text{ nm}$, the thin FM layer thickness $t_F = 3 \text{ nm}$ and zero interface resistance.

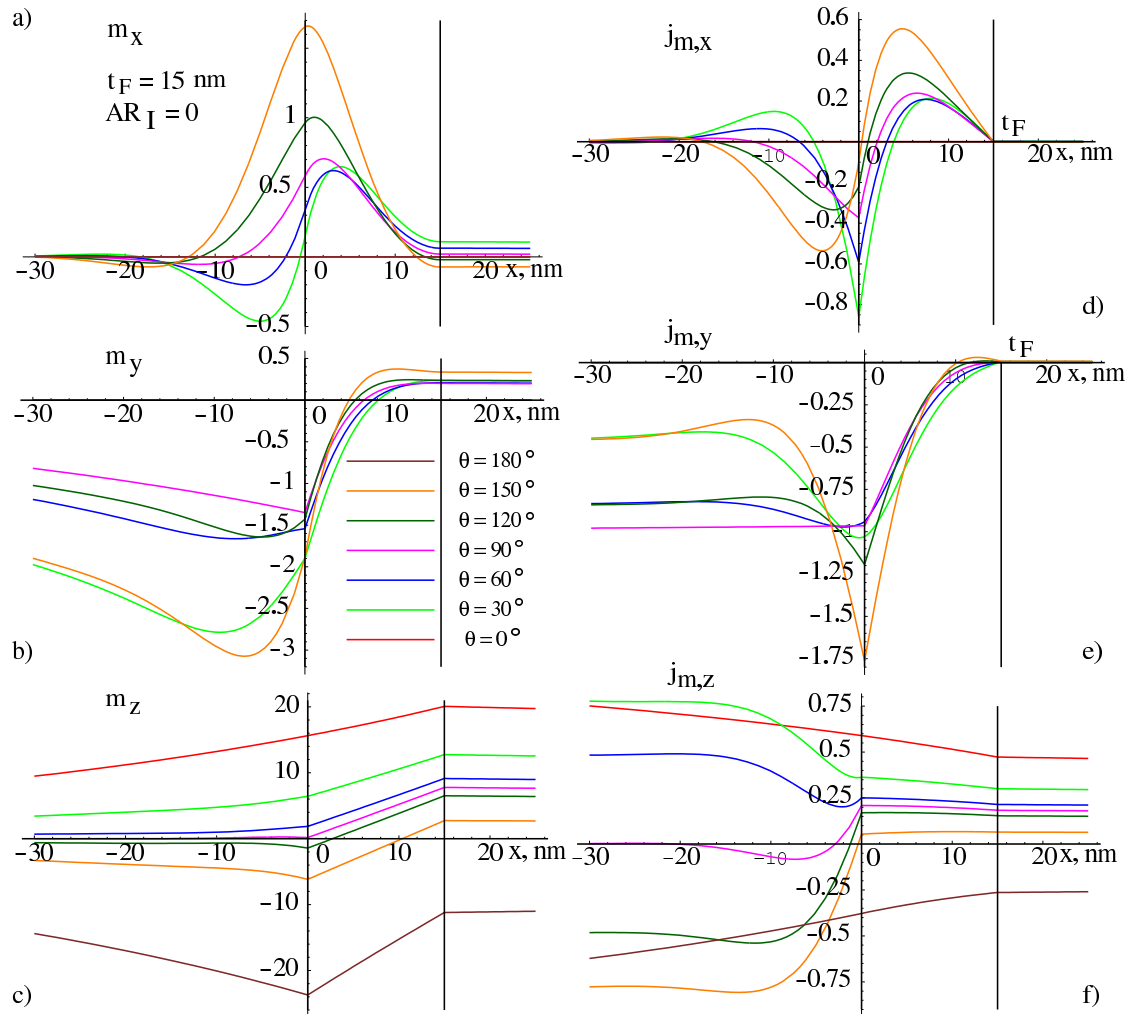


Figure 6.7: x -, y -, and z -components of the spin-accumulation $\mathbf{m}/(\beta j_e/\sqrt{2}\lambda_J J)(\hbar a_0^3/e\mu_B)$ (a-c) and spin-current $\mathbf{j}_m/\beta j_e$ (d-f) distribution in the FM-Sp-FM-NM system with $\lambda_J = 4$ nm, $\lambda_{sdl} = 60$ nm, the thin FM layer thickness $t_F = 15$ nm and zero interface resistance.

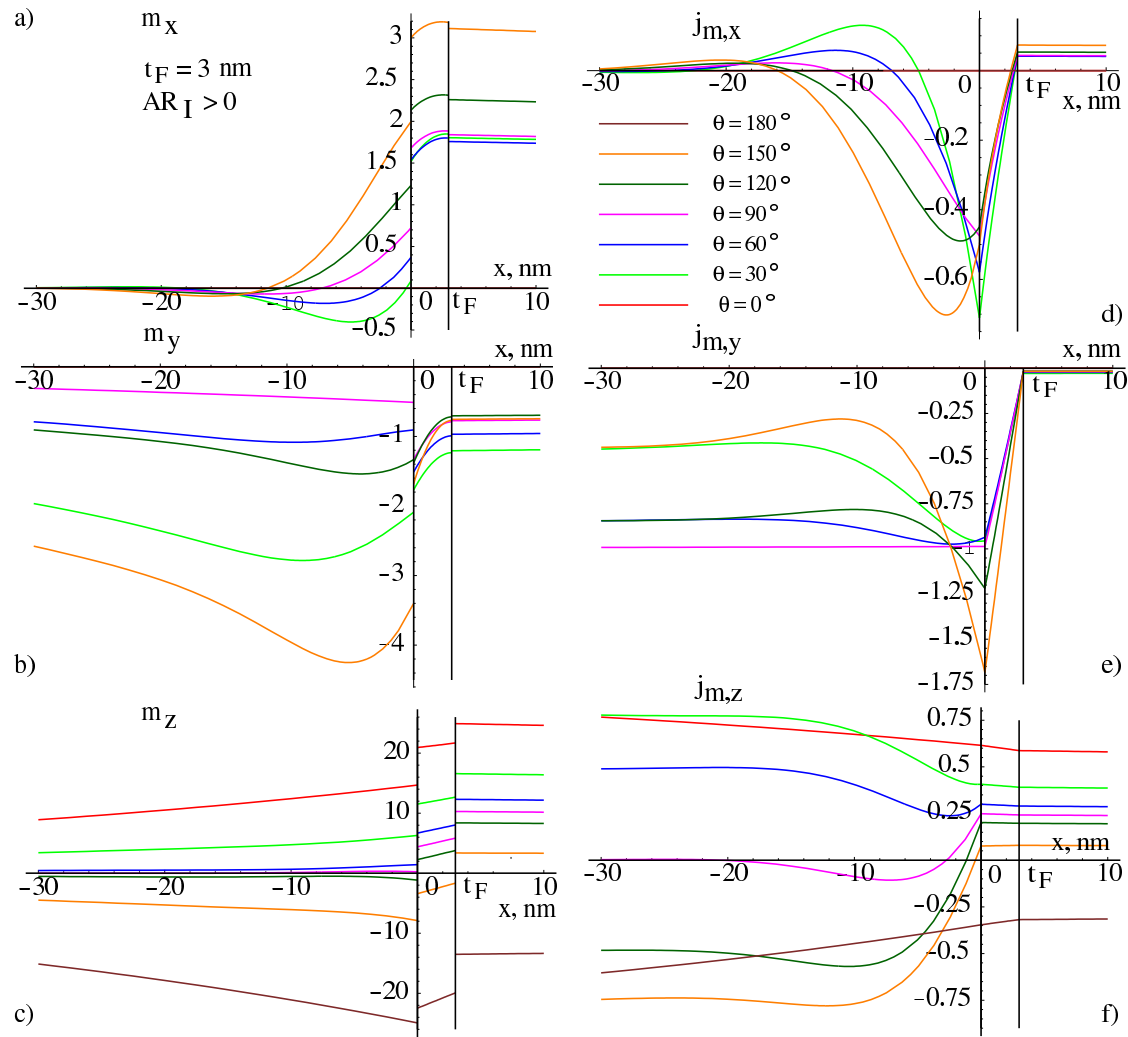


Figure 6.8: x -, y -, and z -components of the spin-accumulation $\mathbf{m}/(\beta j_e/\sqrt{2}\lambda_J J)(\hbar a_0^3/e\mu_B)$ (a-c) and spin-current $\mathbf{j}_m/\beta j_e$ (d-f) distribution in the FM-Sp-FM-NM system with $\lambda_J = 4 \text{ nm}$, $\lambda_{sdl} = 60 \text{ nm}$, the thin FM layer thickness $t_F = 3 \text{ nm}$ and non-zero interface resistance.

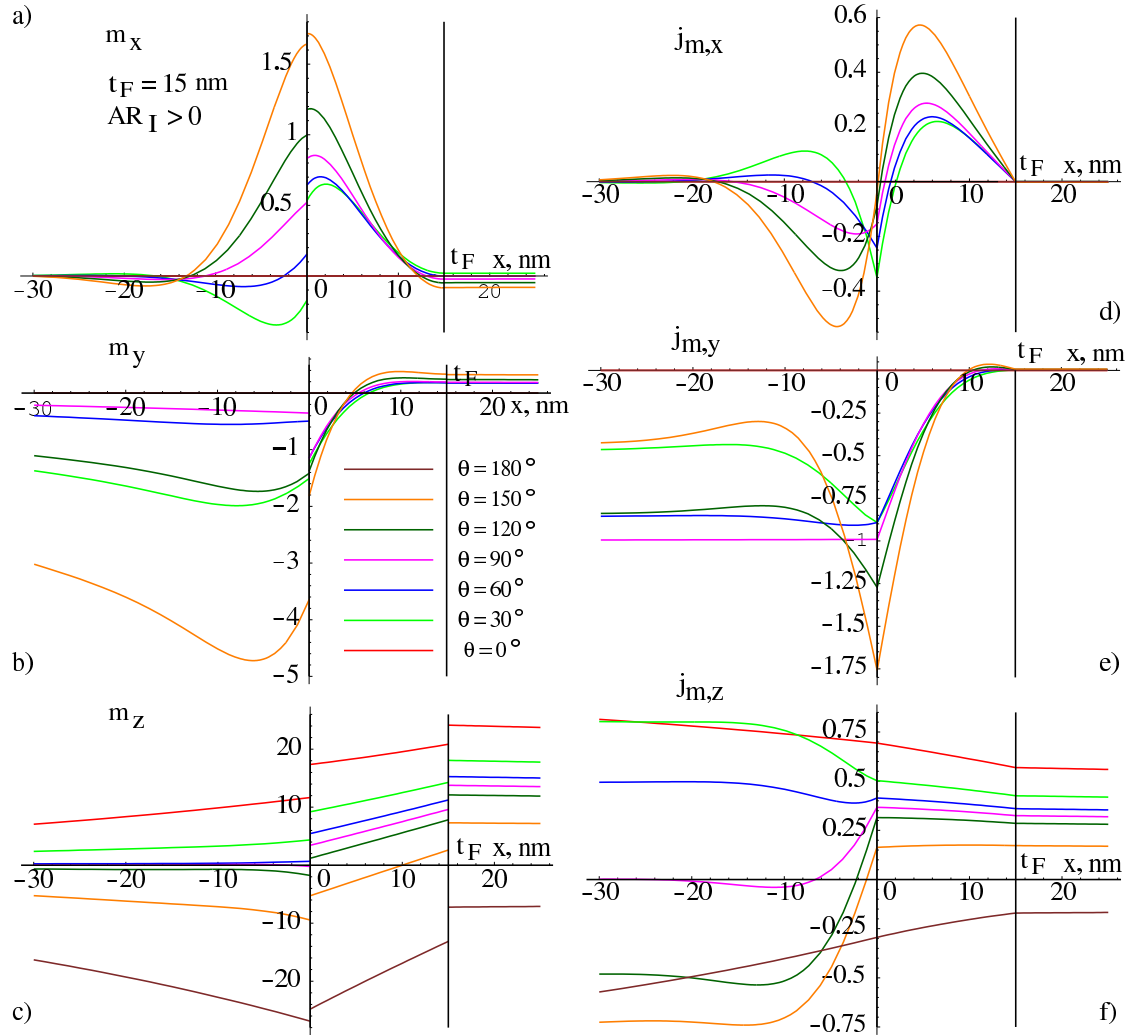


Figure 6.9: x -, y -, and z -components of the spin-accumulation $\mathbf{m}/(\beta j_e/\sqrt{2}\lambda_J J)(\hbar a_0^3/e\mu_B)$ (a-c) and spin-current $\mathbf{j}_m/\beta j_e$ (d-f) distribution in the FM-Sp-FM-NM system with $\lambda_J = 4$ nm, $\lambda_{sdl} = 60$ nm, the thin FM layer thickness $t_F = 15$ nm and non-zero interface resistance.

6.2 Spin current at the interface between ferromagnetic layers

As seen from Figs. 6.6-6.9, the spin current at the interface between the ferromagnetic layers is significantly amplified compared with its bare value $\beta j_e M_d$ for large angles θ between the magnetization directions in the layers. In this section, I derive an analytical expression for the amplification within a simplifying approximation $\lambda_J \ll t_F \ll \lambda_{sf}$.

The spin accumulation distribution in the thin layer takes the form (see appendix B.2):

$$\begin{aligned} m_x^{(1)} &= 2 \sin \theta e^{-\tilde{x}} [\operatorname{Re} G_5 \cos \tilde{x} - \operatorname{Im} G_5 \sin \tilde{x}] \\ &+ 2 \sin \theta e^{\tilde{x}-2\xi} [(\operatorname{Re} G_6 \cos \xi - \operatorname{Im} G_6 \sin \xi) \cos(\tilde{x} - \xi) \\ &+ (\operatorname{Im} G_6 \cos \xi + \operatorname{Re} G_6 \sin \xi) \sin(\tilde{x} - \xi)], \end{aligned} \quad (6.1)$$

$$\begin{aligned} m_y^{(1)} &= 2 \sin \theta e^{-\tilde{x}} [\operatorname{Im} G_5 \cos \tilde{x} + \operatorname{Re} G_5 \sin \tilde{x}] \\ &+ 2 \sin \theta e^{\tilde{x}-2\xi} [(\operatorname{Im} G_6 \cos \xi + \operatorname{Re} G_6 \sin \xi) \cos(\tilde{x} - \xi) \\ &- (\operatorname{Re} G_6 \cos \xi - \operatorname{Im} G_6 \sin \xi) \sin(\tilde{x} - \xi)], \end{aligned} \quad (6.2)$$

$$m_z^{(1)} = G_3 e^{-x/\lambda_{sdl}} + G_4 e^{(x-t_F)/\lambda_{sdl}}, \quad (6.3)$$

where $\tilde{x} = x/\sqrt{2}\lambda_J$, $\xi = t_F/\sqrt{2}\lambda_J$, G_3 , G_4 , G_5 and G_6 are constants of integration found via the boundary conditions (see Appendix B.1). The spin current is calculated as (see Eq. (5.5))

$$\begin{aligned} j_{m,x}^{(1)} &= -\frac{1}{2} \frac{\partial m_x^{(1)}(x)}{\partial x}, \\ j_{m,y}^{(1)} &= -\frac{1}{2} \frac{\partial m_y^{(1)}(x)}{\partial x}, \\ j_{m,z}^{(1)} &= \beta j_e - \frac{1}{2} (1 - \beta \beta') \frac{\partial m_z^{(1)}(x)}{\partial x}. \end{aligned} \quad (6.4)$$

Using the approximation $\lambda_J \ll t_F \ll \lambda_{sf}$, the transverse spin-current at the interface between ferromagnetic layers $x = 0$ in the absence of the interface resistance may be

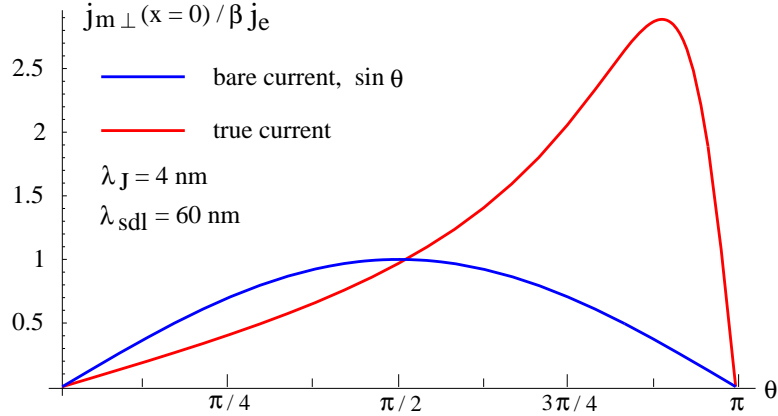


Figure 6.10: True spin current at the interface between the thin and the thick ferromagnetic layers (red line) in comparison with the bare transverse current (blue line) as a function of the angle between the magnetization directions in the layers for $\lambda_J = 4$ nm, $\lambda_{sdl} = 60$ nm.

written as

$$j_{m,x}^{(1)}(x = 0) = (\text{Re}G_5 + \text{Im}G_5) \sin \theta / \sqrt{2} \lambda_J, \quad (6.5)$$

$$j_{m,y}^{(1)}(x = 0) = -(\text{Re}G_5 - \text{Im}G_5) \sin \theta / \sqrt{2} \lambda_J, \quad (6.6)$$

or, after substituting G_5 ,

$$\mathbf{j}_{m,\perp}^{(1)}(x = 0) = -\frac{\beta j_e \sin \theta}{2(\cos^2 \theta/2 + \lambda \sin^2 \theta/2)} \mathbf{e}_y, \quad (6.7)$$

where $\lambda = \sqrt{1 - \beta \beta'} \lambda_J / \sqrt{2} \lambda_{sf}$. Up to the difference in notation, this expression is the same as the one obtained in the previous chapter for the spin current at the interface between two infinite ferromagnetic layers, Eq. (5.21). The magnitude of the spin current at the interface is shown in the Fig. 6.10 (red line) in comparison with the bare value of the transverse current, $\beta j_e \sin \theta$ (blue line). One can see that for the angles θ close to π , the magnitude of the transverse spin current, and, hence, the spin torque acting on the thin layer is enhanced compared to its bare value of $\beta j_e \sin \theta$, reaching its largest value of

$$j_{m,\perp max}^{(1)}(x = 0) = \frac{\beta j_e \sin \theta (1 + \lambda)}{4\lambda} \quad (6.8)$$

for the angle θ^* such that

$$\cos \theta^* = -\frac{1-\lambda}{1+\lambda}. \quad (6.9)$$

This huge enhancement, by a factor of $1/4\lambda$, where λ is of the order of 0.03 for cobalt, comes from the interplay between longitudinal and transverse accumulation; it is the result of the global nature of the spin current even though the transverse components of the spin current and accumulation are absorbed within a region λ_J of the interface.

6.3 Resistance

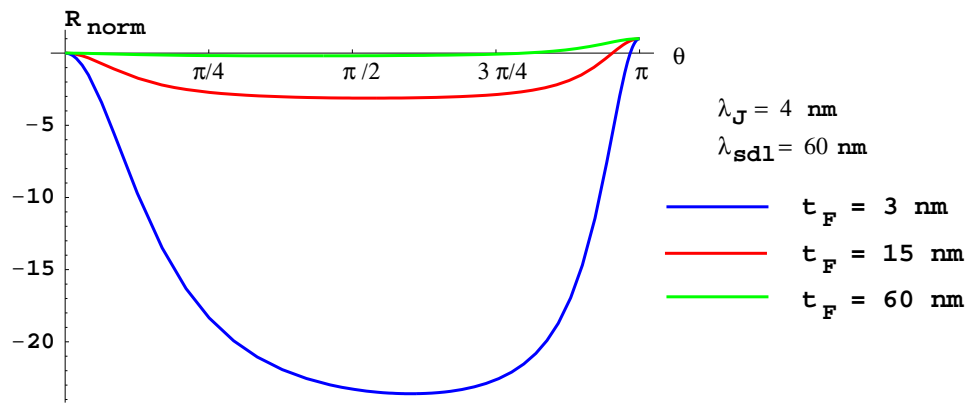
I calculate the resistance of the structure depicted on Fig. 6.1 using the expression for the resistivity in each layer which follows from Eq (5.32) for the electric current:

$$\rho = \frac{1}{2C_0} + \frac{D_0\beta'}{j_e C_0} \frac{\partial m_{||}}{\partial x} \quad (6.10)$$

The sheet resistance of the system AR takes the following form:

$$AR = AR_I + \frac{L}{2C_0} + \frac{\beta\beta'}{2\sqrt{2}j_e C_0} [G_1 + (G_4 - G_3)(1 - e^{-t_F/\lambda_{sdl}})], \quad (6.11)$$

where AR_I is the resistance due to the interfaces, L is the total length of the system, G_1 , G_3 , and G_4 are the constants of integration, defined in the appendix B.2. Figure 6.11 shows the normalized resistance $R_{norm} = (R(\theta) - R(0))/(R(\pi) - R(0))$ as a function of the angle θ between the magnetization directions in the layers for $\lambda_J = 4$ nm, $\lambda_{sdl} = 60$ nm, and several values of the thin layer thickness t_F . One can see that the normalized resistance is a non-monotonic function of the angle between the magnetization directions in the layers (compare with the reference [68]). This is a consequence of the angular momentum transfer from the polarized current to the background magnetization, and the effect it has on the voltage drop across the multilayer.



Chapter 7

Conclusion

Chapters 3 and 4 address the problem of finding the resistance due to the interfaces in the multilayered metallic structures. In Chap. 3, the general method of solving the semi-classical linearized Boltzmann equation in CPP geometry is developed, allowing one to obtain the integral equations for the chemical potentials everywhere in the multilayers in the presence of both specular and diffuse scattering at the interfaces, and diffuse scattering in the bulk of the layers. In Chap. 4, the numerical results for the chemical potential and interface resistance in the multilayered metallic systems are presented. The variation of the chemical potential within a mean-free path of the interface between two semi-infinite metallic layers is investigated. The difference between the potential drop associated with the interface *far* from it and that *at* the interface depends on the amount of diffuse scattering at the interface and can change sign. In the case of the same metal at both sides of the boundary, the different forms of diffuse scattering are classified according to whether the measured resistance is bigger or smaller than that across the interface. For certain forms of diffuse scattering, the chemical potential remains constant outside the immediate interfacial region. Interface resistance in the presence of the diffuse scattering in the bulk of the layers is less than that calculated in the ballistic transport regime. The resistance due to interfaces in the metallic structures consisting of three and five layers is calculated. If one maintains the same interface between layers, its contribution to the total resistance of the system depends on the thickness of the adjacent layers. This contribution is constant only if the distance between interfaces is larger than the electron mean free path. As the thickness of the layers becomes smaller than the electron mean free path in these layers, scattering from interfaces start to interact with each other. The error incurred by neglecting the dependence of the interface resis-

tance on layer thickness depends on the amount of diffuse scattering at interfaces and the height of the potential step at the interface. It reaches 15-20% in Fe-Cr and Co-Cu systems with equal amounts of specular and diffuse scattering at interfaces. In order to observe this effect one should investigate systems where interface resistance dominates total resistance. Hence, the thickness of the layers should be small. Also, by introducing additional scatterers, one should be able to change the ratio of thickness to mean free path without changing the thickness of the layers.

In Chaps. 5 and 6 a mechanism for the magnetization switching that is driven by spin-polarized current in noncollinear magnetic multilayers is studied. I find the spin-torque due to the bulk of the magnetic layers and the diffuse scattering at interfaces for a number of layered structures; the spin transfer that occurs at interfaces is self-consistently determined by embedding it in globally diffusive transport calculations. In Chap. 5 a system consisting of two thick ferromagnetic layers divided by a nonmagnetic spacer is considered. The spin accumulation and the spin current distributions, as well as the spin torques acting on the magnetic layers are found analytically. I obtain an analytical expression for the CPP magnetoresistance that takes into account the effect of the transfer of the spin angular momentum from the polarized current on the voltage drop across the multilayer, and estimate a parameter of the angular dependence of the CPP-MR that gives a correction to the simple $\cos^2(\theta/2)$ dependence of the resistance for cobalt and permalloy. For the latter, this parameter can be compared with the experimental value. While there is a difference between the theoretical and experimental values, the theoretical value is obtained without taking into account the interface resistance, which presence leads to a smaller discrepancy. In Chap. 6 a realistic magnetic multilayer consisting of a thick magnetic layer, a thin magnetic layer that is to be switched, a nonmagnetic spacer layer, and nonmagnetic layers or leads on the backs of the magnetic layers; the current is perpendicular to the plane of the layers. I find the spin-torques acting on the thin magnetic layer, spin accumulation and current profiles in the whole structure for different angles between the magnetization directions in the layers and different thicknesses of the thin layer. The spin angular momentum transferred from the polarized current to the background magnetization of the thin magnetic layer far exceeds the transverse component (to the orientation of the magnetization of the thin layer) of the bare portion of the incoming spin-polarized current (the part proportional to the electric field). Due to the presence of long longitudinal spin-diffusion lengths, the longitudinal and transverse components of the spin accumulations become intertwined from one layer to the next, leading to a significant amplification of the spin torque with respect to the treatments that neglect spin accumulation about the interfaces. I estimate

the scale of the amplification as λ_{sdl}/λ_J , the ratio of the spin-diffusion length to the characteristic length scale of the transverse component of the spin accumulation. The large enhancement of the spin current in the free ferromagnetic layer may lead to the reduction of the critical current necessary to switch spintronics devices.

Appendix A

Appendices for interface resistance chapters

A.1 Calculus related to the problem

In this appendix, several auxiliary equations are obtained, which are used in Chap. 3 to derive the equations for the chemical potential profile in multilayers.

A.1.1 Dirac delta function in ϵ and v space

The Fermi-Dirac equilibrium distribution function has the form

$$f^0(\epsilon) = \frac{1}{\exp(\frac{\epsilon - \epsilon_F}{k_B T}) + 1},$$

where ϵ is an electron energy, ϵ_F is Fermi energy, k_B is Boltzmann constant, and T is temperature. At $T \rightarrow 0$, the derivative of the distribution function over the energy can be approximated by the delta function:

$$\frac{\partial f(\epsilon)}{\partial \epsilon} \sim \delta(\epsilon - \epsilon_F).$$

The electron's energy is a function of its velocity, so delta functions in ϵ space and v space are related via

$$\delta(\epsilon - \epsilon_F) = \frac{\delta(v - v_F)}{\partial \epsilon / \partial v},$$

and, in a free electron model,

$$\delta(\epsilon - \epsilon_F) = \frac{1}{mv} \delta(v - v_F), \quad (\text{A.1})$$

where m is the electron's mass.

A.1.2 Angular averaging

For an arbitrary function $y(|\cos \theta|)$, $y(|\cos \theta|) \sin \theta$ is symmetric around $\theta = \pi/2$, and

$$\int_0^{\pi/2} y(|\cos \theta|) \sin \theta d\theta = \int_{\pi/2}^{\pi} y(|\cos \theta|) \sin \theta d\theta. \quad (\text{A.2})$$

For example, since a correction to the equilibrium distribution function $g(\mathbf{v}, z)$ can be written as a function of z and $|\cos \theta|$ only, where θ is an angle that an electron momentum makes with z axis (Eq. (3.1)), the chemical potential $\mu(z)$ can be written as

$$\begin{aligned} 2\mu(z) &= \int_0^{\pi} g(\theta, z) \sin \theta d\theta \\ &= \int_0^{\pi/2} (g(|\cos \theta|, \cos \theta > 0, z) + g(|\cos \theta|, \cos \theta < 0, z)) \sin \theta d\theta \end{aligned}$$

For an arbitrary function $y(\mathbf{v})$, if it can be written as a function of $|\cos \theta|$ only, it follows from Eq. (A.1) and Eq. (A.2) that

$$\begin{aligned} \int_{FS} d\mathbf{v} |v_z| \delta(\epsilon - \epsilon_F) y(\mathbf{v}) &\sim \int_0^{\infty} \int_0^{\pi} v^2 dv v |\cos \theta| \frac{1}{v} \delta(v - v_F) y(|\cos \theta|) \sin \theta d\theta \\ &= v_F^2 \int_0^{\pi/2} y(|\cos \theta|) \cos \theta \sin \theta d\theta \end{aligned} \quad (\text{A.3})$$

A.1.3 Diffuse scattering term $F(g)$ in the boundary conditions

By using the definition of the correction to the equilibrium distribution function $g(\mathbf{v}, z)$ (Eq. (3.1)), the term in the boundary conditions responsible for the diffuse scattering at an interface $F(g)$ (Eq. (3.7)) can be written as

$$F(g) = \frac{1}{\Omega} \left(\int d\mathbf{v}_2 |v_{2z}^<| \delta(\epsilon - \epsilon_F) g(v_{2z}^<, 0) + \int d\mathbf{v}_1 |v_{1z}^>| \delta(\epsilon - \epsilon_F) g(v_{1z}^>, 0) \right),$$

where \mathbf{v}_i is an electron velocity in i -th layer, and

$$\Omega = \int d\mathbf{v}_2 |v_{2z}^<| \delta(\epsilon - \epsilon_F) + \int d\mathbf{v}_1 |v_{1z}^>| \delta(\epsilon - \epsilon_F).$$

Then, with the help of Eq. (A.3),

$$\begin{aligned} F(g) &= \frac{2v_{F1}^2}{v_{F1}^2 + v_{F2}^2} \int_0^{\pi/2} g(v_{1z}^>, 0) \cos \theta \sin \theta d\theta \\ &+ \frac{2v_{F2}^2}{v_{F1}^2 + v_{F2}^2} \int_0^{\pi/2} g(v_{2z}^<, 0) \cos \theta \sin \theta d\theta \end{aligned} \quad (\text{A.4})$$

is obtained.

A.2 Current conservation across an interface

Electrical current $j(z)$ is defined in terms of the distribution function as

$$j_1(z) = \int_{FS} d\mathbf{v}_1 |v_{1z}| (f(v_{1z}^>, z) - f(v_{1z}^<, z))$$

in the left layer, and

$$j_2(z) = \int_{FS} d\mathbf{v}_1 |v_{2z}| (f(v_{2z}^>, z) - f(v_{2z}^<, z))$$

in the right layer. At an interface, the electron distribution functions $f(v_{1z}^>, 0)$, $f(v_{1z}^<, 0)$, $f(v_{2z}^>, 0)$, and $f(v_{2z}^<, 0)$ are related via boundary conditions (3.6)-(3.7). Since the boundary condition is a linear combination of the specular ($S = 1$) and diffuse ($S = 0$) scattering terms, it is enough to consider current conservation separately for $S = 1$ and

$S = 0$.

If only specular scattering is present at an interface, current to the left of the interface, $j_1(z = 0-, S = 1)$, may be written as

$$j_1(z = 0-, S = 1) = v_{F1}^2 \int_0^{\pi/2} \cos \theta_1 \sin \theta_1 d\theta_1 (g(v_1^>, 0)(1 - R_{12}(\theta_1)) - T_{21}(\theta_2)g(v_2^<, 0)),$$

and current to the right of the interface, $j_2(z = 0+)$, as

$$j_2(z = 0+, S = 1) = v_{F2}^2 \int_0^{\pi/2} \cos \theta_2 \sin \theta_2 d\theta_2 (g(v_1^>, 0)T_{12}(\theta_1) - (1 - R_{21}(\theta_2))g(v_2^<, 0)),$$

where θ_1 (θ_2) is the angle of incidence (transmission) to the left (right) of the interface. In the process of specular scattering, transmission and reflection coefficients are defined so that $T_{ij}(\theta_i) = 1 - R_{ij}(\theta_i)$, and angles θ_1 and θ_2 are related (Appendix A.3), so that

$$v_{F1}^2 \cos \theta_1 \sin \theta_1 d\theta_1 = v_{F2}^2 \cos \theta_2 \sin \theta_2 d\theta_2,$$

and electrical current is conserved at the interface:

$$j_1(z = 0-, S = 1) = j_2(z = 0+, S = 1).$$

If only diffuse scattering is present at an interface, current to the left of the interface, $j_1(z = 0-, S = 0)$, may be written as

$$\begin{aligned} j_1(z = 0-, S = 0) &= v_{F1}^2 \int_0^{\pi/2} \cos \theta_1 \sin \theta_1 d\theta_1 (g(v_1^>, 0) - F(g)) \\ &= v_{F1}^2 \int_0^{\pi/2} \cos \theta_1 \sin \theta_1 d\theta_1 g(v_1^>, 0) - \frac{1}{2} v_{F1}^2 F(g) \end{aligned}$$

where $F(g)$ is given by Eq. (A.4). Then, expression for $j_1(z = 0-, S = 0)$ takes the form

$$j_1(z = 0-, S = 0) = \frac{v_{F1}^2 v_{F2}^2}{v_{F1}^2 + v_{F2}^2} \int_0^{\pi/2} \cos \theta_1 \sin \theta_1 d\theta_1 (g(v_1^>, 0) - g(v_2^<, 0)).$$

Similarly, current to the right of the interface, $j_2(z = 0+, S = 0)$, is

$$j_2(z = 0+, S = 0) = \frac{v_{F1}^2 v_{F2}^2}{v_{F1}^2 + v_{F2}^2} \int_0^{\pi/2} \cos \theta_2 \sin \theta_2 d\theta_2 (g(v_1^>, 0) - g(v_2^<, 0)).$$

Since angles θ_1 and θ_2 are not related in the process of diffuse scattering, it follows that

$$j_1(z = 0-, S = 0) = j_2(z = 0+, S = 0).$$

If both specular and diffuse scattering are present at an interface, so that $S \neq 0$ and $S \neq 1$, the total electrical current $j_{1(2)}(z = 0)$ can be written as a linear combination of $j_{1(2)}(z = 0, S = 1)$ and $j_{1(2)}(z = 0, S = 0)$:

$$j_1(z = 0-) = S j_1(z = 0-, S = 1) + (1 - S) j_1(z = 0-, S = 0)$$

$$j_2(z = 0+) = S j_2(z = 0+, S = 1) + (1 - S) j_2(z = 0+, S = 0)$$

Hence, total electrical current at the interface is conserved by the boundary conditions (3.6)-(3.7):

$$j_1(z = 0-) = j_2(z = 0+) \tag{A.5}$$

A.3 Specular reflection and transmission at the potential step

Consider an electron with the Fermi energy ϵ_F moving in a one-dimensional step-like potential $V(z) = V_1$ if $z < 0$, $V(z) = V_2$ if $z > 0$. (Fig. A.1a)) For example, this corresponds to a free electron motion across an interface between two layers of different metals, or layers of the same magnetic metals with antiparallel magnetization directions.

If electron energy is referenced from ϵ_F , so that $\epsilon_F = 0$, energy conservation law takes the following form:

$$V_1 + \frac{mv_{F1}^2}{2} = V_2 + \frac{mv_{F2}^2}{2} = \epsilon_F = 0, \tag{A.6}$$

where an effective electron mass m is assumed to be the same in both materials. Electron Fermi velocities v_{F1} to the left of the step ($z < 0$) and v_{F2} to the right of the step ($z > 0$)

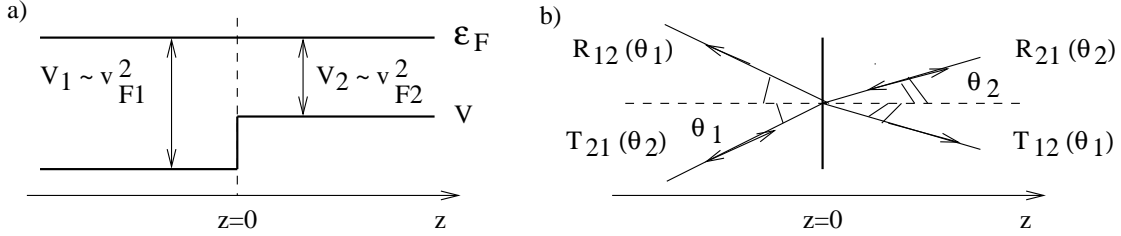


Figure A.1: Specular scattering at the potential barrier: a) Motion in a step-like potential, b) reflection and transmission at an interface.

are related via

$$\frac{v_{F1}}{v_{F2}} = \sqrt{\frac{|V_1|}{|V_2|}}.$$

Electron velocity \mathbf{v} and momentum \mathbf{k} are related as $m\mathbf{v} = \hbar\mathbf{k}$. From the one-dimensional geometry of the problem it follows that the component of an electron momentum parallel to $z = 0$ plane is conserved, so that the energy conservation law (Eq. (A.6)) can be written in terms of z -component of the momentum $k_z = k_F \cos \theta$ only:

$$-\frac{2m|V_1|}{\hbar^2} + k_{F1}^2 \cos^2 \theta_1 = -\frac{2m|V_2|}{\hbar^2} + k_{F2}^2 \cos^2 \theta_2, \quad (\text{A.7})$$

where θ_1 (θ_2) is the angle that an electron momentum makes with z axis in the left (right) layer.

Condition (A.7) means that at an interface, the angle of incidence of an electron traveling from left to right θ_1 and its angle of transmittance θ_2 , or, vice versa, the angle of incidence of an electron traveling from right to left θ_2 and its angle of transmittance θ_1 are related as follows (Fig. A.1b)):

$$\left\{ \begin{array}{lcl} \cos \theta_2 & = & \cos \theta_1 \frac{v_{F1}}{v_{F2}} \operatorname{Re} \sqrt{1 - \frac{1}{\cos^2 \theta_1} + \frac{v_{F2}^2}{v_{F1}^2} \frac{1}{\cos^2 \theta_1}} \\ \sin \theta_2 d\theta_2 & = & \sin \theta_1 d\theta_1 \frac{v_{F1}}{v_{F2}} \frac{1}{\operatorname{Re} \sqrt{1 - \frac{1}{\cos^2 \theta_1} + \frac{v_{F2}^2}{v_{F1}^2} \frac{1}{\cos^2 \theta_1}}}, \end{array} \right. \quad (\text{A.8})$$

or

$$\begin{cases} \cos \theta_1 = \cos \theta_2 \frac{v_{F2}}{v_{F1}} \operatorname{Re} \sqrt{1 - \frac{1}{\cos^2 \theta_2} + \frac{v_{F1}^2}{v_{F2}^2} \frac{1}{\cos^2 \theta_2}} \\ \sin \theta_1 d\theta_1 = \sin \theta_2 d\theta_2 \frac{v_{F2}}{v_{F1}} \frac{1}{\operatorname{Re} \sqrt{1 - \frac{1}{\cos^2 \theta_2} + \frac{v_{F1}^2}{v_{F2}^2} \frac{1}{\cos^2 \theta_2}}}. \end{cases} \quad (\text{A.9})$$

Quantum mechanically, an electron is described by the wave function ψ , which, in the case of the electron moving in a constant potential, has the form of a plane wave, $\psi = e^{i\mathbf{k}\mathbf{r}}$. At the potential barrier along z direction, an electron experiences scattering, so that its wave function is only partially transmitted across the barrier, and partially reflected. For an electron moving from left to right, two plane waves, incident and reflected, are present in the left layer, and transmitted plane wave is present in the right layer: (Fig. A.1b))

$$\begin{cases} \psi_1 \sim e^{ik_{1z}z} + re^{-ik_{1z}z} \\ \psi_2 \sim te^{ik_{2z}z}, \end{cases} \quad (\text{A.10})$$

where r (t) is the reflection (transmission) coefficient for the wave function ψ . At an interface between layers, both electrical charge density, proportional to $|\psi|^2$, and quantum mechanical flux density, proportional to $\psi\psi'^* - \psi'^*\psi'$, have to be conserved, which requires continuity of both ψ and ψ' at $z = 0$:

$$\psi_1(z = 0) = \psi_2(z = 0), \quad \psi'_1(z = 0) = \psi'_2(z = 0).$$

These continuity conditions, together with the expressions for the wave function in the left and right layers (A.10) lead to the following expressions for the reflection and transmission coefficients for the wave function:

$$\begin{cases} 1 + r = t \\ k_{1z}(1 - r) = k_{2z}t \end{cases} \Rightarrow \begin{cases} r = \frac{k_{1z} - k_{2z}}{k_{1z} + k_{2z}} \\ t = \frac{2k_{1z}}{k_{1z} + k_{2z}} \end{cases} \quad (\text{A.11})$$

In the boundary conditions (3.6) for the semiclassical Boltzmann equation, reflection and transmission coefficients for an electron *flux* are required. It follows from the quantum mechanical flux conservation condition that r and t are related via

$$1 = |r|^2 + \frac{k_{2z}}{k_{1z}} |t|^2,$$

so it is convenient to define the reflection (transmission) coefficient for the flux in terms of the reflection (transmission) coefficient for the wave function as

$$R = |r|^2, \quad T = \frac{k_{2z}}{k_{1z}} |t|^2,$$

so that the condition $T = 1 - R$ is satisfied. Reflection coefficient for the electron flux going from left to right takes the following form:

$$R_{12}(\theta_1) = |r_{12}(\theta_1)|^2 = \left| \frac{1 - \sqrt{1 - \frac{1}{\cos^2 \theta_1} + \frac{v_{F2}^2}{v_{F1}^2} \frac{1}{\cos^2 \theta_1}}}{1 + \sqrt{1 - \frac{1}{\cos^2 \theta_1} + \frac{v_{F2}^2}{v_{F1}^2} \frac{1}{\cos^2 \theta_1}}} \right|^2. \quad (\text{A.12})$$

In a similar fashion, reflection coefficient for the electron flux going from the right to the left layer can be obtained:

$$R_{21}(\theta_2) = |r_{21}(\theta_2)|^2 = \left| \frac{1 - \sqrt{1 - \frac{1}{\cos^2 \theta_2} + \frac{v_{F1}^2}{v_{F2}^2} \frac{1}{\cos^2 \theta_2}}}{1 + \sqrt{1 - \frac{1}{\cos^2 \theta_2} + \frac{v_{F1}^2}{v_{F2}^2} \frac{1}{\cos^2 \theta_2}}} \right|^2. \quad (\text{A.13})$$

Expressions (A.12)-(A.13) together with the relations on the angles θ_1 and θ_2 (A.9)-(A.8) lead to the microscopic reversibility condition

$$R_{ij}(\theta_i) = R_{ji}(\theta_j). \quad (\text{A.14})$$

Figure A.2 shows schematically how the reflection coefficients R_{12} and R_{21} depend on the cosine of the angle of incidence θ_1 or θ_2 for two different geometries of the potential barrier, $V_2 > V_1$ and $V_2 < V_1$.

A.4 Equations for chemical potential for three-layered system

In this appendix, equations for the chemical potential profile in the system consisting of three metallic layers (Fig. A.3) are presented without derivation. The same electron relaxation time τ is assumed in all three metals, and a dimensionless variable $\xi = z/l_i$

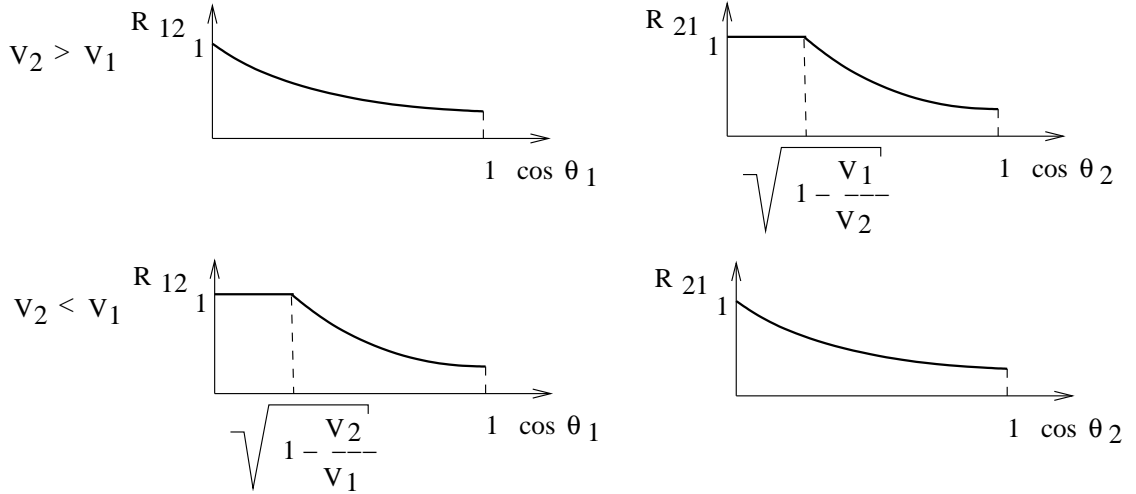


Figure A.2: Reflection coefficient at the potential barrier as a function of the angle of incidence

is introduced, where $l_i = v_{F_i}\tau$ is an electron's mean free path in the i -th layer, so that $\mu_i = \mu_i(\xi = z/l_i)$, and $d_i = d/l_i$, where $2d$ is the thickness of the middle layer.

$$\begin{aligned}
 2\mu_1(\xi) &= eE_1 l_1 \int_0^{\pi/2} \left[(1 + SR_{12}(\theta_1)) \cos \theta_1 - \frac{v_{F1}^2}{v_{F2}^2} ST_{12}(\theta_1) \cos \theta_2(\theta_1) \right] \\
 &\times \exp\left(\frac{\xi + d_1}{\cos \theta_1}\right) \sin \theta_1 d\theta_1
 \end{aligned} \tag{A.15}$$

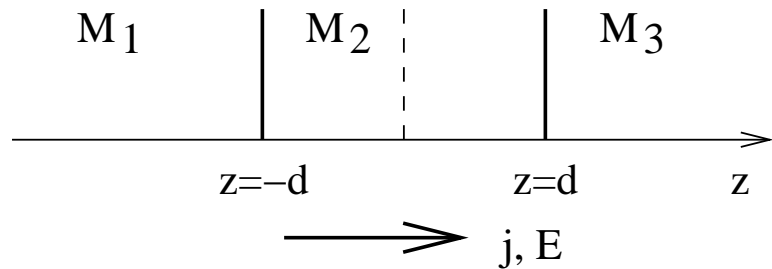


Figure A.3: System consisting of three layers.

$$\begin{aligned}
& + \int_{-\infty}^{-d_1} \mu_1(\xi') d\xi' \\
& \times \int_0^{\pi/2} \left(\exp\left(-\frac{|\xi - \xi'|}{\cos \theta_1}\right) + SR_{12}(\theta_1) \exp\left(\frac{\xi + \xi' + 2d_1}{\cos \theta_1}\right) \right) \tan \theta_1 d\theta_1 \\
& + \int_{-d_2}^{d_2} \mu_2(\xi') d\xi' \\
& \times \int_0^{\pi/2} ST_{12}(\theta_1) \exp\left(\frac{-\xi' - d_2}{\cos \theta_2(\theta_1)}\right) \exp\left(\frac{-\xi + d_1}{\cos \theta_1}\right) \frac{\sin \theta_1}{\cos \theta_2(\theta_1)} d\theta_1 \\
& + \frac{2(1-S)v_{F1}^2}{v_{F1}^2 + v_{F2}^2} \int_{-\infty}^{-d_1} \mu_1(\xi') d\xi' \int_0^{\pi/2} \exp\left(\frac{\xi' + d_1}{\cos \theta}\right) \sin \theta \\
& \times \int_0^{\pi/2} \exp\left(\frac{\xi + d_1}{\cos \theta}\right) \sin \theta \\
& + \frac{2(1-S)v_{F2}^2}{v_{F1}^2 + v_{F2}^2} \int_{-d_2}^{d_2} \mu_2(\xi') d\xi' \int_0^{\pi/2} \exp\left(\frac{-\xi' - d_2}{\cos \theta}\right) \sin \theta \\
& \times \int_0^{\pi/2} \exp\left(\frac{\xi + d_1}{\cos \theta}\right) \sin \theta \\
& + \int_0^{\pi/2} ST_{21}(\theta_2) A(\theta_2) \exp\left(\frac{-2d_2}{\cos \theta_2}\right) \exp\left(\frac{\xi + d_1}{\cos \theta_1(\theta_2)}\right) \sin \theta_1(\theta_2) d\theta_1(\theta_2) \\
& + \frac{2(1-S)v_{F2}^2}{v_{F1}^2 + v_{F2}^2} \int_0^{\pi/2} A(\theta_2) \exp\left(\frac{-2d_2}{\cos \theta}\right) \sin \theta d\theta \int_0^{\pi/2} \exp\left(\frac{\xi + d_1}{\cos \theta}\right) \sin \theta d\theta
\end{aligned}$$

$$\begin{aligned}
2\mu_2(\xi) & = \int_{-d_2}^{d_2} \mu_2(\xi') d\xi' \int_0^{\pi/2} \exp\left(-\frac{|\xi - \xi'|}{\cos \theta_2}\right) \tan \theta_2 d\theta_2 \\
& + \int_0^{\pi/2} A(\theta_2) \exp\left(\frac{\xi - d_2}{\cos \theta_2}\right) \sin \theta_2 d\theta_2 \\
& + \int_0^{\pi/2} B(\theta_2) \exp\left(\frac{-\xi - d_2}{\cos \theta_2}\right) \sin \theta_2 d\theta_2
\end{aligned} \tag{A.16}$$

$$2\mu_3(\xi) = -eE_3l_3 \int_0^{\pi/2} \left[(1 + SR_{32}(\theta_3)) \cos \theta_3 - \frac{v_{F3}^2}{v_{F2}^2} ST_{32}(\theta_3) \cos \theta_2(\theta_3) \right]$$

$$\begin{aligned}
& \times \exp\left(\frac{-\xi + d_3}{\cos \theta_3}\right) \sin \theta_3 d\theta_3 \\
& + \int_{d_3}^{\infty} \mu_3(\xi') d\xi' \\
& \times \int_0^{\pi/2} \left(\exp\left(-\frac{|\xi - \xi'|}{\cos \theta_3}\right) + SR_{32}(\theta_3) \exp\left(\frac{-\xi - \xi' + 2d_3}{\cos \theta_3}\right) \right) \tan \theta_3 d\theta_3 \\
& + \int_{-d_2}^{d_2} \mu_2(\xi') d\xi' \\
& \times \int_0^{\pi/2} ST_{32}(\theta_3) \exp\left(\frac{\xi' - d_2}{\cos \theta_2(\theta_3)}\right) \exp\left(\frac{-\xi + d_3}{\cos \theta_3}\right) \frac{\sin \theta_3}{\cos \theta_2(\theta_3)} d\theta_3 \\
& + \frac{2(1-S)v_{F3}^2}{v_{F3}^2 + v_{F2}^2} \int_{d_3}^{\infty} \mu_3(\xi') d\xi' \int_0^{\pi/2} \exp\left(\frac{-\xi' + d_3}{\cos \theta}\right) \sin \theta \\
& \times \int_0^{\pi/2} \exp\left(\frac{-\xi + d_3}{\cos \theta}\right) \sin \theta \\
& + \frac{2(1-S)v_{F2}^2}{v_{F3}^2 + v_{F2}^2} \int_{-d_2}^{d_2} \mu_2(\xi') d\xi' \int_0^{\pi/2} \exp\left(\frac{\xi' - d_2}{\cos \theta}\right) \sin \theta \\
& \times \int_0^{\pi/2} \exp\left(\frac{-\xi + d_3}{\cos \theta}\right) \sin \theta \\
& + \int_0^{\pi/2} ST_{23}(\theta_2) B(\theta_2) \exp\left(\frac{-2d_2}{\cos \theta_2}\right) \exp\left(\frac{-\xi + d_3}{\cos \theta_3(\theta_2)}\right) \sin \theta_3(\theta_2) d\theta_3(\theta_2) \\
& + \frac{2(1-S)v_{F2}^2}{v_{F3}^2 + v_{F2}^2} \int_0^{\pi/2} B(\theta_2) \exp\left(\frac{-2d_2}{\cos \theta}\right) \sin \theta d\theta \int_0^{\pi/2} \exp\left(\frac{-\xi + d_3}{\cos \theta}\right) \sin \theta d\theta
\end{aligned} \tag{A.17}$$

where

$$\begin{aligned}
A(\theta_2) & = eE_2 l_2 |\cos \theta_2| (1 + SR_{23}(\theta_2)) - ST_{23}(\theta_2) eE_3 l_3 |\cos \theta_3(\theta_2)| \\
& + SR_{23}(\theta_2) B(\theta_2) \exp\left(\frac{-2d_2}{\cos \theta_2}\right) + \frac{2(1-S)v_{F2}^2}{v_{F3}^2 + v_{F2}^2} \int_0^{\pi/2} B(\theta) \exp\left(\frac{-2d_2}{\cos \theta}\right) \sin \theta d\theta \\
& + SR_{23}(\theta_2) \int_{-d_2}^{d_2} \exp\left(\frac{\xi' - d_2}{\cos \theta_2}\right) \frac{\mu_2(\xi')}{\cos \theta_2} d\xi' \\
& + ST_{23}(\theta_2) \int_{d_3}^{\infty} \exp\left(\frac{-\xi' + d_3}{\cos \theta_3(\theta_2)}\right) \frac{\mu_3(\xi')}{\cos \theta_3(\theta_2)} d\xi'
\end{aligned} \tag{A.18}$$

$$\begin{aligned}
& + \frac{2(1-S)v_{F2}^2}{v_{F3}^2 + v_{F2}^2} \int_{-d_2}^{d_2} \mu_2(\xi') d\xi' \int_0^{\pi/2} \exp\left(\frac{\xi' - d_2}{\cos \theta}\right) \sin \theta d\theta \\
& + \frac{2(1-S)v_{F3}^2}{v_{F3}^2 + v_{F2}^2} \int_{d_3}^{\infty} \mu_3(\xi') d\xi' \int_0^{\pi/2} \exp\left(\frac{-\xi' + d_3}{\cos \theta}\right) \sin \theta d\theta \\
\\
B(\theta_2) & = -eE_2 l_2 |\cos \theta_2| (1 + SR_{21}(\theta_2)) + ST_{21}(\theta_2) eE_1 l_1 |\cos \theta_1(\theta_2)| \\
& + SR_{21}(\theta_2) A(\theta_2) \exp\left(\frac{-2d_2}{\cos \theta_2}\right) + \frac{2(1-S)v_{F2}^2}{v_{F1}^2 + v_{F2}^2} \int_0^{\pi/2} A(\theta) \exp\left(\frac{-2d_2}{\cos \theta}\right) \sin \theta d\theta \\
& + SR_{21}(\theta_2) \int_{-d_2}^{d_2} \exp\left(\frac{-\xi' - d_2}{\cos \theta_2}\right) \frac{\mu_2(\xi')}{\cos \theta_2} d\xi' \\
& + ST_{21}(\theta_2) \int_{-\infty}^{-d_1} \exp\left(\frac{\xi' + d_1}{\cos \theta_1(\theta_2)}\right) \frac{\mu_1(\xi')}{\cos \theta_1(\theta_2)} d\xi' \\
& + \frac{2(1-S)v_{F2}^2}{v_{F1}^2 + v_{F2}^2} \int_{-d_2}^{d_2} \mu_2(\xi') d\xi' \int_0^{\pi/2} \exp\left(\frac{-\xi' - d_2}{\cos \theta}\right) \sin \theta d\theta \\
& + \frac{2(1-S)v_{F1}^2}{v_{F1}^2 + v_{F2}^2} \int_{-\infty}^{-d_1} \mu_1(\xi') d\xi' \int_0^{\pi/2} \exp\left(\frac{\xi' + d_1}{\cos \theta}\right) \sin \theta d\theta
\end{aligned} \tag{A.19}$$

A.5 Equations for chemical potential for five-layered system

In this appendix, equations for the chemical potential profile in the system consisting of five metallic layers (Fig. A.4) are presented without derivation. For simplicity, only symmetrical structures $M_1\text{-}M_2\text{-}M_3\text{-}M_2\text{-}M_1$ are considered. The same electron relaxation time τ is assumed in all three metals, and a dimensionless variable $\xi = z/l_i$ is introduced, where $l_i = v_{Fi}\tau$ is an electron mean free path in the i -th layer, so that $\mu_i = \mu_i(\xi = z/l_i)$, and $d_i = d/l_i$, $b_i = b/l_i$, where $2d$ is the thickness of the middle layer, $2b$ is the thickness of the second and fourth layers.

$$2\mu_1(\xi) = \int_{-\infty}^{-d_1-2b_1} \mu_1(\xi') d\xi' \int_0^{\pi/2} \exp\left(-\frac{|\xi - \xi'|}{\cos \theta_1}\right) \tan \theta_1 d\theta_1 \tag{A.20}$$

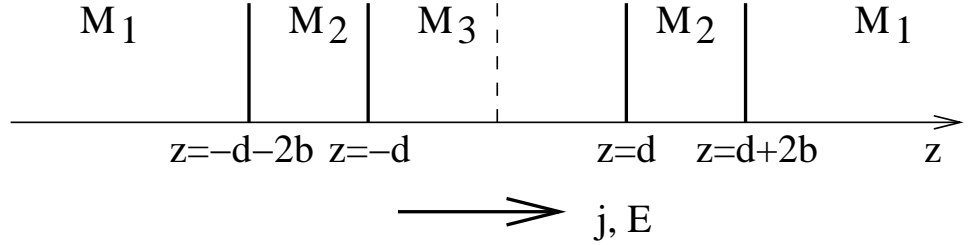


Figure A.4: System consisting of five layers.

$$+ \int_0^{\pi/2} A(\theta_1) \exp\left(\frac{\xi + d_1 + 2b_1}{\cos \theta_1}\right) \sin \theta_1 d\theta_1$$

$$\begin{aligned} 2\mu_2(\xi) &= \int_{-d_2-2b_2}^{-d_2} \mu_2(\xi') d\xi' \int_0^{\pi/2} \exp\left(-\frac{|\xi - \xi'|}{\cos \theta_2}\right) \tan \theta_2 d\theta_2 \quad (\text{A.21}) \\ &+ \int_0^{\pi/2} B_1(\theta_2) \exp\left(-\frac{\xi + d_2 + 2b_2}{\cos \theta_2}\right) \sin \theta_2 d\theta_2 \\ &+ \int_0^{\pi/2} B_2(\theta_2) \exp\left(\frac{\xi + d_2}{\cos \theta_2}\right) \sin \theta_2 d\theta_2 \end{aligned}$$

$$\begin{aligned} 2\mu_3(\xi) &= \int_{-d_3}^{d_3} \mu_3(\xi') d\xi' \int_0^{\pi/2} \exp\left(-\frac{|\xi - \xi'|}{\cos \theta_3}\right) \tan \theta_3 d\theta_3 \quad (\text{A.22}) \\ &+ \int_0^{\pi/2} C(\theta_3) \left(\exp\left(\frac{-\xi - d_3}{\cos \theta_3}\right) - \exp\left(\frac{\xi - d_3}{\cos \theta_3}\right) \right) \sin \theta_3 d\theta_3 \end{aligned}$$

$$\mu_4(\xi) = -\mu_2(-\xi) \quad (\text{A.23})$$

$$\mu_5(\xi) = -\mu_1(-\xi) \quad (\text{A.24})$$

where

$$\begin{aligned}
A(\theta_1) = & eE_1l_1(1 + SR_{12}(\theta_1))\cos\theta_1 - eE_2l_2ST_{12}(\theta_1)\cos\theta_2(\theta_1) \\
& + SR_{12}(\theta_1) \int_{-\infty}^{-d_1-2b_1} \exp\left(\frac{\xi' + d_1 + 2b_1}{\cos\theta_1}\right) \frac{\mu_1(\xi')}{\cos\theta_1} d\xi' \\
& + \frac{2(1-S)v_{F1}^2}{v_{F1}^2 + v_{F2}^2} \int_{-\infty}^{-d_1-2b_1} \mu_1(\xi') d\xi' \int_0^{\pi/2} \exp\left(\frac{\xi' + d_1 + 2b_1}{\cos\theta}\right) \sin\theta d\theta \\
& + ST_{12}(\theta_1) \int_{-d_2-2b_2}^{-d_2} \exp\left(\frac{-\xi' - d_2 - 2b_2}{\cos\theta_2(\theta_1)}\right) \frac{\mu_2(\xi')}{\cos\theta_2(\theta_1)} d\xi' \\
& + \frac{2(1-S)v_{F2}^2}{v_{F1}^2 + v_{F2}^2} \int_{-d_2-2b_2}^{-d_2} \mu_2(\xi') d\xi' \int_0^{\pi/2} \exp\left(\frac{-\xi' - d_2 - 2b_2}{\cos\theta}\right) \sin\theta d\theta \\
& + ST_{12}(\theta_1)B_2(\theta_2(\theta_1)) \exp\left(\frac{-2b_2}{\cos\theta_2(\theta_1)}\right) \\
& + \frac{2(1-S)v_{F2}^2}{v_{F1}^2 + v_{F2}^2} \int_0^{\pi/2} B_2(\theta) \exp\left(\frac{-2b_2}{\cos\theta}\right) \cos\theta \sin\theta d\theta
\end{aligned} \tag{A.25}$$

$$\begin{aligned}
B_1(\theta_1) = & -eE_2l_2(1 + SR_{21}(\theta_2))\cos\theta_2 + eE_1l_1ST_{21}(\theta_2)\cos\theta_1(\theta_2) \\
& + ST_{21}(\theta_2) \int_{-\infty}^{-d_1-2b_1} \exp\left(\frac{\xi' + d_1 + 2b_1}{\cos\theta_1(\theta_2)}\right) \frac{\mu_1(\xi')}{\cos\theta_1(\theta_2)} d\xi' \\
& + \frac{2(1-S)v_{F1}^2}{v_{F1}^2 + v_{F2}^2} \int_{-\infty}^{-d_1-2b_1} \mu_1(\xi') d\xi' \int_0^{\pi/2} \exp\left(\frac{\xi' + d_1 + 2b_1}{\cos\theta}\right) \sin\theta d\theta \\
& + SR_{21}(\theta_2) \int_{-d_2-2b_2}^{-d_2} \exp\left(\frac{-\xi' - d_2 - 2b_2}{\cos\theta_2}\right) \frac{\mu_2(\xi')}{\cos\theta_2} d\xi' \\
& + \frac{2(1-S)v_{F2}^2}{v_{F1}^2 + v_{F2}^2} \int_{-d_2-2b_2}^{-d_2} \mu_2(\xi') d\xi' \int_0^{\pi/2} \exp\left(\frac{-\xi' - d_2 - 2b_2}{\cos\theta}\right) \sin\theta d\theta \\
& + SR_{21}(\theta_2)B_2(\theta_2) \exp\left(\frac{-2b_2}{\cos\theta_2}\right) \\
& + \frac{2(1-S)v_{F2}^2}{v_{F1}^2 + v_{F2}^2} \int_0^{\pi/2} B_2(\theta) \exp\left(\frac{-2b_2}{\cos\theta}\right) \cos\theta \sin\theta d\theta
\end{aligned} \tag{A.26}$$

$$\begin{aligned}
B_2(\theta_2) = & eE_2l_2(1 + SR_{23}(\theta_2)) \cos \theta_2 - eE_3l_3ST_{23}(\theta_2) \cos \theta_3(\theta_2) \\
& + SR_{23}(\theta_2) \int_{-d_2-2b_2}^{-d_2} \exp\left(\frac{\xi' + d_2}{\cos \theta_2}\right) \frac{\mu_2(\xi')}{\cos \theta_2} d\xi' \\
& + \frac{2(1-S)v_{F2}^2}{v_{F3}^2 + v_{F2}^2} \int_{-d_2-2b_2}^{-d_2} \mu_2(\xi') d\xi' \int_0^{\pi/2} \exp\left(\frac{\xi' + d_2}{\cos \theta}\right) \sin \theta d\theta \\
& + ST_{23}(\theta_2) \int_{-d_3}^{d_3} \exp\left(\frac{-\xi' - d_3}{\cos \theta_3(\theta_2)}\right) \frac{\mu_3(\xi')}{\cos \theta_3(\theta_2)} d\xi' \\
& + \frac{2(1-S)v_{F3}^2}{v_{F3}^2 + v_{F2}^2} \int_{-d_3}^{d_3} \mu_3(\xi') d\xi' \int_0^{\pi/2} \exp\left(\frac{-\xi' - d_3}{\cos \theta}\right) \sin \theta d\theta \\
& + SR_{23}(\theta_2) B_1(\theta_2) \exp\left(\frac{-2b_2}{\cos \theta_2}\right) \\
& + \frac{2(1-S)v_{F2}^2}{v_{F3}^2 + v_{F2}^2} \int_0^{\pi/2} B_1(\theta) \exp\left(\frac{-2b_2}{\cos \theta}\right) \cos \theta \sin \theta d\theta \\
& - ST_{23}(\theta_2) C(\theta_2) \exp\left(\frac{-2d_3}{\cos \theta_3(\theta_2)}\right) \\
& - \frac{2(1-S)v_{F3}^2}{v_{F3}^2 + v_{F2}^2} \int_0^{\pi/2} C(\theta) \exp\left(\frac{-2d_3}{\cos \theta}\right) \cos \theta \sin \theta d\theta
\end{aligned} \tag{A.27}$$

$$\begin{aligned}
C(\theta_3(1 + SR_{32}(\theta_3))) \exp\left(\frac{2d_3}{\cos \theta_3}\right) = & -eE_3l_3(1 + SR_{32}(\theta_3)) \cos \theta_3 + eE_2l_2ST_{32}(\theta_3) \cos \theta_2(\theta_3) \\
& + ST_{32}(\theta_3) \int_{-d_2-2b_2}^{-d_2} \exp\left(\frac{\xi' + d_2}{\cos \theta_2(\theta_3)}\right) \frac{\mu_2(\xi')}{\cos \theta_2(\theta_3)} d\xi' \\
& + \frac{2(1-S)v_{F2}^2}{v_{F3}^2 + v_{F2}^2} \int_{-d_2-2b_2}^{-d_2} \mu_2(\xi') d\xi' \int_0^{\pi/2} \exp\left(\frac{\xi' + d_2}{\cos \theta}\right) \sin \theta d\theta \\
& + SR_{32}(\theta_3) \int_{-d_3}^{d_3} \exp\left(\frac{-\xi' - d_3}{\cos \theta_3}\right) \frac{\mu_3(\xi')}{\cos \theta_3} d\xi' \\
& + \frac{2(1-S)v_{F3}^2}{v_{F3}^2 + v_{F2}^2} \int_{-d_3}^{d_3} \mu_3(\xi') d\xi' \int_0^{\pi/2} \exp\left(\frac{-\xi' - d_3}{\cos \theta}\right) \sin \theta d\theta
\end{aligned} \tag{A.28}$$

$$\begin{aligned}
& + ST_{32}(\theta_2)C(\theta_2(\theta_3)) \exp\left(\frac{-2b_2}{\cos\theta_2(\theta_3)}\right) \\
& + \frac{2(1-S)v_{F2}^2}{v_{F3}^2 + v_{F2}^2} \int_0^{\pi/2} B_1(\theta) \exp\left(\frac{-2b_2}{\cos\theta}\right) \cos\theta \sin\theta d\theta \\
& - \frac{2(1-S)v_{F3}^2}{v_{F3}^2 + v_{F2}^2} \int_0^{\pi/2} C(\theta) \exp\left(\frac{-2d_3}{\cos\theta}\right) \cos\theta \sin\theta d\theta
\end{aligned}$$

A.6 Numerical procedure of solving the Fredholm equation of the second kind

In this Appendix, the numerical procedure of solving the Fredholm equation of the second kind, Eq. (3.4), will be briefly discussed. The general form of the Fredholm equation of the second kind is the following:

$$f(x) = \int_a^b K(x, y) f(y) dy + g(x), \quad (\text{A.29})$$

where $f(x)$ is an unknown function defined on the interval $[a, b]$ of the real axis, $K(x, y)$ is the kernel of the integral, and $g(x)$ is the source.

The Nystrom routine is used in to solve the equation (A.29). [69] It transforms the integral equation into the system of N linear equations for the unknown vector $f(x_i)$, where x_i are the points of the mesh at the interval $[a, b]$, given by the N -point Gauss-Legendre rule. This standard rule [69] gives the points of the mesh with weights:

$$gauleg(a, b, \mathbf{x}, \mathbf{w}, N),$$

where a and b are the boundaries of the interval of interest, \mathbf{x} is the vector of the points of the mesh, \mathbf{w} is the vector of the weights, and N is the number of points in the mesh. The equation for the vector $f(x_i)$ takes the following form:

$$f(x_i) = \sum_{j=1}^N K(x_i, y_j) f(y_j) w_j + g(x_i), \quad (\text{A.30})$$

or

$$f_i = \sum_{j=1}^N \bar{K}_{ij} f_j + g_i, \quad (\text{A.31})$$

where $\bar{K}_{ij} = w_j K(x_i, y_j)$, or, in the matrix form,

$$(\hat{\mathbf{1}} - \hat{\bar{K}})\mathbf{f} = \mathbf{g}. \quad (\text{A.32})$$

In the case of a singularity in the kernel, for instance if $K(x, y) \rightarrow \infty$ when $x = y$, this singularity is removed from the integral by writing

$$\int_a^b K(x, y) f(y) dy = \int_a^b K(x, y) (f(y) - f(x)) dy + r(x) f(x),$$

where $r(x) = \int_a^b K(x, y) dy$. Instead of the Eq. (A.31), the following system of equations is obtained:

$$f_i(1 - r_i + \sum_{j=1, j \neq i}^N \bar{K}_{ij}) = \sum_{j=1, j \neq i}^N \bar{K}_{ij} f_j + g_i. \quad (\text{A.33})$$

The systems of linear equations (A.31) or (A.33) are solved using the *ludcmp* and *lubksb* routines. [69] In order to work with the vectors and matrices, the standard NR.h package is used, which contains also the standard numerical routines *gauleg*, *ludcmp*, and *lubksb*.

The numerical procedure for solving the system of the Fredholm equations of the second kind, Eq. (3.5), is identical to the one for solving a single equation, and will not be covered here.

A.7 Parameters entering the equations for the chemical potentials for Co-Cu and Fe-Cr systems

A.7.1 Electrons Fermi velocities ratios for Co-Cu system

In this appendix, the ratio of the electrons Fermi velocities in the Co-Cu structure v_{FCu}/v_{FCo} for majority and minority electrons is obtained using the results presented in Ref. [70] for the transmission probabilities averaged over the Fermi surface. The probability for an electron to be transmitted through an interface between metals i and j as a

function of the angle of incidence takes the following form (see Appendix A.3):

$$T_{ij}(\cos \theta) = \frac{4\sqrt{1 + (v_{Fj}^2/v_{Fi}^2 - 1)/\cos^2 \theta}}{1 + \sqrt{1 + (v_{Fj}^2/v_{Fi}^2 - 1)/\cos^2 \theta}}, \quad (\text{A.34})$$

where v_{Fi}^2 and v_{Fj}^2 are the electron Fermi velocities in the metals i and j . After averaging over the Fermi surface, the expression for the transmission probability takes the following form:

$$T(A) = \frac{1}{2} \int_0^\pi T_{ij}(\cos \theta, A) \sin \theta d\theta = 4A \int_0^{1/A} \frac{\sqrt{1 + 1/x^2}}{1 + \sqrt{1 + 1/x^2}}, \quad (\text{A.35})$$

where $A = v_{Fj}^2/v_{Fi}^2 - 1$. The equation $T(A) = T^*$ is solved numerically, with T^* equal to 0.44 for the minority electrons, and 0.66 for the majority electrons. [70] In this illustration, a (110) interface has been chosen, and the electrons were assumed to go from Cu into Co. The ratio v_{FCu}/v_{FCo} is found to be 1.05 for majority electrons, and 1.18 for minority electrons. If the motion from Co into Cu is considered, the same ratio of v_{FCu}/v_{FCo} is obtained for majority electrons, but different ratio is obtained for minority electrons; this suggests that the free electron approximation used to obtain the transmission probability expression (A.34) is reasonable for majority states, but not for minority states. Within the free electron model, the averaging over the Fermi surface is performed, and the information about the true electron momenta is lost, which leads to different values of v_{FCu}/v_{FCo} for different directions of motion.

A.7.2 The summary of the Fermi velocities ratios entering the equations for the chemical potentials

The following table summarizes the correspondence between the equations that have to be solved in order to find the resistances of up and down electrons $R \uparrow$ and $R \downarrow$ in different geometries and magnetization configurations (Fig. 4.9) and the electron Fermi velocities ratios entering these equations:

		Two layers	Three or five layers	
		Eqs.(3.14)-(3.15)	Eqs.(A.15)-(A.19) or (A.20)-(A.28)	
			parallel	anti-parallel
CoCu	$R \uparrow$	$\frac{v_{F2}}{v_{F1}} = 1.05$	$\frac{v_{F2}}{v_{F1}} = \frac{v_{F2}}{v_{F3}} = 1.05$	$\frac{v_{F2}}{v_{F1}} = 1.05; \frac{v_{F2}}{v_{F3}} = 1.18$
	$R \downarrow$	$\frac{v_{F2}}{v_{F1}} = 1.18$	$\frac{v_{F2}}{v_{F1}} = \frac{v_{F2}}{v_{F3}} = 1.18$	$\frac{v_{F2}}{v_{F1}} = 1.18; \frac{v_{F2}}{v_{F3}} = 1.05$
FeCr	$R \uparrow$	$\frac{v_{F2}}{v_{F1}} = 0.837$	$\frac{v_{F2}}{v_{F1}} = \frac{v_{F2}}{v_{F3}} = 0.837$	$\frac{v_{F2}}{v_{F1}} = 0.837; \frac{v_{F2}}{v_{F3}} = 1.003$
	$R \downarrow$	$\frac{v_{F2}}{v_{F1}} = 1.003$	$\frac{v_{F2}}{v_{F1}} = \frac{v_{F2}}{v_{F3}} = 1.003$	$\frac{v_{F2}}{v_{F1}} = 1.003; \frac{v_{F2}}{v_{F3}} = 0.837$

Appendix B

Appendices for torques chapters

B.1 Derivation of the boundary conditions for spin-accumulation and spin-current between the layers

In this appendix, the boundary conditions at the interfaces between the layers in Fig. 1.11 are derived. To achieve this goal, I consider a sub-system shown in Fig. B.1 which consists of a semi-infinite FM layer with $x < 0$ with the local magnetization $\mathbf{M} = \cos \theta \mathbf{e}_z - \sin \theta \mathbf{e}_y$, a diffuse interfacial layer I between $0 < x < d^I$ with the same local magnetization as in the FM layer, and a semi-infinite NM layer for $x > d^I$. When d^I is infinitesimally small, this sub-system represents the three FM-NM interfaces in Fig. 1.11, i.e., between the thick FM and spacer layers, between the spacer and thin FM layers (when spatially inverted), and between the thin FM and back NM layers. Both spin accumulation and current are assumed to be continuous at the FM-I and I-NM interfaces, and one can derive the relation between spin accumulation and current at $x = 0$ with the same quantities at $x = d^I$ as the thickness of the interfacial layer d^I goes to zero. In this limit the parameters of the interfacial layer, such as λ_{mfp}^I , τ_{sf}^I , J^I , λ_J^I , and, most important, its resistance AR_I remain constant; the latter condition implies that the diffusion constant of the interfacial layer $D_0^I \sim d^I$ as $d^I \rightarrow 0$.

Equations (5.9), (5.10) for the spin accumulation are solved, and the Eq. (5.5) is used to find spin current in the ferromagnetic and interfacial layers. By adopting a set of local coordinates $(\bar{x}, \bar{y}, \bar{z})$ such that the *local* magnetization is $\mathbf{M}_{\bar{z}} = \mathbf{e}_{\bar{z}}$ the spin accumulation

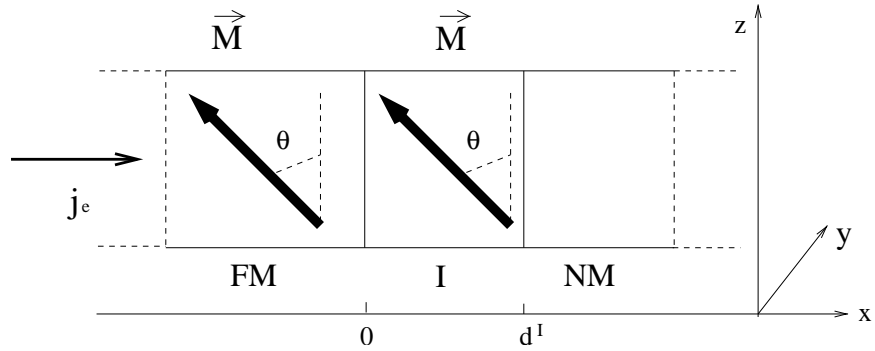


Figure B.1: Structure of the interface between the layers at Fig.1.11. FM is a semi-infinite ferromagnetic layer with the local magnetization $\mathbf{M}_d^{(2)} = \cos \theta \mathbf{e}_z - \sin \theta \mathbf{e}_y$, I is a diffuse interfacial layer with the same local magnetization as in FM layer, and NM is a semi-infinite nonmagnetic layer.

and current in the FM layer take the form:

$$\begin{cases} m_{\bar{x}}^F = 2Re \left(G_2 \exp \left(\frac{x}{l_+^F} \right) \right) \\ m_{\bar{y}}^F = 2Im \left(G_2 \exp \left(\frac{x}{l_+^F} \right) \right) \\ m_{\bar{z}}^F = G_1 \exp \left(\frac{x}{\lambda_{sdl}^F} \right), \end{cases} \quad (\text{B.1})$$

and

$$\begin{cases} j_{m,\bar{x}}^F = -4D_0^F Re \left(\frac{G_2}{l_+^F} \exp \left(\frac{x}{l_+^F} \right) \right) \\ j_{m,\bar{y}}^F = -4D_0^F Im \left(\frac{G_2}{l_+^F} \exp \left(\frac{x}{l_+^F} \right) \right) \\ j_{m,\bar{z}}^F = \beta j_e - \frac{2D_0^F(1-\beta\beta')}{\lambda_{sdl}^F} G_1 \exp \left(\frac{x}{\lambda_{sdl}^F} \right). \end{cases} \quad (\text{B.2})$$

In the interfacial layer, spin accumulation and spin current take the form:

$$\begin{cases} m_{\bar{x}}^I = 2\operatorname{Re} \left(G_5 \exp\left(\frac{x}{l_+^I}\right) \right) + 2\operatorname{Re} \left(G_6 \exp\left(-\frac{x}{l_+^I}\right) \right) \\ m_{\bar{y}}^I = 2\operatorname{Im} \left(G_5 \exp\left(\frac{x}{l_+^I}\right) \right) + 2\operatorname{Im} \left(G_6 \exp\left(-\frac{x}{l_+^I}\right) \right) \\ m_{\bar{z}}^I = G_3 \exp\left(\frac{x}{\lambda_{sdl}^I}\right) + G_4 \exp\left(-\frac{x}{\lambda_{sdl}^I}\right), \end{cases} \quad (\text{B.3})$$

and

$$\begin{cases} j_{m,\bar{x}}^I = -4D_0^I \left[\operatorname{Re} \left(\frac{G_5}{l_+^I} \exp\left(\frac{x}{l_+^I}\right) \right) - \operatorname{Re} \left(\frac{G_6}{l_+^I} \exp\left(-\frac{x}{l_+^I}\right) \right) \right] \\ j_{m,\bar{y}}^I = -4D_0^I \left[\operatorname{Im} \left(\frac{G_5}{l_+^I} \exp\left(\frac{x}{l_+^I}\right) \right) - \operatorname{Im} \left(\frac{G_6}{l_+^I} \exp\left(-\frac{x}{l_+^I}\right) \right) \right] \\ j_{m,\bar{z}}^I = \gamma j_e - \frac{2D_0^I(1-\gamma\gamma')}{\lambda_{sdl}^I} \left[G_3 \exp\left(\frac{x}{\lambda_{sdl}^I}\right) - G_4 \exp\left(-\frac{x}{\lambda_{sdl}^I}\right) \right]. \end{cases} \quad (\text{B.4})$$

Here β, β' are spin-polarization parameters for the conductivity and diffusion constant in the bulk of the ferromagnetic layer, defined in Chap. 5; γ, γ' are similar parameters for the conductivity and diffusion constant in the interfacial layer, defined as

$$\begin{aligned} \mathbf{C}_I &= \gamma C_0^I \mathbf{M}_d, \\ \mathbf{D}_I &= \gamma' D_0^I \mathbf{M}_d. \end{aligned} \quad (\text{B.5})$$

and

$$(l_+^{F,I})^{-1} = \sqrt{\frac{1}{(\lambda_{sf}^{F,I})^2} - \frac{i}{(\lambda_J^{F,I})^2}} \approx \frac{1-i}{\sqrt{2}\lambda_J^{F,I}}, \quad (\text{B.6})$$

when $\lambda_J^{F,I} \ll \lambda_{sf}^{F,I}$.

The boundary conditions for the continuity of the spin accumulation and current at

the interface between ferromagnetic and interfacial layer $x = 0$ take the form:

$$\begin{cases} 2ReG_2 = 2ReG_5 + 2ReG_6 \\ 2ImG_2 = 2ImG_5 + 2ImG_6 \\ G_1 = G_3 + G_4, \end{cases} \quad (\text{B.7})$$

and

$$\begin{cases} -4D_0^F Re\left(\frac{G_2}{l_+^F}\right) = -4D_0^I Re\left(\frac{G_5 - G_6}{l_+^I}\right) \\ -4D_0^F Im\left(\frac{G_2}{l_+^F}\right) = -4D_0^I Im\left(\frac{G_5 - G_6}{l_+^I}\right) \\ \beta j_e - \frac{2D_0^F(1-\beta\beta')}{\lambda_{sdl}^F} G_1 = \gamma j_e - \frac{2D_0^I(1-\gamma\gamma')}{\lambda_{sdl}^I} (G_3 - G_4). \end{cases} \quad (\text{B.8})$$

To relate $\mathbf{m}^F(0)$ to $\mathbf{m}^I(d^I)$, and $\mathbf{j}_m^F(0)$ to $\mathbf{j}_m^I(d^I)$, one can use the assumption that as the thickness of the interfacial layer goes to zero, other parameters of the interfacial layer, such as λ_{sdl}^I , J^I , and λ_J^I remain constant, but the diffusion constant D_0^I goes to zero with the same rate as d^I , so that $d^I/D_0^I = \text{const}$. Then, for example, for small $d^I \ll \lambda_J^I$ the \bar{x} -component of the spin-accumulation at $x = d^I$ may be written as

$$m_{\bar{x}}^I(d^I \rightarrow 0) \approx 2Re(G_5 + G_6) + 2Re\left((G_5 - G_6)\frac{d^I}{l_+^I}\right). \quad (\text{B.9})$$

By comparing this expression with Eqs. (B.7) and (B.8), the following relation between the \bar{x} -components of spin accumulation and current at $x = 0$ and $x = d^I$ is obtained:

$$m_{\bar{x}}^I(d^I \rightarrow 0) = m_{\bar{x}}^F(0) - j_{m,\bar{x}}^F(0)\frac{d^I}{2D_0^I}, \quad (\text{B.10})$$

and similarly,

$$m_{\bar{y}}^I(d^I \rightarrow 0) = m_{\bar{y}}^F(0) - j_{m,\bar{y}}^F(0)\frac{d^I}{2D_0^I}, \quad (\text{B.11})$$

$$m_{\bar{z}}^I(d^I \rightarrow 0) = m_{\bar{z}}^F(0) + j_e\frac{\gamma}{2(1-\gamma\gamma')}\frac{d^I}{D_0^I} - j_{m,\bar{z}}^F(0)\frac{1}{2(1-\gamma\gamma')}\frac{d^I}{D_0^I}. \quad (\text{B.12})$$

In a manner similar to Eq. (B.9) the \bar{x} -component of spin current at $x = d^I$ may be

written as

$$j_{m,\bar{x}}^I(d^I \rightarrow 0) \approx -4D_0^I \operatorname{Re} \left(\frac{G_5 - G_6}{l_+^I} \right) - 2 \operatorname{Re} (i(G_5 + G_6)) \frac{d^I J^I}{\hbar}.$$

By comparing this expression with Eqs. (B.7) and (B.8), one finds the continuity condition for the \bar{x} -component of spin current:

$$j_{m,\bar{x}}^I(d^I \rightarrow 0) = j_{m,\bar{x}}^F(0) - m_{\bar{y}}^F(0) \frac{d^I J^I}{\hbar}, \quad (\text{B.13})$$

and, similarly,

$$j_{m,\bar{y}}^I(d^I \rightarrow 0) = j_{m,\bar{y}}^F(0) + m_{\bar{x}}^F(0) \frac{d^I J^I}{\hbar}, \quad (\text{B.14})$$

and

$$j_{m,\bar{z}}^I(d^I \rightarrow 0) = j_{m,\bar{z}}^F(0) - m_{\bar{z}}^F(0) \frac{d^I J^I}{\tau_{sf}^I}. \quad (\text{B.15})$$

With these relations, the boundary conditions at the three interfaces in the multilayered structure depicted in Fig. 1.11 can now be obtained.

By using the conditions Eqs. (B.10)-(B.15), the boundary conditions at the interface between the thin (first) ferromagnetic and non-magnetic (N) layers of the structure shown in Fig. 1.11 at $x = t_F$ may be written immediately, since in the thin FM layer the local coordinate system $(\bar{x}, \bar{y}, \bar{z})$ coincides with the global axes (x, y, z) ; one finds

$$\begin{cases} m_x^N(t_F) - m_x^{(1)}(t_F) = -r j_{m,x}^{(1)}(t_F) \\ m_y^N(t_F) - m_y^{(1)}(t_F) = -r j_{m,y}^{(1)}(t_F) \\ m_z^N(t_F) - m_z^{(1)}(t_F) = r j_e \frac{\gamma}{1-\gamma\gamma'} - r j_{m,z}^{(1)}(t_F) \frac{1}{1-\gamma\gamma'}, \end{cases} \quad (\text{B.16})$$

and

$$\begin{cases} j_{m,x}^N(t_F) - j_{m,x}^{(1)}(t_F) = -m_y^{(1)}(t_F) \frac{d^I J^I}{\hbar} \\ j_{m,y}^N(t_F) - j_{m,y}^{(1)}(t_F) = m_x^{(1)}(t_F) \frac{d^I J^I}{\hbar} \\ j_{m,z}^N(t_F) - j_{m,z}^{(1)}(t_F) = -m_z^{(1)}(t_F) \frac{d^I J^I}{\tau_{sf}^I}, \end{cases} \quad (\text{B.17})$$

where $r = d^I/2D_0^I$. Similarly, the boundary conditions at the interface between the non-magnetic spacer (S) and the thin (first) FM layer at $x = 0$ take the form:

$$\begin{cases} m_x^S(0) - m_x^{(1)}(0) = rj_{m,x}^{(1)}(0) \\ m_y^S(0) - m_y^{(1)}(0) = rj_{m,y}^{(1)}(0) \\ m_z^S(0) - m_z^{(1)}(0) = -rj_e \frac{\gamma}{1-\gamma\gamma'} + rj_{m,z}^{(1)}(0) \frac{1}{1-\gamma\gamma'}, \end{cases} \quad (\text{B.18})$$

and

$$\begin{cases} j_{m,x}^S(0) - j_{m,x}^{(1)}(0) = m_y^{(1)}(0) \frac{d^I J^I}{\hbar} \\ j_{m,y}^S(0) - j_{m,y}^{(1)}(0) = -m_x^{(1)}(0) \frac{d^I J^I}{\hbar} \\ j_{m,z}^S(0) - j_{m,z}^{(1)}(0) = m_z^{(1)}(0) \frac{d^I}{\tau_{sf}^I}, \end{cases} \quad (\text{B.19})$$

Note that spin-current conservation condition at the interfaces, which means that there are no torques acting at the interfaces, is due to the infinitely small thickness of the interfacial layers $d^I \rightarrow 0$. To write the boundary conditions at the interface between the thick FM and NM spacer layers at $x = 0$, one have to change from the local coordinate system $(\bar{x}, \bar{y}, \bar{z})$, related to the magnetization direction in the thick FM layer, to the global (x, y, z) system. Any vector \mathbf{a} will be transformed according to the following rule:

$$\begin{cases} a_{\bar{x}} = a_x \\ a_{\bar{y}} = a_y \cos \theta + a_z \sin \theta \\ a_{\bar{z}} = -a_y \sin \theta + a_z \cos \theta. \end{cases} \quad (\text{B.20})$$

By applying this transformation to the conditions, Eqs. (B.10)-(B.15), one obtain the following boundary conditions at the interface between the thick (second) FM and non-

magnetic spacer (S) layers:

$$\left\{ \begin{array}{l} m_x^S(0) - m_x^{(2)}(0) = -rj_{m,x}^{(2)}(0) \\ m_y^S(0) - m_y^{(2)}(0) = -rj_e \frac{\gamma}{1-\gamma\gamma'} \sin \theta - rj_{m,y}^{(2)}(0) \frac{1-\gamma\gamma' \cos^2 \theta}{1-\gamma\gamma'} \\ \quad + rj_{m,z}^{(2)}(0) \sin \theta \cos \theta \frac{\gamma\gamma'}{1-\gamma\gamma'} \\ m_z^S(0) - m_z^{(2)}(0) = rj_e \frac{\gamma}{1-\gamma\gamma'} \cos \theta + rj_{m,y}^{(2)}(0) \sin \theta \cos \theta \frac{\gamma\gamma'}{1-\gamma\gamma'} \\ \quad + rj_{m,z}^{(2)}(0) \frac{1-\gamma\gamma' \sin^2 \theta}{1-\gamma\gamma'}, \end{array} \right. \quad (\text{B.21})$$

and

$$\left\{ \begin{array}{l} j_{m,x}^S(0) - j_{m,x}^{(2)}(0) = -m_y^{(2)}(0) \cos \theta \frac{d^I J^I}{\hbar} - m_z^{(2)}(0) \sin \theta \frac{d^I J^I}{\hbar} \\ j_{m,y}^S(0) - j_{m,y}^{(2)}(0) = m_x^{(2)}(0) \cos \theta \frac{d^I J^I}{\hbar} - m_y^{(2)}(0) \sin^2 \theta \frac{d^I}{\tau_{sf}^I} \\ \quad + m_z^{(2)}(0) \sin \theta \cos \theta \frac{d^I}{\tau_{sf}^I} \\ j_{m,z}^S(0) - j_{m,z}^{(2)}(0) = m_x^{(2)}(0) \sin \theta \frac{d^I J^I}{\hbar} + m_{2y}(0) \sin \theta \cos \theta \frac{d^I}{\tau_{sf}^I} \\ \quad - m_z^{(2)}(0) \cos^2 \theta \frac{d^I}{\tau_{sf}^I}, \end{array} \right. \quad (\text{B.22})$$

Note that as the thickness of the interfacial layer d^I goes to zero, for diffuse scattering considered here, large discontinuities in the spin-accumulation (Eqs. (B.16), (B.18), (B.21)) are produced, proportional to finite $r = d^I/2D_0^I$, but small discontinuities in the spin-currents (Eqs. (B.17), (B.19), (B.22)) proportional to d^I , because J_I does not increase and τ_{sf}^I does not decrease as $d^I \rightarrow 0$. Since the torque acting at the interface is proportional to the discontinuity of the spin-current at the interface (see Eq. (5.14)), the finite thickness of the interfacial layer is essential for torque production at the interface. As the infinitely small interfacial thicknesses $d^I \rightarrow 0$ are considered, one obtains spin-current conservation conditions at each interface:

$$\mathbf{j}_m^N(t_F) = \mathbf{j}_m^{(1)}(t_F), \quad (\text{B.23})$$

$$\mathbf{j}_m^S(0) = \mathbf{j}_m^{(1)}(0), \quad (\text{B.24})$$

and

$$\mathbf{j}_m^{(2)}(0) = \mathbf{j}_m^S(0). \quad (\text{B.25})$$

By eliminating $m^S(0)$ and $j_m^S(0)$ from Eqs. (B.18), (B.21), (B.24), and (B.25), one obtains the boundary conditions at the interface between thick (second) and thin (first) FM layers at $x = 0$ (of course there is the NM spacer in-between, however its thickness t_N is irrelevant for these boundary conditions as long as $t_N \ll \lambda_{sdl}^N$):

$$\left\{ \begin{array}{l} m_x^{(1)}(0) - m_x^{(2)}(0) = -2rj_{m,x}^{(1)}(0) \\ m_y^{(1)}(0) - m_y^{(2)}(0) = -rj_e \frac{\gamma}{1-\gamma\gamma'} \sin \theta - rj_{m,y}^{(1)}(0) \frac{2-\gamma\gamma'(1+\cos^2 \theta)}{1-\gamma\gamma'} \\ \quad + rj_{m,z}^{(1)}(0) \sin \theta \cos \theta \frac{\gamma\gamma'}{1-\gamma\gamma'} \\ m_z^{(1)}(0) - m_z^{(2)}(0) = rj_e \frac{\gamma}{1-\gamma\gamma'} (1 + \cos \theta) + rj_{m,y}^{(1)}(0) \sin \theta \cos \theta \frac{\gamma\gamma'}{1-\gamma\gamma'} \\ \quad - rj_{m,z}^{(1)}(0) \frac{2-\gamma\gamma' \sin^2 \theta}{1-\gamma\gamma'}, \end{array} \right. \quad (\text{B.26})$$

and

$$\mathbf{j}_m^{(1)}(0) = \mathbf{j}_m^{(2)}(0) \quad (\text{B.27})$$

Finally, I show that parameter $r = d^I/2D_0^I$ is proportional to the interface resistance AR_I found from CPP transport measurements [23]. By considering the expression (5.3) for the electrical current in the interfacial layer, and the assumptions that $D_0^I \sim d^I$ and λ_{sdl}^I remains constant as the thickness of the interfacial layer $d^I \rightarrow 0$, one finds $AR_I = d^I/2C_0^I$, or $r = \frac{d^I}{2D_0^I} = AR_I \frac{C_0^I}{D_0^I}$. Parameters C_0^I and D_0^I may be related via Einstein's relation

$$\hat{C}_I = e^2 \hat{N}_I(\epsilon_F) \hat{D}_I, \quad (\text{B.28})$$

where

$$\left\{ \begin{array}{l} \hat{C} = C_0 \hat{I} + \boldsymbol{\sigma} \cdot \mathbf{C} \\ \hat{D} = D_0 \hat{I} + \boldsymbol{\sigma} \cdot \mathbf{D} \\ \hat{N} = N_0 \hat{I} + \boldsymbol{\sigma} \cdot \mathbf{N}, \end{array} \right. \quad (\text{B.29})$$

$\boldsymbol{\sigma}$ is the Pauli matrix. In Eqs. (B.29), as well as in the equations below, the subscript I is omitted for simplicity, as only the parameters of the interfacial layer are considered.

Using the definitions of γ and γ' , Eqs. (B.5), and introducing a spin-polarization parameter for the density of states γ'' , such that

$$\mathbf{N} = \gamma'' N_0 \mathbf{M}_d \quad (\text{B.30})$$

equations (B.29) may be written as

$$\begin{cases} \hat{C} = C_0(\hat{I} + \gamma\hat{\sigma}_z) \\ \hat{D} = D_0(\hat{I} + \gamma'\hat{\sigma}_z) \\ \hat{N} = N_0(\hat{I} + \gamma''\hat{\sigma}_z). \end{cases} \quad (\text{B.31})$$

The product of \hat{N} and \hat{D} then takes the form

$$\hat{N}\hat{D} = N_0 D_0((1 + \gamma'\gamma'')\hat{I} + (\gamma' + \gamma'')\hat{\sigma}_z),$$

and from the Einstein's relation (B.28) it follows that

$$\begin{cases} C_0 = e^2 N_0 D_0(1 + \gamma'\gamma'') \\ \gamma C_0 = e^2 N_0 D_0(\gamma' + \gamma''). \end{cases} \quad (\text{B.32})$$

The experimental value of γ may be found in the Ref. [23], the value of γ'' may be found from the density of states of up and down electrons, N_\uparrow and N_\downarrow correspondingly, since \hat{N} may be written as

$$\hat{N} = \begin{pmatrix} N_\uparrow & 0 \\ 0 & N_\downarrow \end{pmatrix},$$

and comparing this matrix with the expression for \hat{N} in (B.31), one obtains

$$\begin{cases} \gamma'' = \frac{N_\uparrow - N_\downarrow}{N_\uparrow + N_\downarrow} \\ N_0 = \frac{N_\uparrow + N_\downarrow}{2}. \end{cases} \quad (\text{B.33})$$

From the equation (B.32) the spin-polarization parameter γ' can be expressed in terms of γ and γ'' as

$$\gamma' = \frac{\gamma - \gamma''}{1 - \gamma\gamma''}, \quad (\text{B.34})$$

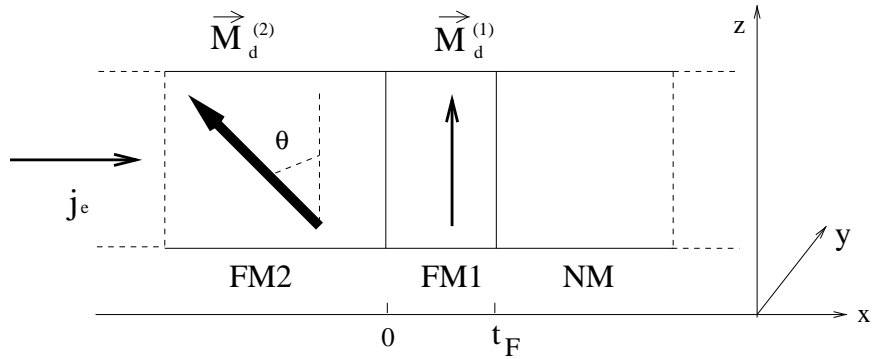


Figure B.2: Three-layered structure used for current induced reversal of a magnetic layer. FM2 is a thick ferromagnetic layer with the thickness exceeding λ_{sdl}^F and local magnetization $\mathbf{M}_d^{(2)} = \cos \theta \mathbf{e}_z - \sin \theta \mathbf{e}_y$, FM1 is a thin ferromagnetic layer with the thickness t_F and local magnetization $\mathbf{M}_d^{(1)} = \mathbf{e}_z$, and NM is a nonmagnetic back layer.

so that the parameter r takes the form:

$$r = A R_I e^2 N_0^I(\epsilon_F) \frac{1 - \gamma''^2}{1 - \gamma \gamma'}, \quad (\text{B.35})$$

where e is the electron charge, $N_0^I(\epsilon_F)$ is the density of states at the interface at Fermi energy.

B.2 Solution of the diffusion equation for spin-accumulation

In this appendix, I present the expressions for the spin-accumulation and spin-current in the multilayered system shown on the Fig. B.2.

Equations. (5.9), (5.10) for the spin accumulation in each of three layers are solved, and the spin currents are found using Eq. (5.5). In the thick ferromagnetic layer, spin

accumulation and current take the form

$$\begin{cases} m_x^{(2)} = 2Re \left(G_2 \exp\left(\frac{x}{l_+}\right) \right) \\ m_y^{(2)} = 2Im \left(G_2 \exp\left(\frac{x}{l_+}\right) \right) \cos \theta - G_1 \exp\left(\frac{x}{\lambda_{sdl}^F}\right) \sin \theta \\ m_z^{(2)} = 2Im \left(G_2 \exp\left(\frac{x}{l_+}\right) \right) \sin \theta + G_1 \exp\left(\frac{x}{\lambda_{sdl}^F}\right) \cos \theta, \end{cases} \quad (\text{B.36})$$

and

$$\begin{cases} j_{m,x}^{(2)} = -4D_0 Re \left(\frac{G_2}{l_+} \exp\left(\frac{x}{l_+}\right) \right) \\ j_{m,y}^{(2)} = -\beta j_e \sin \theta - 4D_0 Im \left(\frac{G_2}{l_+} \exp\left(\frac{x}{l_+}\right) \right) \cos \theta \\ \quad + \frac{2D_0(1-\beta\beta')}{\lambda_{sdl}} G_1 \exp\left(\frac{x}{\lambda_{sdl}^F}\right) \sin \theta \\ j_{m,z}^{(2)} = \beta j_e \cos \theta - 4D_0 Im \left(\frac{G_2}{l_+} \exp\left(\frac{x}{l_+}\right) \right) \sin \theta - \frac{2D_0(1-\beta\beta')}{\lambda_{sdl}^F} G_1 \exp\left(\frac{x}{\lambda_{sdl}^F}\right) \cos \theta. \end{cases} \quad (\text{B.37})$$

In the thin ferromagnetic layer

$$\begin{cases} m_x^{(1)} = 2Re \left(G_5 \exp\left(-\frac{x}{l_+}\right) \right) + 2Re \left(G_6 \exp\left(\frac{x-t_F}{l_+}\right) \right) \\ m_y^{(1)} = 2Im \left(G_5 \exp\left(-\frac{x}{l_+}\right) \right) + 2Im \left(G_6 \exp\left(\frac{x-t_F}{l_+}\right) \right) \\ m_z^{(1)} = G_3 \exp\left(-\frac{x}{\lambda_{sdl}^F}\right) + G_4 \exp\left(\frac{x-t_F}{\lambda_{sdl}^F}\right), \end{cases} \quad (\text{B.38})$$

and

$$\begin{cases} j_{m,x}^{(1)} = 4D_0 \left[Re \left(\frac{G_5}{l_+} \exp\left(-\frac{x}{l_+}\right) \right) - Re \left(\frac{G_6}{l_+} \exp\left(\frac{x-t_F}{l_+}\right) \right) \right] \\ j_{m,y}^{(1)} = 4D_0 \left[Im \left(\frac{G_5}{l_+} \exp\left(-\frac{x}{l_+}\right) \right) - Im \left(\frac{G_6}{l_+} \exp\left(\frac{x-t_F}{l_+}\right) \right) \right] \\ j_{m,z}^{(1)} = \beta j_e + \frac{2D_0(1-\beta\beta')}{\lambda_{sdl}^F} \left[G_3 \exp\left(-\frac{x}{\lambda_{sdl}^F}\right) - G_4 \exp\left(\frac{x-t_F}{\lambda_{sdl}^F}\right) \right]. \end{cases} \quad (\text{B.39})$$

where $l_+^{-1} = \sqrt{\frac{1}{\lambda_{sf}^2} - \frac{i}{\lambda_J^2}} \approx \frac{1-i}{\sqrt{2}\lambda_J}$, and λ_{sdl}^F is spin-diffusion length in FM layer. In the non-magnetic layer,

$$\mathbf{m}^N = \mathbf{A} \exp\left(-\frac{x - t_F}{\lambda_{sdl}^N}\right), \quad (\text{B.40})$$

and

$$\mathbf{j}_m^N = \frac{2D_0^N}{\lambda_{sdl}^N} \mathbf{A} \exp\left(-\frac{x - t_F}{\lambda_{sdl}^N}\right). \quad (\text{B.41})$$

To obtain the 12 unknown constants $A_x, A_y, A_z, G_1, \text{Re}G_2, \text{Im}G_2, G_3, G_4, \text{Re}G_5, \text{Im}G_5, \text{Re}G_6, \text{Im}G_6$, one can use the boundary conditions (see Appendix B.1, Eqs. (B.16), (B.26), (B.23), and (B.27)):

$$\begin{cases} m_x^N(t_F) - m_x^{(1)}(t_F) = -rj_{m,x}^{(1)}(t_F) \\ m_y^N(t_F) - m_y^{(1)}(t_F) = -rj_{m,y}^{(1)}(t_F) \\ m_z^N(t_F) - m_z^{(1)}(t_F) = rj_e \frac{\gamma}{1-\gamma\gamma'} - rj_{m,z}^{(1)}(t_F) \frac{1}{1-\gamma\gamma'}, \end{cases} \quad (\text{B.42})$$

and

$$\begin{cases} m_x^{(1)}(0) - m_x^{(2)}(0) = -2rj_{m,x}^{(1)}(0) \\ m_y^{(1)}(0) - m_y^{(2)}(0) = -rj_e \frac{\gamma}{1-\gamma\gamma'} \sin \theta - rj_{m,y}^{(1)}(0) \frac{2-\gamma\gamma'(1+\cos^2 \theta)}{1-\gamma\gamma'} \\ \quad + rj_{m,z}^{(1)}(0) \sin \theta \cos \theta \frac{\gamma\gamma'}{1-\gamma\gamma'} \\ m_z^{(1)}(0) - m_z^{(2)}(0) = rj_e \frac{\gamma}{1-\gamma\gamma'} (1 + \cos \theta) + rj_{m,y}^{(1)}(0) \sin \theta \cos \theta \frac{\gamma\gamma'}{1-\gamma\gamma'} \\ \quad - rj_{m,z}^{(1)}(0) \frac{2-\gamma\gamma' \sin^2 \theta}{1-\gamma\gamma'}, \end{cases} \quad (\text{B.43})$$

where the parameter r is proportional to the interface resistance AR_I , $r = AR_I e^2 N_0 (1 - \gamma''^2) / (1 - \gamma\gamma')$, e is the electron charge, N_0 is the density of states at the interface, $\gamma, \gamma', \gamma''$ are the spin polarization parameters for the conductivity, diffusion constant, and density of states at the interfaces (see Appendix B.1). The other six boundary conditions

come from the conservation of spin current at the interfaces:

$$\mathbf{j}_m^N(t_F) = \mathbf{j}_m^{(1)}(t_F), \quad (\text{B.44})$$

$$\mathbf{j}_m^{(1)}(0) = \mathbf{j}_m^{(2)}(0). \quad (\text{B.45})$$

In order to find the torque a and effective field b acting on the thin ferromagnetic layer, one can use the definition of a and b (Eq. (5.12)):

$$J\mathbf{m}_\perp^{(1)} = a\mathbf{M}_d^{(2)} \times \mathbf{M}_d^{(1)} + b\mathbf{M}_d^{(1)} \times (\mathbf{M}_d^{(2)} \times \mathbf{M}_d^{(1)}) = -a \sin \theta \mathbf{e}_x - b \sin \theta \mathbf{e}_y. \quad (\text{B.46})$$

From the other hand,

$$J\mathbf{m}_\perp^{(1)} = Jm_x^{(1)}\mathbf{e}_x + Jm_y^{(1)}\mathbf{e}_y. \quad (\text{B.47})$$

Comparing these expressions, one can see that the torque a and effective field b per unit length can be obtained by averaging the x - and y - components of the spin accumulation over the thickness t_F of the thin layer.

Bibliography

- [1] S. Maekawa and T. Shinjo, in *Electronic Transport in Mesoscopic Systems* (Taylor and Francis, London and New York, 2002), Chap. 1.
- [2] M. N. Baibich *et al.*, Physical Review Letters **61**, 2472 (1988).
- [3] S. Maekawa and T. Shinjo, in *Electronic Transport in Mesoscopic Systems* (Taylor and Francis, London and New York, 2002), Chap. 2.
- [4] K.-M. H. Lenssen *et al.*, Sensors and Actuators **85**, 1 (2000).
- [5] M. Johnson, Physical Review Letters **67**, 3594 (1991).
- [6] T. Valet and A. Fert, Physical Review B **48**, 7009 (1993).
- [7] J. C. Slonczewski, Journal of Magnetism and Magnetic Materials **159**, L1 (1996).
- [8] J. C. Slonczewski, Journal of Magnetism and Magnetic Materials **195**, L261 (1999).
- [9] J. C. Slonczewski, Journal of Magnetism and Magnetic Materials **247**, 324 (2002).
- [10] L. Berger, Physical Review B **54**, 9353 (1996).
- [11] L. Berger, Journal of Applied Physics **89**, 5521 (2001).
- [12] E. B. Myers *et al.*, Science **285**, 867 (1999).
- [13] M. Tsoi *et al.*, Physical Review Letters **80**, 4281 (1998).
- [14] B. Ozyilmaz *et al.*, Physical Review Letters **61**, 067203 (2003).
- [15] J. Bass *et al.*, cond-mat/0310467 (unpublished).

- [16] A. Fert *et al.*, cond-mat/0310737 (unpublished).
- [17] T. Valet and A. Fert, Journal of Magnetism and Magnetic Materials **121**, 378 (1993).
- [18] J. Barnas and A. Fert, Physical Review B **49**, 12835 (1994).
- [19] J. Barnas and A. Fert, Journal of Magnetism and Magnetic Materials **136**, 260 (1994).
- [20] S. Zhang and P. M. Levy, Journal of Applied Physics **69**, 4786 (1991).
- [21] W. P. P. Jr. *et al.*, Journal of Magnetism and Magnetic Materials **126**, 406 (1993).
- [22] J. Bass *et al.*, Comments on Condensed Matter Physics **18**, 223 (1998).
- [23] J. Bass and W. P. P. Jr., Journal of Magnetism and Magnetic Materials **200**, 274 (1999).
- [24] S. Zhang and P. M. Levy, Physical Review B **57**, 5336 (1998).
- [25] W. H. Butler *et al.*, Journal of Applied Physics **87**, 5173 (2000).
- [26] D. R. Penn and M. D. Stiles, Physical Review B **59**, 13338 (1999).
- [27] B. Laikhtman and S. Luryi, Physical Review B **49**, 17177 (1994).
- [28] C. Kunze, Physical Review B **51**, 14085 (1995).
- [29] R. Landauer, Physical Review B **52**, 11225 (1995).
- [30] K. M. Schep *et al.*, Physical Review B **56**, 10805 (1997).
- [31] K. Xia *et al.*, cond-mat/0005314 (unpublished).
- [32] A. Shapiro and P. M. Levy, Physical Review B **63**, 014419 (2000).
- [33] X. Waintal *et al.*, Physical Review B **62**, 12317 (2000).
- [34] A. Brataas *et al.*, Physical Review Letters **84**, 2481 (2000).
- [35] D. H. Hernando *et al.*, Physical Review B **62**, 5700 (2000).

- [36] S. Zhang *et al.*, Physical Review Letters **88**, 236601 (2002).
- [37] A. Shapiro *et al.*, Physical Review B **67**, 104430 (2003).
- [38] J. Zhang and P. M. Levy, unpublished .
- [39] J. Zhang, P. M. Levy, and V. P. Antropov, unpublished .
- [40] V. P. Antropov, unpublished (unpublished).
- [41] R. L. Cooper and E. A. Uehling, Physical Review **164**, 662 (1967).
- [42] P. Dauguet *et al.*, Physical Review B **54**, 1083 (1996).
- [43] J. W. P. Pratt, private communication (unpublished).
- [44] R. Landauer, IBM Journal of Research and Development **1**, 223 (1957).
- [45] R. Landauer, Journal of Mathematical Physics **37**, 5259 (1996).
- [46] R. Landauer, Zeitschrift für Physik B - Condensed Matter **68**, 217 (1987).
- [47] S. Datta, in *Electronic Transport in Mesoscopic Systems* (Cambridge University Press, New York, 1995), Chap. 2.
- [48] J. M. Ziman, in *Principles of the Theory of Solids* (Cambridge University Press, New York, 1972), Chap. 7.
- [49] N. W. Ashcroft and N. D. Mermin, in *Solid State Physics* (Saunders College Publishing, Fort Worth, 1976), Chap. 16.
- [50] N. W. Ashcroft and N. D. Mermin, in *Solid State Physics* (Saunders College Publishing, Fort Worth, 1976), Chap. 13.
- [51] M. Büttiker *et al.*, Physical Review B **31**, 6207 (1985).
- [52] Y. Imry *et al.*, Review of Modern Physics **71**, S306 (1999).
- [53] N. W. Ashcroft and N. D. Mermin, in *Solid State Physics* (Saunders College Publishing, Fort Worth, 1976), Chap. 2.

- [54] S. Doniach and E. H. Sondheimer, in *Green's Functions for Solid State Physists* (W.A.Benjamin, New York, 1974), Chap. 5.
- [55] B. Laikhtman and S. Luryi, Physical Review B **49**, 17177 (1994).
- [56] A. Shapiro *et al.*, in *Proceedings of the Fall 2001 Materials Research Society Meeting* (Materials Research Society, Pittsburgh, Pennsylvania, 2001).
- [57] R. Q. Hood and L. M. Falicov, Physical Review B **46**, 8287 (1992).
- [58] G. Baym, in *Lectures on Quantum Mechanics* (W.A.Benjamin, New York, 1969).
- [59] S. Zhang and P. M. Levy, Physical review B **65**, 052409 (2002).
- [60] H. E. Camblong *et al.*, Physical review B **47**, 4735 (1993).
- [61] K. Wang *et al.*, Philosophical Magazine **83**, 1255 (2003).
- [62] I. I. Mazin, Physical Review Letters **83**, 1427 (1999).
- [63] B. Nadgorny *et al.*, Physical Review B **61**, R3788 (2000).
- [64] J. A. Katine *et al.*, Physical Review Letters **84**, 3149 (2000).
- [65] F. J. Albert *et al.*, Applied Physics Letter **77**, 3809 (2000).
- [66] J. Grollier *et al.*, Applied Physics Letter **78**, 3663 (2001).
- [67] S. Wolfram, in *Mathematica. A System for Doing Mathematics by Computer* (Addison-Wesley Publishing Company, Redwood City, Calif., 1988).
- [68] J. Manschot *et al.*, cond-mat/0309252 (unpublished).
- [69] W. H. Press *et al.*, in *Numerical Recipes in C. The Art of Scientific Computing* (Cambridge University Press, New York, 1992), Chap. 2,18.
- [70] M. D. Stiles, Journal of Applied Physics **79**, 5805 (1996).